

2013

Development of a co-firing fuel from biomass-derived binder and crushed coal

Andrew Friend
Iowa State University

Follow this and additional works at: <http://lib.dr.iastate.edu/etd>

 Part of the [Mechanical Engineering Commons](#), and the [Oil, Gas, and Energy Commons](#)

Recommended Citation

Friend, Andrew, "Development of a co-firing fuel from biomass-derived binder and crushed coal" (2013). *Graduate Theses and Dissertations*. 13192.

<http://lib.dr.iastate.edu/etd/13192>

This Thesis is brought to you for free and open access by the Graduate College at Iowa State University Digital Repository. It has been accepted for inclusion in Graduate Theses and Dissertations by an authorized administrator of Iowa State University Digital Repository. For more information, please contact digirep@iastate.edu.

Development of a co-firing fuel from biomass-derived binder and crushed coal

by

Andrew James Friend

A thesis submitted to the graduate faculty
in partial fulfillment of the requirements for the degree of
MASTER OF SCIENCE

Co-majors: Mechanical Engineering; Biorenewable Resources and Technology

Program of Study Committee:

Robert Brown, Major Professor
D. Raj Raman
Terrence Meyer
R. Christopher Williams

Iowa State University

Ames, Iowa

2013

Copyright © Andrew James Friend, 2013. All rights reserved.

TABLE OF CONTENTS

LIST OF FIGURES	iv
LIST OF TABLES	vi
ACKNOWLEDGEMENTS	vii
ABSTRACT	viii
CHAPTER 1. INTRODUCTION	1
1.1 Motivation	1
1.2 Overview of thesis.....	1
CHAPTER 2. BACKGROUND AND LITERATURE REVIEW	2
2.1 Introduction	2
2.2 Current regulations which target electrical utilities	2
2.3 Greenhouse gas mitigation strategies.....	5
2.3.1 Biomass Fuels	5
2.3.2 Biomass Combustion Technologies.....	6
2.3.3 Co-firing advantages and challenges	8
2.4 Densification technologies	11
2.4.1 Biomass pelletization	12
2.4.2 Torrefaction.....	14
2.4.3 Fast pyrolysis	14
2.4.4 Coal pelletization	16
2.4.5 Co-fire pellets.....	16
CHAPTER 3. EXPERIMENTAL METHODS	17
3.1 Experimental objective.....	17
3.2 Design of experiments.....	17
3.3 Experimental test procedure.....	22
3.3.1 Production of bio-oil	22
3.3.2 Separation of sugars and phenolic oligomers	24
3.3.3 Preparation of coal	25
3.3.4 Pelletization of coal using clean phenolic oligomers as binder	26
3.4 Analysis of products.....	28
CHAPTER 4. RESULTS AND DISCUSSION.....	33
4.1 Higher heating value	33
4.2 Proximate analysis.....	42
4.2.1 Moisture	42
4.2.2 Volatiles	44
4.2.3 Fixed carbon.....	47
4.2.4 Ash	49
4.3 Ultimate Analysis.....	52
4.3.1 Carbon.....	52
4.3.2 Sulfur.....	54

4.4	Durability	55
4.4.1	Indirect tensile strength.....	55
4.4.2	Impact resistance.....	57
4.4.3	Abrasion resistance	58
4.5	Other analysis.....	60
4.5.1	Density	60
4.5.2	Ash fusibility.....	62
CHAPTER 5. CONCLUSIONS		64
5.1	Experimental Conclusions.....	64
5.2	Future Work	65
BIBLIOGRAPHY.....		67
APPENDIX A: PELLET MOLD DRAWINGS		70
APPENDIX B: EXPERIMENTAL DATA		77
APPENDIX C: STATISTICAL MODELS		83

LIST OF FIGURES

Figure 1: Summary of renewable portfolio requirements by state	4
Figure 2: Common types of combustors:(a) grate-fired, (b) suspension, (c) fluidized bed.....	7
Figure 3: Deposit build-up on superheaters after one week of co-firing coal and straw	10
Figure 4: Pellet mill schematic	12
Figure 5: Mechanical or hydraulic briquette press	13
Figure 6: Screw extruder.....	13
Figure 7: Fast pyrolysis system.....	15
Figure 8: Co-fire pellets	16
Figure 9: Central composite design for three factors.....	18
Figure 10: Fast pyrolysis unit coupled with fractionating bio-oil recovery system	23
Figure 11: Product distribution from fast pyrolysis unit shown in Figure 10.....	23
Figure 12: The phenolic oligomer fraction of bio-oil (CPO).....	25
Figure 13: Riffle type sample splitter	25
Figure 14: (left) coal-CPO mixture, (right) pellet mold filled with coal-CPO mixture.....	27
Figure 15: Mold baseplate closed (left), and open (right)	27
Figure 16: Pellet press setup	28
Figure 17: Indirect tensile strength test before (left) and after (right)	30
Figure 18: Abrasion test apparatus	31
Figure 19: Modeled pellet higher heating value with respect to coal moisture content and coal particle size.....	34
Figure 20: Modeled pellet higher heating value with respect to cure temperature and CPO binder fraction.....	35
Figure 21: Pellet higher heating values on a wet basis sorted by experiment number	36
Figure 22: Pellet higher heating values on an ASTM dry basis sorted by experiment number	37
Figure 23: Predicted pellet higher heating values.....	38
Figure 24: Pellet higher heating values predicted by the correlation developed by Sheng et al.....	38
Figure 25: FTIR analysis of the coal, pellets, and CPO	40
Figure 26: Heat flow test of a coal - CPO mixture using a thermogravimetric analyzer	41
Figure 27: Modeled pellet moisture content with respect to coal moisture content and cure temperature	43
Figure 28: Modeled pellet moisture content with respect to CPO binder fraction and coal particle size	44
Figure 29: Modeled pellet volatile content with respect to coal particle size and coal moisture content.....	46
Figure 30: Modeled pellet volatile content with respect to CPO binder fraction and cure temperature	47

Figure 31: Modeled pellet fixed carbon content with respect to coal particle size and coal moisture content.....	48
Figure 32: Modeled pellet fixed carbon content with respect to CPO binder fraction and cure temperature.....	49
Figure 33: Modeled pellet ash content with respect to coal particle size and CPO binder fraction	51
Figure 34: Pellet ash content with respect to CPO binder fraction.....	51
Figure 35: Modeled pellet elemental carbon content with respect to CPO binder fraction and coal particle size.....	53
Figure 36: Modeled pellet elemental carbon content with respect to cure temperature and coal moisture content	53
Figure 37: Modeled pellet elemental sulfur content with respect to CPO binder fraction and coal moisture content	55
Figure 38: Indirect tensile strength comparison.....	56
Figure 39: Impact resistance statistical model residuals vs. predicted values	57
Figure 40: Impact resistance comparison	58
Figure 41: Abrasion resistance statistical model residuals vs. predicted values.....	59
Figure 42: Abrasion resistance comparison.....	59
Figure 43: Modeled pellet particle density with respect to CPO binder fraction and coal moisture content.....	61
Figure 44: Modeled pellet particle density with respect to coal particle size and cure temperature	62
Figure 45: Ash fusibility test points.....	62
Figure 46: Ash fusibility comparison for coal and co-fire pellets	63

LIST OF TABLES

Table 1: National ambient air quality standards	3
Table 2: List of considered factors for experimental design.....	19
Table 3: Design of experiment factor-level combinations.....	19
Table 4: List of experiments for central composite design.....	21
Table 5: Coal size reduction parameters	26
Table 6: Precision of Leco CHNS analyzer	29
Table 7: Pellet heating value reduced model summary	33
Table 8: Pellet moisture content reduced model summary.....	42
Table 9: Pellet volatile content reduced model summary.....	45
Table 10: Pellet fixed carbon content reduced model summary.....	47
Table 11: Pellet ash content reduced model summary.....	50
Table 12: Pellet elemental carbon content reduced model summary	52
Table 13: Pellet elemental sulfur content reduced model summary	54
Table 14: Pellet indirect tensile strength reduced model summary	56
Table 15: Pellet particle density reduced model summary	60

ACKNOWLEDGEMENTS

I would like to acknowledge Dr. Robert Brown for his idea of creating the co-fire pellet. In addition, I would like to thank him for the opportunity and funding to be able to further develop the co-fire pellets.

Special thanks go to the staff and students of CSET, particularly Marge Rover, Patrick Johnson, Lysle Whitmer, Ryan Smith, Marty Haverly, Jordan Funkhouser, John Hoyt, and Mat Dorn, for their guidance and help with the research process.

I would like to recognize Dr. Chris Williams for his help in the initial development stages of the co-fire pellet. I would like to thank Dr. Thomas Wheelock for his help through the use of his coal analysis laboratory. I would also like to thank Dr. Max Morris for his invaluable advice concerning the statistical analysis of my data.

Thanks go to Dr. Brown, Dr. Williams, Dr. Raj Raman, and Dr. Terry Meyer for agreeing to serve on my graduate committee. I would also like to recognize the Iowa Farm Bureau for funding this project.

Finally, I would like to recognize the immense support and love my wife Naomi has showed me while I worked on this project. She always had helpful suggestions when unexplained problems confronted me in my research. Many cherished moments were spent with her as we worked on our graduate theses together.

ABSTRACT

The focus of this work was the development of a co-firing boiler fuel for use in the coal power plant industry. This fuel, known as co-fire pellets, is a densified product comprised of crushed coal and a renewable binder derived from the liquid product of the fast pyrolysis of lignocellulosic biomass. The co-fire pellets can help meet certain state and federal regulations related to electricity production. A central composite design of experiments was used to evaluate properties of the co-fire pellets based on four factors relating to the makeup of the pellets. These factors are coal particle size, coal moisture content, binder percentage, and pellet cure time. Properties of the pellets were investigated using the following tests: higher heating value, proximate analysis, ultimate analysis, mass density, particle density, indirect tensile strength, impact resistance, and abrasion resistance. The experimental data was modeled using linear regression techniques. The pyrolyzed biomass binder fraction had the largest impact on pellet properties, while cure temperature was determined to be a nonessential treatment.

CHAPTER 1. INTRODUCTION

1.1 Motivation

By 2050, the world population is expected to reach 9 billion. Most of the population growth between now and 2050 is expected to occur in developing countries [1]. Proportional to population growth, energy demand between 2008 and 2035 is expected to increase 0.6 percent in developed countries. In developing countries where most of the population growth is expected to occur, energy demand is expected to increase 2.3 percent during the same time period [2]. This increase in energy demand is projected to occur over all energy sources.

As developing countries continue to industrialize, residents of these countries are expecting the same luxuries that developed countries already enjoy, such as access to inexpensive electricity. Currently, coal provides the largest share in electrical power generation worldwide [1]. However, coal also emits harmful emissions, more so than most energy sources. Therefore, it is heavily regulated by government agencies, most notably the United States Environmental Protection Agency. In light of this, the goal of this research is to develop a partially renewable boiler fuel that allows current and future electrical power plants to be able to reduce coal consumption and harmful emissions while adapting to the ever increasing worldwide electrical demand.

1.2 Overview of thesis

This thesis consists of four chapters which follow this introduction. Chapter 2 consists of a brief literature review that summarizes current technology as it relates to coal combustion, emission regulations, and solid fuel densification technologies. Chapter 3 serves as an overview of the experimental methods that were used to explore properties of the co-fire pellets. Chapter 4 presents a discussion of the results from the experiments. A summary of the conclusions that can be drawn from this work and recommendations for future work are presented in Chapter 5. Supplemental information necessary to understand this work in detail can be found in the Appendices.

CHAPTER 2. BACKGROUND AND LITERATURE REVIEW

2.1 Introduction

This literature review will serve as an overview of current environmental regulations as they relate to coal combustion. In order to combat these regulations, utilities are considering a number of options, including supplementing their boiler feed with renewable fuels. These options will be discussed. An overview of fast pyrolysis will be given, along with a summary of processes used in the mechanical densification of biomasses and coal. Finally, an introduction will be given to the concept of a co-fire pellet.

2.2 Current regulations which target electrical utilities

Regulations which target coal-fired power plants can be divided into two categories. The first is regulations that limit the emission of certain air pollutants. The second is state and federal regulations that indirectly lower the emissions of air pollutants through the required or encouraged use of alternative sources of energy, such as biomass, wind, and solar.

Air pollutant regulations. In the United States, air pollutant regulations are set in place by the Environmental Protection Agency (EPA). EPA regulations, as they relate to coal-fired boilers, can be broken down into the following rules.

The Clean Air Act was first passed by Congress in 1970; it was revised in 1990. It required the EPA to set up the National Ambient Air Quality Standards (NAAQS) for regulating six hazardous air pollutants: carbon monoxide, lead, nitrogen dioxide, ozone, particulate matter, and sulfur dioxide. The current maximum levels for these pollutants are shown in Table 1. In addition to the NAAQS, the 1990 revision of the Clean Air Act created the Maximum Achievable Control Technology (MACT) rule that specifically targeted toxic air emissions from power plants. The MACT rule has been recently revised as the Mercury and Air Toxics Standards (MATS) rule. This latest revision has received considerable pushback from the utility industry as it limits the emissions of mercury and acid gases to a level that the utility industry considers to be severe. The U.S. judicial courts have ordered the EPA to reconsider the limits of the current MATS rule. Because of this court ruling, the most current revision of the MATS rule has not yet been implemented [3].

Table 1: National ambient air quality standards [4]

Pollutant [final rule cite]		Primary/ Secondary	Averaging Time	Level	Form
Carbon Monoxide [76 FR 54294, Aug 31, 2011]		primary	8-hour	9 ppm	Not to be exceeded more than once per year
			1-hour	35 ppm	
Lead [73 FR 66964, Nov 12, 2008]		primary and secondary	Rolling 3 month average	0.15 µg/m ³ (1)	Not to be exceeded
Nitrogen Dioxide [75 FR 6474, Feb 9, 2010] [61 FR 52852, Oct 8, 1996]		primary	1-hour	100 ppb	98th percentile, averaged over 3 years
		primary and secondary	Annual	53 ppb (2)	Annual Mean
Ozone [73 FR 16436, Mar 27, 2008]		primary and secondary	8-hour	0.075 ppm (3)	Annual fourth-highest daily maximum 8-hr concentration, averaged over 3 years
Particle Pollution Dec 14, 2012	PM _{2.5}	primary	Annual	12 µg/m ³	annual mean, averaged over 3 years
		secondary	Annual	15 µg/m ³	annual mean, averaged over 3 years
		primary and secondary	24-hour	35 µg/m ³	98th percentile, averaged over 3 years
	PM ₁₀	primary and secondary	24-hour	150 µg/m ³	Not to be exceeded more than once per year on average over 3 years
Sulfur Dioxide [75 FR 35520, Jun 22, 2010] [38 FR 25678, Sept 14, 1973]		primary	1-hour	75 ppb (4)	99th percentile of 1-hour daily maximum concentrations, averaged over 3 years
		secondary	3-hour	0.5 ppm	Not to be exceeded more than once per year

Another EPA regulation is the Cross State Air Pollution Rule, or CSAPR. This rule seeks to limit power plant emissions that cross state lines. Sulfur dioxide and nitrogen oxides are the main compounds targeted as they are known to react with each other to produce ground level ozone and particulate matter. With a similar fate to the MATS rule, CSAPR was struck down by a federal court in August 2012. Until the EPA revises CSAPR satisfactorily to the court's demands, an earlier rule, the Clean Air Interstate Rule (CAIR) remains in effect [5].

In addition to the pollutants that are hazardous to human health, the EPA is considering limiting the emission of carbon dioxide, a known greenhouse gas (GHG). Currently, the EPA only requires the reporting of CO₂, but does not limit it. In an effort to cut carbon emissions, the EPA proposed a rule in March 2012 that would limit CO₂ emissions from power plants to 1000 lbs/MWh of generated electricity [6].

Other federal and state regulations. While the EPA’s air pollutant regulations may indirectly reduce the use of fossil fuels, many states already have regulations in place that require or encourage the use of renewable resources for power production. These regulations are called renewable portfolio standards (RPS), or renewable electricity standards (RES). An RPS is a policy that ensures that a minimum amount of renewable energy is included in a state’s electrical generating portfolio [7]. Some of the renewable sources that are covered include solar, wind, hydro, geothermal, and biomass. Others may include landfill gas, municipal solid waste, and tidal energy. The setup of an RPS depends on each state; not all states utilize this regulation. An RPS specifies an amount of renewable electrical generating capacity that must be achieved by a future point in time. The RPS may include regular scheduled increases up to the future target [8]. As shown in Figure 1, Iowa’s RPS is somewhat outdated with the requirement of 105 MW by 1999. Congress has attempted to institute a national RPS, but no legislative progress has been made on that front [9].

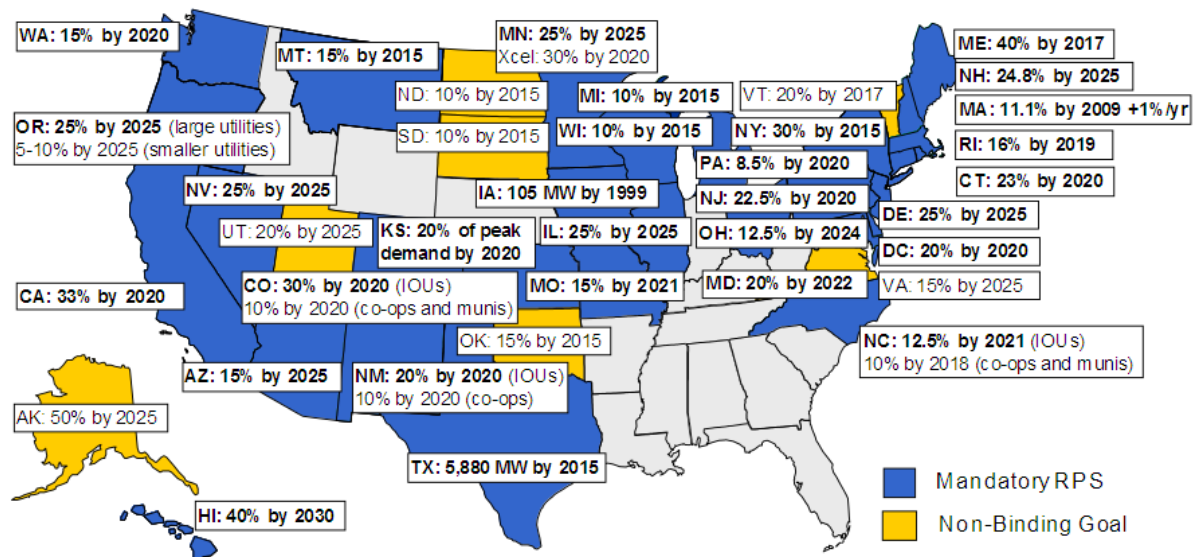


Figure 1: Summary of renewable portfolio requirements by state [10]

2.3 Greenhouse gas mitigation strategies

Current GHG mitigation tactics include pre-combustion, combustion, and post-combustion strategies. Post-combustion strategies, known as carbon capture and storage (CCS), employ devices that treat and capture carbon dioxide in the combustion exhaust gases. Combustion mitigation strategies concentrate the levels of carbon dioxide in the exhaust gases, rendering it easier to capture and store. Pre-combustion strategies include the pretreatment of boiler fuel, co-firing of renewable fuels, such as biomass, and integrated gasification combined cycle (IGCC).

While each of the technologies listed above represent a theoretical avenue for reducing GHG emissions, biomass co-firing is the only technology that can be implemented in the near future without extensive capital investment. Biomass co-firing offers the lowest cost option among the several technologies available for greenhouse gas reduction. The cost of CO₂ capture and sequestration is in the range of 40-60 US\$/ton of CO₂. The high capital investment for carbon sequestration technology could potentially increase the cost of the electricity by as much as 60% [11].

2.3.1 Biomass Fuels

Biomass can be defined as any material of recent, biological origin. The adjective “recent” distinguishes biomass from fossil fuels which are also thought to have originated from plant materials.

Two main classes characterize biomass: residues and energy crops. Residues include materials such as wood chips, agricultural co-products, and industrial wastes. Energy crops are grown specifically for energy use and include annual grains, short rotation woody crops, and herbaceous perennial grasses. Residual biomasses are usually classified as waste materials. They have little apparent economic value making them an inexpensive fuel for power plants. In contrast, dedicated energy crops can provide a more reliable and uniform fuel source, but are typically sold at a premium when compared to biomass residues [12].

The physical and chemical structures of biomass vary significantly depending on type. Three plant polymers comprise biomass: cellulose, hemicellulose, and lignin. Cellulose and hemicellulose polymers act as structural fibers to give biomass its shape and rigidity. Lignin acts as glue which binds the fiber matrix together. Chemically, biomass is

comprised of carbon, hydrogen, nitrogen, oxygen, sulfur, and chlorine as well as many trace alkali and alkaline earth metals such as Si, Al, Ti, Fe, Ca, Mg, Na, K, S, and P [13].

2.3.2 Biomass Combustion Technologies

Two main methods exist for the combustion of biomass for heat and power. It can be either fired in dedicated biomass boilers, or co-fired alongside coal in existing coal-fired boilers.

Dedicated biomass boilers. Solid fuel boiler types include grate-fired, suspension, and fluidized bed, see Figure 2. In grate-fired boilers, biomass is fed onto a moving grate. Primary combustion air is blown through the bottom of the grate. As the biomass moves through the boiler, it slowly combusts and the remaining ash is deposited at the end of the boiler. Secondary air can be blown in above the grate fuel bed in order to improve the combustion efficiency by burning out remaining carbon in the flue gas. Grate fired boilers can handle large, heterogeneous biomass particles with high moisture contents [14]. However, they can rarely achieve combustion efficiencies exceeding 90% [12].

Suspension burners, also known as pulverized coal boilers, achieve high combustion efficiencies through the suspension of fine fuel particles in a stream of rising air. The fuel is ground to less than 100 micron particle size, and is subsequently entrained in the primary combustion airflow. Secondary air is injected to help complete the combustion process. While suspension burners can achieve combustion efficiencies exceeding 99%, they are not well suited to burning large, fibrous biomass particles [12].

Fluidized bed boilers employ a bed of sand or other granular material that is suspended via air injected into the bottom of the boiler. The granular bed provides high rates of heat and mass transfer, suitable for burning a wide range of biomass types and moisture contents. However, they are very sensitive to bed agglomeration, leading to unscheduled shutdowns [12,14].

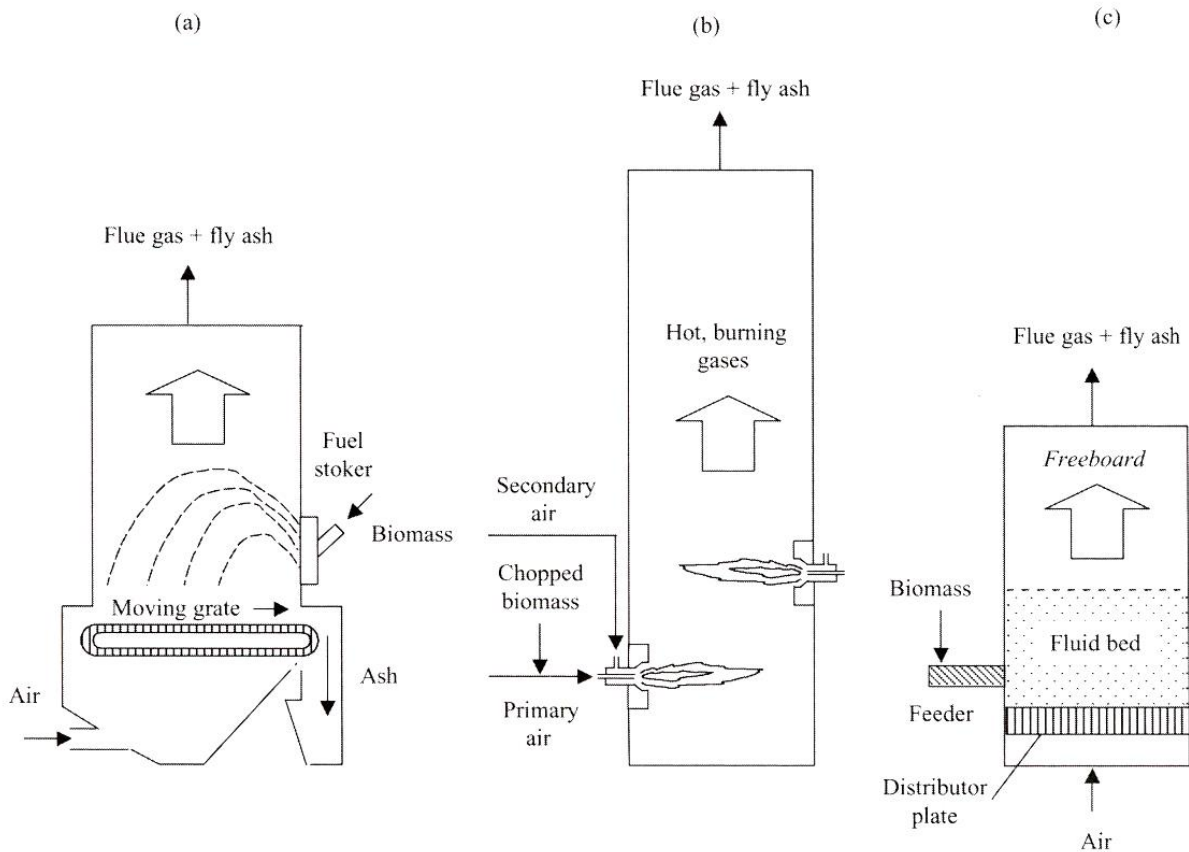


Figure 2: Common types of combustors:(a) grate-fired, (b) suspension, (c) fluidized bed [12]

Biomass co-firing techniques. Along with direct firing, each of the boiler types previously discussed may also be used for the co-firing of coal and biomass. Co-firing technology can be classified under three main types: direct, indirect, or gasification co-firing.

Direct co-firing involves the combustion of biomass and coal in the same boiler. This can be achieved four ways. First, the biomass can be co-processed in the same size reduction mills as the coal, and then fed into the boiler. Second, the biomass can be ground separately from the coal and then mixed with the coal feed before insertion into the boiler. Third, the biomass can be ground separately and fed into a different section of the boiler. Finally, the biomass can be used as a reburn fuel for NO_x emission control. Direct co-firing does not require large amounts of capital input due to the utilization of existing coal infrastructure. However, biomass-coal feed ratios typically do not exceed 10% due to the lower heat input from the biomass.

Indirect co-firing employs a separate boiler for biomass combustion. The resulting steam is combined with steam from coal-fired boilers. An advantage of this method is that some processes or equipment can be shared between the biomass and coal boilers, resulting in a lower capital cost compared to standalone biomass boilers. Another advantage is that the flue gas of the biomass boiler does not come in contact with the heating tubes in the coal boiler, thereby avoiding biomass related fouling or corrosion.

Finally, gasification co-firing employs a thermochemical process known as gasification. Biomass is heated to high temperatures in an oxygen starved environment to yield a syngas theoretically comprised of hydrogen and carbon monoxide. The syngas is then injected into a coal-fired boiler. The advantages of this method include easy removal of biomass alkali metals via the biochar, and the ability to handle a wide range of biomass types. When compared to direct, or indirect co-firing, gasification co-firing requires a large capital investment [11].

2.3.3 Co-firing advantages and challenges

One of the largest advantages of biomass co-firing is emissions reduction. The elemental composition of biomass is naturally low in sulfur, mercury, and other heavy metals, thereby reducing SO_x and heavy metal emissions. When compared to coal, the amount of net CO_2 released into the atmosphere is substantially lower for biomass. This is due to the fact that biomass removes carbon from the atmosphere during its growth cycle. The carbon is then released back into the atmosphere during combustion, and removed again during the next growth cycle of the biomass. Another advantage is that co-firing allows for the easy disposal of biomass wastes that may be expensive to landfill. Biomass co-firing also reduces fouling issues associated with boilers that only burn biomass [12].

The challenges associated with biomass co-firing may outweigh the advantages. The properties of biomass span a wide range, and widely differ from that of traditional fossil fuels. As such, many difficulties are encountered in the process of combusting or co-firing biomass. These challenges include:

- fuel preparation, storage, and delivery
- ash deposition and corrosion
- fuel conversion

- pollutant formation
- fly ash utilization
- impacts on SCR systems [15]

Fuel preparation, storage, and delivery. Owing mostly to its low bulk density, biomass contains roughly two-thirds the energy content of coal. Large amounts of biomass must therefore be fed into a coal boiler in order to keep the steam output constant. Biomass must also be sourced near the power plant in order to keep transportation costs low. Biomass is generally produced during the summer months of the year, and harvested in the fall. It therefore requires large amounts of storage to support year round operations. Finally, the fibrous nature of biomass inhibits size reduction necessary for co-firing operations, especially for pulverized coal boilers.

Ash deposition and corrosion. Ash deposition and corrosion can be traced back to biomass composition. In general, herbaceous biomasses produce high deposit rates while many woody biomasses produce relatively lower deposit rates [13]. Alkali metals, sulfur, chlorine, and silica are all elements found in biomass that are known to cause corrosion and fouling problems in boilers. Chlorine combines with alkali metals found in biomass to form alkali chlorides which impinge on boiler tubes. Once in contact with the iron elements, chlorine can act as a catalyst in the oxidation of iron to form iron oxides [14]. The reaction of alkali with silica or sulfur forms low melting point compounds that easily stick to heat transfer surfaces [16]. As shown in Figure 3, once the alkali chloride deposits form, fly ash begins to deposit on superheaters, creating a very large deposit. The deposit is usually very porous, making it an effective insulator which reduces the boiler efficiency [14]. Certain elemental compounds are known to affect the melting point of ash. Magnesium and calcium are known to increase the melting temperature, while potassium and alkali chlorides decrease the melting temperature. As the melting temperature of ash decreases, it begins to liquefy; a condition known as slagging. Slagging coats the walls of boilers and increases the effort needed to remove the ash.



Figure 3: Deposit build-up on superheaters after one week of co-firing coal and straw [17]

Fuel conversion. During biomass combustion, a larger amount of volatiles (85-95% initial mass) are released than during coal combustion (50-65%). This large release of volatiles occurs over a relatively short time span. In contrast, the char burnout time of biomass combustion is much longer, especially for large particle sizes and high moisture contents. Unless precautionary measures are taken, the co-firing of biomass and coal may result in an increase of carbon in the flue gas due to the slow biomass char burnout time, especially for boilers with short residence times [13,15].

Pollutant formation. Products of incomplete combustion include carbon monoxide (CO), hydrocarbons, tars, polyaromatic hydrocarbons (PAH), and char particles [13]. These pollutants can be avoided by raising the combustion temperature, adjusting the air-to-fuel ratio, and increasing the residence of the combustion gas in the combustion zone. Biomass may generate incomplete combustion products due to its high moisture content and long char burnout time.

Other combustion derived pollutants include particulate matter, nitrogen oxides (NO_x), sulfur oxides (SO_x), acid gases and heavy metals [13]. Biomass can help decrease particulate emissions during co-firing due to its low ash content. Sulfur emissions, primarily SO₂, can also be reduced since biomass is naturally low in sulfur. The emission of NO_x compounds from biomass combustion varies greatly. For most boilers, biomass combustion does not result in thermal NO_x because of relatively low combustion temperatures. Rather, nitrogen bound in the fuel produces nitric oxides [16]. Acid gases, such as HCl are known to be a problem in coal combustion emissions. Biomass may lower acidic gas emissions

depending on the chlorine content in the biomass. Herbaceous biomass sources generally contain higher levels of chlorine than woody biomass. Heavy metal emissions depend largely on the biomass type. Industrial wastes, such as refuse derived fuel (RDF), contain high concentrations of heavy metals which are known to condense on alkali-derived fly ash particles in the flue gas [13].

Fly ash utilization. Markets exist for coal fly ash, depending on the rank of coal used in the combustion process. The concrete market represents one of the best utilization opportunities for coal-derived fly ash. In this market, ash is sealed in concrete during construction of roads and other stationary structures. In order to avoid fracture during freeze/thaw cycles, air is introduced into concrete via air-entraining agents (AEA). Unburned carbon in fly ash is known to absorb the AEA. Biomass derived fly ash is especially troublesome due to its higher carbon content when compared to coal fly ash [15,18]. Currently, most biomass-coal derived ashes do not meet the ASTM C618 specification for fly ash utilization [12].

Impacts on selective catalytic reduction (SCR) systems. SCR is used in coal-fired boilers and other industrial applications to convert NO_x into N_2 and water using a catalyst. Evidence indicates that co-firing biomass with coal could deactivate SCR catalysts. This deactivation may be caused by the poisoning of the catalyst by the alkali and alkaline earth metals found in biomass. The deactivation may also be due to plugging on the surface of the catalyst, rather than the poisoning of the catalyst itself. If this is indeed the case, the catalyst can be regenerated [15]. Regardless, biomass combustion can increase the cost needed to operate SCR systems.

2.4 Densification technologies

As discussed in the previous section, biomass is being considered for use by electrical utilities in order to meet environmental and state level regulations. Compared with coal, biomass is usually inferior in terms of heating value, bulk density, moisture content, alkali metal content and homogeneity [12]. Methods to increase the usability of biomass through densification will be discussed in this section.

2.4.1 Biomass pelletization

One way to overcome the limitations of biomass is through mechanical densification, or pelletization. Compared to loose or raw biomass, pelletized biomass offers increased bulk density, higher heating values, and improved homogeneity. Some of the common densification systems used in industry include the pellet mill, briquette press, and screw extruder [19].

Pellet mill. A pellet mill consists of a series of rollers that rotate around a stationary die, as shown in Figure 4. Before entering the pelletizing chamber, the biomass is usually pretreated with steam in order to partially gelatinize the carbohydrate portion of the biomass, which makes for more durable pellets. The softened biomass is then fed into a stationary die where a series of rollers force feed the biomass through holes in the die. Knives mounted around the outer perimeter of the die cut the pellets as they are extruded, so that pellets with uniform lengths are produced [19].

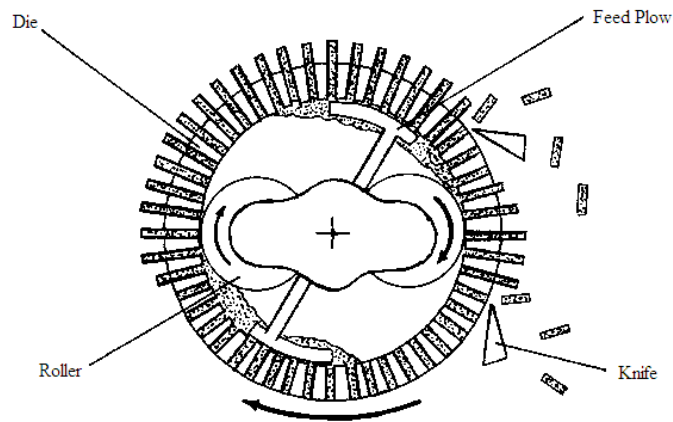


Figure 4: Pellet mill schematic [20]

Briquette press. Compared with a pellet mill, a briquette press can handle larger particle sizes and a wider range of moisture contents. During the briquetting process, moisture in the biomass forms steam under high pressure. The steam helps to hydrolyze the hemicellulose and lignin into lower molecular weight compounds that act as adhesives and help bind the biomass particles together. Different types of briquette presses include the hydraulic piston press, the mechanical piston press, and the tabletizer [19]. An example of a

hydraulic or mechanical press is shown in Figure 5. The hydraulic briquette press closely resembles the press used to make co-fire pellets, as will be discussed in Section 3.3.4.

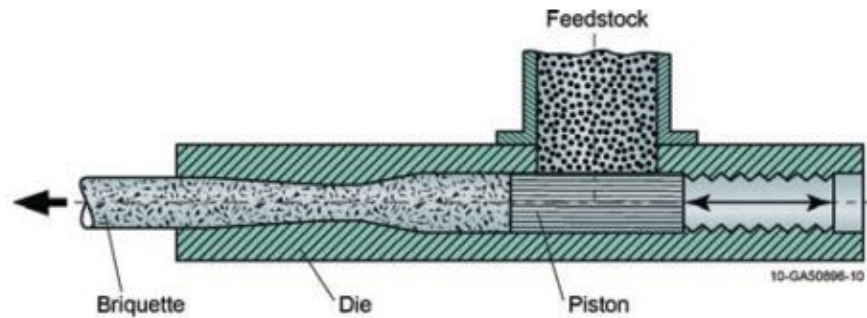


Figure 5: Mechanical or hydraulic briquette press [19]

Screw extruder: A screw extruder (Figure 6) utilizes particle sizes less than 4 mm so that the act of bringing biomass particles close together creates strong inter-particle forces, resulting in a durable product. During the extrusion process, biomass moves progressively through a rotating screw and then through a barrel and die. Throughout the process, the biomass particles experience significant pressure and friction gradients, leading to an increase in the temperature of the biomass. Similar to the pellet mill, the high process temperatures soften the biomass, leading to the formation of local bridges and interlocking particles. The high temperature, which can reach magnitudes close to 300 C, slightly chars the biomass, making it suitable for burning or co-firing applications [19].

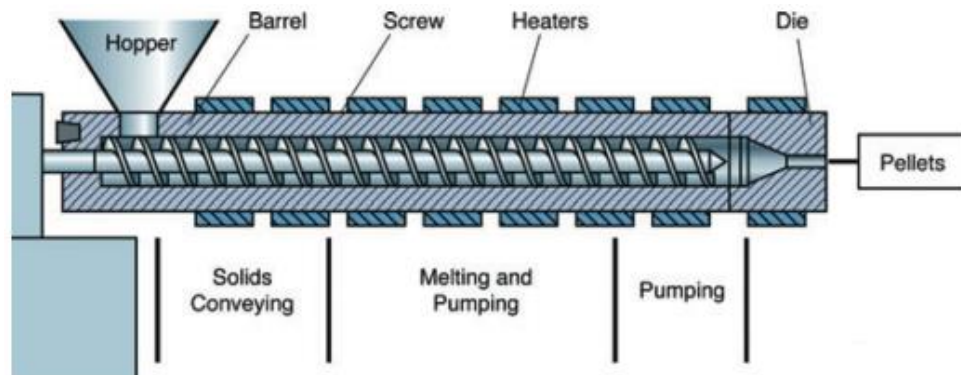


Figure 6: Screw extruder [19]

2.4.2 Torrefaction

Torrefaction is a thermochemical process characterized by moderate temperatures (200-300°C), low particle heating rates (< 50 °C/min.), and long residence times (30 min. - 2 hr.). During torrefaction, biomass partially volatilizes, yielding a solid, charred product. Compared with the raw biomass, torrefied biomass boasts lower moisture contents and an increase in bulk density, which translates into an increase in heating value. Torrefied biomass accounts for 70% of the original mass, and nearly 90% of the initial energy content. Other advantages include increased product uniformity, and an increase in hydrophobicity due to the destruction of OH groups during the torrefaction process [21].

Due to its brittle nature, torrefied biomass is a popular candidate for co-firing applications. In fact, torrefied biomass has been dubbed “bio-coal” due to its increased grindability and dense energy content. With regard to Section 2.4.1 on pelletization, synergetic effects can be realized through the combination of torrefaction and pelletization. Torrefaction is easily applied to a wide variety of biomasses, while pelletization subsequently increases the energy density and durability of the torrefied biomass. The resulting product is believed to be a competitive candidate for power production [22].

2.4.3 Fast pyrolysis

Fast pyrolysis is the rapid decomposition of biomass at high temperatures and in the absence of oxygen to yield three products: a solid known as biochar, a liquid bio-oil, and a weak synthesis gas. Biochar can be used as a soil fertilizer or combusted for heat and power. Bio-oil can be upgraded to fuels and chemicals, or combusted for heat and power. The syngas product, comprised mainly of carbon dioxide, carbon monoxide and light oxygenates, is usually combusted to provide heat for the pyrolysis reactor [23].

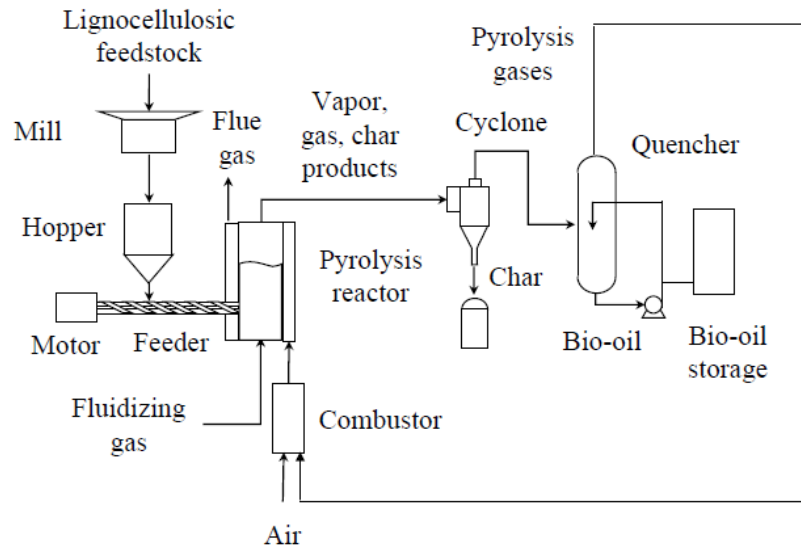


Figure 7: Fast pyrolysis system [12]

Bio-oil. Bio-oil is often compared to crude oil, but it is instead better thought of as liquid biomass from the perspective of its elemental composition. Bio-oil holds many advantages over raw biomass. This energy dense liquid simplifies transportation and processing. Compared with raw biomass it is relatively homogeneous, making for easier upgrading. Although bio-oil is an ideal product when compared to biomass, crude oil bests bio-oil in terms of energy content and ease of upgrading. Bio-oil is comprised of hundreds of oxygenated compounds, which makes the upgrading processing difficult for refineries. Because of this, the traditional end use of bio-oil is combustion in a boiler for steam and power production. However, the high water content and acidic nature of bio-oil make it a less desirable boiler fuel when compared to coal or heavy fuel oil [23].

Clean phenolic oligomers (CPO). CPO can be produced from the heavy ends of bio-oil via a simple water washing process in which bio-oil is mixed with water in order to recover the sugars present in bio-oil. The resulting “sugar water” is decanted from the mixture, leaving behind the lignin fraction of bio-oil. The advantage of this water washing process is that the high value sugars present in bio-oil are recovered separately from the CPO and are then upgraded to fuels or commodity chemicals [23,24]. The physical properties of CPO are similar to the heavy ends of bio-oil. CPO can be used as a liquid fuel for use in

coal-fired boilers, or as an asphalt additive [25]. The use of CPO as an energy dense binder will be discussed in Section 2.4.5.

2.4.4 Coal pelletization

The mining, transport and processing of coal produces very small particles known as fines that are difficult to use despite their high calorific value. Generally, for bituminous coals, the amount of cleaning waste coal fines equals the amount of clean coal produced [26]. These fines are sometimes disposed of in dumps and slurry ponds, which pose environmental problems and aggravate the risk of spontaneous combustion [23]. Attempts to reclaim these waste coal fines via pelletization techniques are being attempted by the electrical utility industry. The most popular recovery technique is agglomeration with an oil-type binder. Agglomeration is accomplished by tumbling the coal fines with a binder. Through the repeated act of rotation, the coal particles bind together to form sufficient sized spheres [19]. The agglomerated spheres are easier to transport and store than the coal fines [27]. An alternative method for coal fines recovery is the production of co-fire pellets, as discussed in the next section.

2.4.5 Co-fire pellets

Known as “co-fire pellets,” these energy dense capsules are produced by mixing the lignin-derived fraction of bio-oil with crushed coal. The resulting mixture is then compressed to form a dense pellet (1” diameter by 2” height). The coal forms the bulk of the pellet, while the bio-oil acts as a binder occupying up to 35% of pellet mass. The bio-oil binder can be either the heavy ends of conventional bio-oil, or the CPO fraction of bio-oil as discussed in section 2.4.3.



Figure 8: Co-fire pellets

CHAPTER 3. EXPERIMENTAL METHODS

3.1 Experimental objective

The objective of these experiments was to investigate certain properties of the novel co-fire pellet technology based on the factors of coal particle size, coal moisture content, phenolic oligomer binder weight percentage, and pellet cure time. A central composite design of experiments was developed to explore properties of the pellets by subjecting them to the following analyses: higher heating value, proximate analysis, ultimate analysis, mass density, particle density, indirect tensile strength, impact resistance, and abrasion resistance.

3.2 Design of experiments

A response surface methodology (RSM) experimental design is used to explore the relationship between several factors with one or more response variables. Through the investigation of the effect of two treatments on a response variable, a three dimensional response surface is generated. This response surface allows the researcher to visually inspect the response over a region of interesting factor levels. It also enables the researcher to determine the optimum factor-level combinations used to yield a desired response [28]. In order to quantify factor-response relationships via second order polynomials, a full factorial design is required. However, full factorial designs become increasingly cumbersome as the number of factors increases. Therefore, a central composite design was chosen because it minimizes the total number of experimental runs. It is also very efficient in determining main effects, two factor interaction effects, and the quadratic effects [29]. Central composite designs are comprised of a 2^n factorial design along with additional treatment combinations called axial points which test conditions outside the main design space. In addition, a number of replications are added to the center of the design to establish the variance within the system. Figure 9 shows a central composite design for three factors. Each of the dots in the figure represent a different set of factor-level combinations, or treatments.

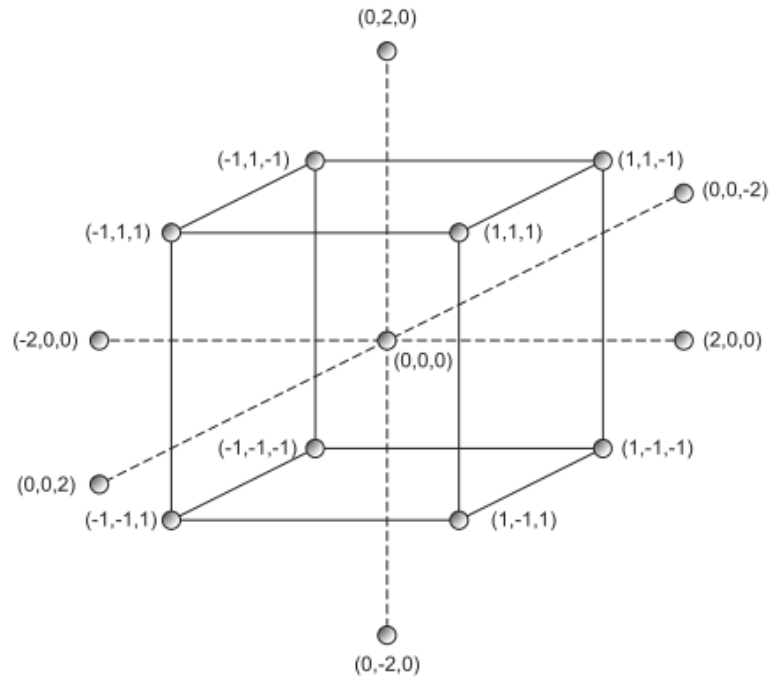


Figure 9: Central composite design for three factors [30]

The production of co-fire pellets is influenced by many factors. In order to decide which factors would be chosen for the central composite design, a list was made of all the factors which impact the production of the pellets as shown in Table 2. After preliminary experiments were conducted, the darkened factors were chosen for use in the four factor central composite design.

The levels for each factor were determined from a review of the literature and from preliminary experiments performed for this thesis research. Table 3 shows the four factors and their associated levels. The coded levels represent the points shown in Figure 9 where “0” is the center point, “-1/+1” correspond with edge of the design space, and “ $-\alpha/\alpha$ ” correspond with points outside the design space. In this experimental design, $\alpha = 2$ since the step between the levels 0 and 1 is the same as between 1 and α . Unlike the other levels, coal particle size does not have evenly spaced levels due to the equipment available for size reduction. Each of the levels for coal particle size was quantified experimentally via sieve analysis. Levels for the other three factors are theoretical and are close approximations of the value actually achieved for each experiment.

Table 2: List of considered factors for experimental design

Factor Number	Factory Category	Factor
1	Coal Preparation	Coal Moisture Content
2		Coal Particle Size
3		Coal Rank
4	CPO Binder Production	Bio-oil Feedstock
5		Pyrolyzer Operating Conditions
6		Bio-oil Stage Fraction
7		Ratio of Water-to-Bio-oil
8		CPO Moisture Content
9	Pellet Production	CPO Binder wt% in Pellet
10		Temperature of CPO
11		Compaction Pressure
12		Hold Time at Maximum Pressure
13		Pellet Shape and Size
14	Post-Processing	Pellet Cure Temperature
15		Pellet Cure Time

Table 3: Design of experiment factor-level combinations

Variable	Factor	Coded Level & Actual Level				
		$-\alpha$	-1	0	1	$+\alpha$
x_1	Coal Mean Particle Size (μm)	114	174	1081	1923	2298
x_2	Coal Moisture Content (wt%)	0.0	3.0	6.0	9.0	12.0
x_3	CPO Binder wt% in Pellet	12	18	24	30	36
x_4	Pellet Aging Temperature ($^{\circ}\text{C}$)	20	70	120	170	220

Table 4 gives the factor-level combinations for each of the 31 experiments. The Exp. ID column lists the order of experiments as dictated by the central composite design. As shown in the Run ID column, all experiments were performed in a random sequence in order to minimize any confounding effects between experimental setups.

After the experiments were performed, the results were fitted to a model using the Statistical Analysis System (SAS) Institute's JMP 10.0 statistical software. Each model generated from JMP can be represented by Equation 1 where Y_i is the model response, β_0 is the intercept, β_i , β_{ii} and β_{ij} are model coefficients, and x_i , $x_i x_j$, and x_i^2 are single terms,

interaction terms, and quadratic terms, respectively. The x terms correspond with the four factors shown in Table 3.

$$Y_i = \beta_0 + \sum_i \beta_i x_i + \sum_{ij} \beta_{ij} x_i x_j + \sum_{ii} \beta_{ii} x_i^2 \quad \text{Equation 1}$$

The significance of each statistical model was determined using values from JMP generated reports. A confidence interval of 95% was used for all models. The first step in evaluating a model is to observe a plot of residuals versus experimental data. Residuals are a quantification of the distance between actual experimental data and predicted values. If the data scatter in the residuals plot occurs in a random fashion, then the assumption is validated that a linear model is appropriate. Next, the R^2 value (percentage of variation that can be explained by the model) should be examined to ensure that it is sufficiently high, ideally 0.80 or greater. In the analysis of variance (ANOVA) table, the f-test probability value (p-value) should be inspected to ensure that it is less than 0.05, which indicates a model is significant. Finally, the lack-of-fit (LOF) p-value should be observed to confirm that it is greater than 0.05. A significant LOF indicates that another model type may fit the experimental data better.

In order to condense the full model into a simpler form, a reduced model can be constructed by examining the p-values for each of the terms in the full model. A p-value less than 0.05 indicates that the term is significant. Non-significant terms with low p-values (less than 0.3 typically) can be included since they may increase the overall accuracy of the reduced model. In order to determine its significance, the reduced model is subjected to the same tests as the full model. In comparison with the full model, the R^2 adjusted value (percentage of variation explained by the significant terms) should be greater. A reduced model should also have a lower root mean squared error (RMSE). The RMSE is a quantification of the error between values predicted by the model and values actually observed. Model reports and residual plots for both full and reduced models are shown in Appendix C.

Table 4: List of experiments for central composite design

Type	Exp. ID	Run ID	Factor			
			Coal Particle Size (μm)	Coal Moisture (wt%)	CPO Binder (wt%)	Pellet Cure Temp. ($^{\circ}\text{C}$)
Center Point	1	20	1081	6	24	120
	2	16	1081	6	24	120
	3	24	1081	6	24	120
	4	15	1081	6	24	120
	5	22	1081	6	24	120
	6	13	1081	6	24	120
	7	9	1081	6	24	120
Axial Experiments	8	14	114	6	24	120
	9	31	2298	6	24	120
	10	17	1081	0	24	120
	11	5	1081	12	24	120
	12	29	1081	6	12	120
	13	18	1081	6	36	120
	14	25	1081	6	24	20
	15	12	1081	6	24	220
Factorial Experiments	16	26	174	3.0	18.0	70
	17	3	174	3.0	18.0	170
	18	11	174	3.0	30.0	70
	19	10	174	3.0	30.0	170
	20	4	174	9.0	18.0	70
	21	30	174	9.0	18.0	170
	22	28	174	9.0	30.0	70
	23	27	174	9.0	30.0	170
	24	8	1923	3.0	18.0	70
	25	7	1923	3.0	18.0	170
	26	23	1923	3.0	30.0	70
	27	6	1923	3.0	30.0	170
	28	2	1923	9.0	18.0	70
	29	1	1923	9.0	18.0	170
	30	21	1923	9.0	30.0	70
	31	19	1923	9.0	30.0	170

3.3 Experimental test procedure

The experimental procedure consisted of the following sequence. First the bio-oil was produced, and the sugars were removed from the heavy fraction of bio-oil via a water wash procedure. Second, the coal was ground and sieved to the appropriate size distributions. Third, the CPO and the coal were mixed together and compressed to form pellets. Finally, a series of tests were performed to investigate the properties of the co-fire pellets. Further details are provided below.

3.3.1 Production of bio-oil

Bio-oil was produced using an 8 kg/hr fast pyrolysis reactor that was coupled with a novel fractionating bio-oil recovery system as described by Pollard et al. [31]. Red oak was ground through a 1/8" inch screen, and subsequently dried to below 10 wt% moisture before being fed into the fast pyrolysis reactor. The sand bed in the reactor was fluidized with hot nitrogen, and held at a constant temperature of 500°C.

The stream exiting a fast pyrolysis reactor contains vapors, aerosols, and solids. Conventional bio-oil recovery uses quench vessels or condensers that collect the bio-oil into one or two fractions. In contrast, the fractionating bio-oil recovery system described by Pollard et al. recovers compounds in the pyrolysis stream based on dew point, yielding five distinct bio-oil fractions (See Figure 10). These stage fractions consist of the following components. Stage 1 is a shell and tube heat exchanger. Viscous in nature, bio-oil recovered in Stage 1 consists of high boiling point compounds such as levoglucosan and phenolic oligomers. Stage 2 consists of an electrostatic precipitator (ESP) that collects phenolic oligomers and polysaccharides in the form of aerosols. Stage 3 is another shell and tube exchanger which recovers phenol type compounds. Stage 4 is an ESP that collects aerosols which have formed in the vapor stream after the second stage fraction. The final fraction, Stage 5, is a shell and tube heat exchanger designed to collect water, furans, and light oxygenated compounds [32]. A typical product distribution for this system is shown in Figure 11.

A significant advantage of the fractionating system is the ability to recover water, acids, and other light oxygenated compounds into a separate fraction, thereby creating four

high value bio-oil fractions [31]. Due to their viscous nature, the first two bio-oil stage fractions were utilized for the production of the co-fire pellet binder.

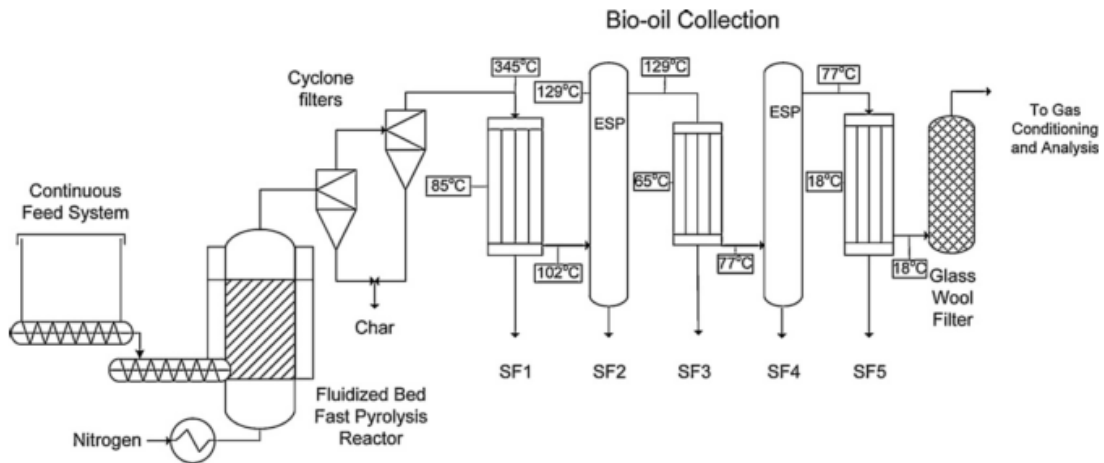


Figure 10: Fast pyrolysis unit coupled with fractionating bio-oil recovery system [31]

Fast pyrolysis product distribution

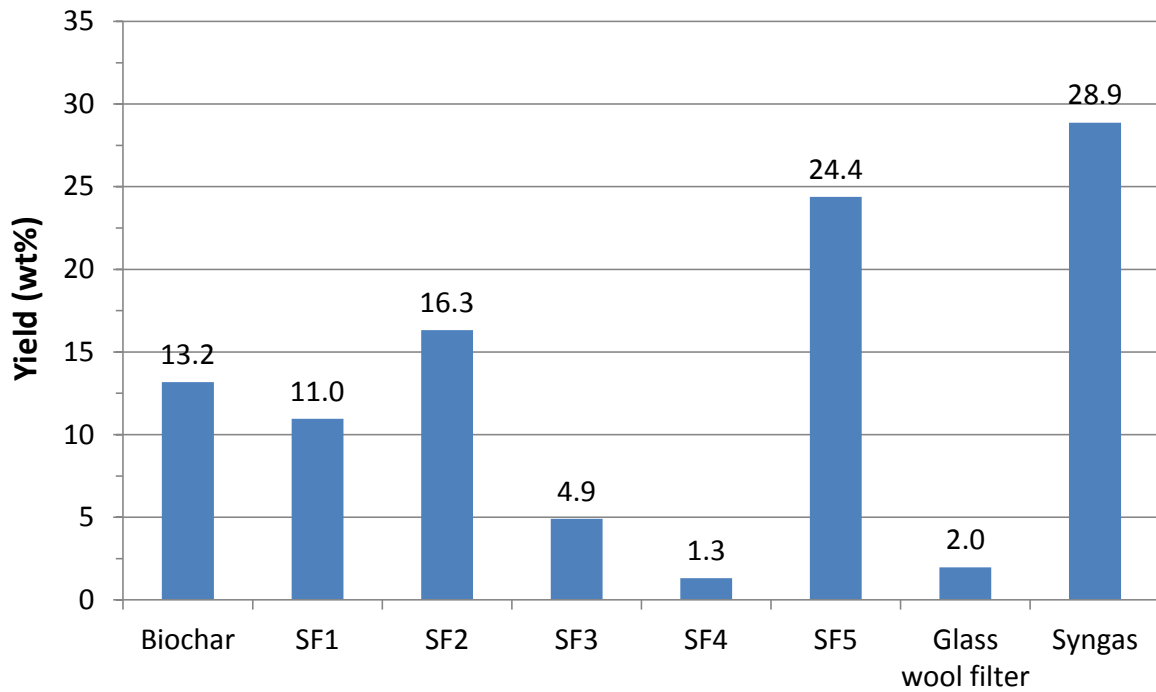


Figure 11: Product distribution from fast pyrolysis unit shown in Figure 10

3.3.2 Separation of sugars and phenolic oligomers

As discussed in the previous section, the first two bio-oil stage fractions are rich in sugars and phenolic oligomers that are respectively derived from the carbohydrate and lignin portions of biomass. As demonstrated by Rover et al. [24], the sugar fraction of bio-oil can be separated from the lignin fraction via a simple water washing procedure. Since most of the sugars present in bio-oil are water soluble, they can be recovered by mixing equal mass portions of bio-oil from stage fractions 1 and 2 with water, which dissolves the sugars into the water.

A KitchenAid 5 quart stand mixer was used to agitate the bio-oil-water mixture. In order to combine the first two stage fractions, approximately 0.5 liters of both stage fraction 1 and 2 were mixed with a corresponding amount of deionized water (DI) on a mass basis. The mixture was agitated using a flat beater at the lowest speed setting available on the mixer. A plastic bag was fastened between the mixer head and the 5 quart bowl in order to contain the bio-oil-water mixture inside the mixer bowl during agitation. After a half hour of mixing, the top sugar-rich phase was poured off into a 1 L Nalgene bottle. The bottom phenolic oligomer rich phase was then poured into a separate 1L Nalgene bottle.

The sugar solution contains up to 93 wt% of the sugars recovered in stage fractions 1 and 2. These high value sugars can be fermented or catalytically upgraded to biofuels [33]. The insoluble fraction (raffinate) remaining is mostly oligomers derived from the lignin fraction of the biomass. Known as clean phenolic oligomers (CPO), this material is less viscous and sticky than the original bio-oil stage fractions [24]. These properties make CPO a desirable candidate for binding coal particles together.

Due to the nature of the mixing process, some moisture was trapped in the CPO fraction after decanting the sugar-rich phase. In order to remove as much moisture as possible, the CPO fraction was centrifuged for 1 hour, at 17,000 rpm in an Avanti high performance centrifuge, model J-26 XPI. After centrifugation, the CPO had an average moisture content of 16.04 ± 1.90 wt%. Both the bio-oil and CPO were refrigerated between use.



Figure 12: The phenolic oligomer fraction of bio-oil (CPO)

3.3.3 Preparation of coal

High volatile C bituminous coal was obtained from the Iowa State University power plant. It is originally sourced from coal mines in western Kentucky and Southern Illinois. The coal is transported via barge up the Mississippi river to Muscatine, IA. From there, it is trucked to the Iowa State power plant. The coal was collected into 5 gallon buckets from random locations in the Iowa State power plant coal pile. In order to minimize error, the coal was separated into 32 separate samples via a riffle type sample splitter (see Figure 13).

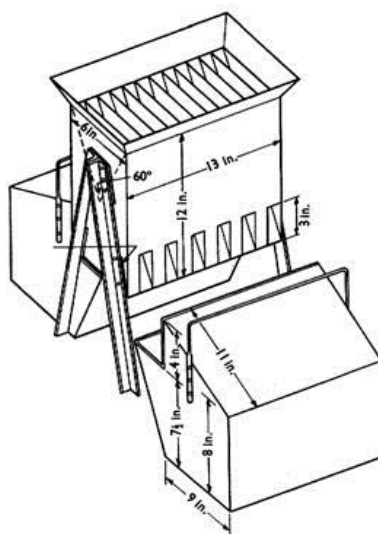


Figure 13: Riffle type sample splitter [34]

After sample division, the coal was ground to correspond with the coal particle size factor levels shown in Table 3. In order to achieve the required factor level, the coal was sent through the combination of a jaw crusher, roll mill, pulverizer, and sieve (see Table 5). The coal grinding equipment is located in Sweeny Hall at Iowa State University. For example, coal for the center point factor level was passed through a jaw crusher, roll mill, and then through a sieve with 2.36 mm openings. In order to simulate coal fines, factor level $-\alpha$ coal was additionally ball milled for 1 to achieve a particle size as small as possible. The Mikro-Pulverizer was fitted with a 1/8 inch screen, and was manufactured by Hosokawa Micron Powder Systems.

Table 5: Coal size reduction parameters

Factor Level	Targeted Coal Mean Particle Size (μm)	Jaw					Sieve Size
		Crusher	Roll Mill	Pulverizer	Ball Mill		
+ α	2298	x	--	--	--	6.3 mm	
+1	1923	x	x	--	--	4.75 mm	
0	1081	x	x	--	--	2.36 mm	
-1	174	x	x	x	--	--	
$-\alpha$	114	x	x	x	x	--	

After size reduction was completed, the respective coal distributions were sieved in order to quantify the mean coal particle size, see Appendix B. Coal samples were stored in Ziploc bags between use.

3.3.4 Pelletization of coal using clean phenolic oligomers as binder

Centrifuged CPO was preheated to 80 °C in order to insure sufficient fluidity for mixing with coal. The moisture content was determined using an Ohaus MB25 moisture analyzer. Depending on the desired moisture content, the coal was then either dried in a gravity convection furnace, or supplemented with DI water. A KitchenAid 5 quart stand mixer with flat beater attachment was used to mix the hot CPO and coal. The mixture was agitated for approximately one minute. A custom designed pellet mold (Figure 14) was filled with 30 g of the coal-CPO mixture to yield approximately a 1" diameter by 2" height pellet.



Figure 14: (left) coal-CPO mixture, (right) pellet mold filled with coal-CPO mixture

After filling four molds, the mixture was compressed into pellets using the setup in Figure 16. An Enerpac 10 ton manual hydraulic press (10000 psi maximum) fitted with an Omega digital pressure gauge was used for the pelletization procedure. The mixture in each mold was compressed to a hydraulic line pressure of 2000 psi, or 8000 psi total when compressing four molds simultaneously. After one minute at 8000 psi, the pressure was released, the baseplate was opened, and the pellets were pushed out the bottom (see Figure 15). The pelletization procedure was conducted at ambient temperatures. Between each batch of four molds, the coal-CPO mixture was kept in a gravity convection oven at 80°C.

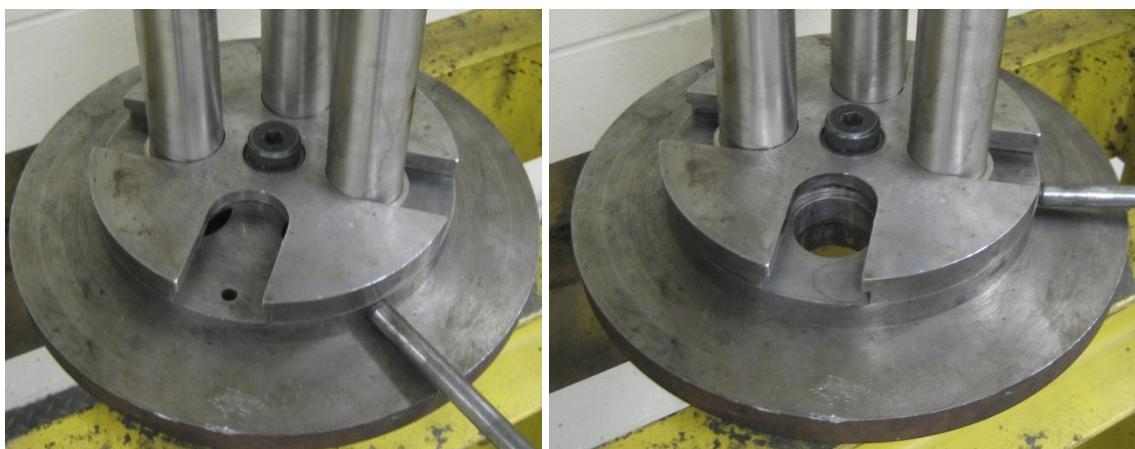


Figure 15: Mold baseplate closed (left), and open (right)



Figure 16: Pellet press setup

After all of the pellets were produced for a particular experiment, they were heat cured in a gravity convection oven at the temperature specified in Table 3. The cure time was fixed at 15 minutes. Following the cure treatment, the pellets were stored in sealed Ziploc bags until needed for analysis.

3.4 Analysis of products

A broad range of analysis techniques were used to study properties of the pellets produced from the 31 experiment RSM. The red oak feedstock, biochar, non-condensable gases, CPO, and coal were analyzed to allow for comparison with the pellets. Analysis procedures will be discussed in the following sections. Unless otherwise noted, all tests were performed in triplicate. The ultimate analysis, proximate analysis, higher heating value, and particle density tests were conducted at the Biorenewable Resources Laboratory. Unless otherwise noted, all other tests were conducted at the BioCentury Research Farm.

Higher heating value. A Parr oxygen bomb calorimeter, model 6400, was used to determine the heating value of the pellets. ASTM D5865 was the standard test method used. This calorimeter has a repeatability of $\pm 0.10\%$. From this point forward, the term “heating value” will be used in place of “higher heating value” unless otherwise indicated.

Proximate analysis. A Mettler Toledo thermo-gravimetric analysis (TGA/DSC 1) was used to analyze the moisture, volatiles, fixed carbon, and ash content of the pellets. ASTM D7582 was referenced for the method; the sample size ranged from 90-150 mg. The precision of the balance used to weigh the sample inside the TGA is $\pm 10 \mu\text{g}$.

Ultimate analysis. For this analysis, a Leco TruSpec CHN and TruSpec S analyzer were used to measure the carbon, hydrogen, nitrogen and sulfur content of a sample. For high carbon samples, such as the pellets, coal, and biochar, ASTM D5373 was used to determine the carbon, hydrogen and nitrogen content, while ASTM D4239 was used to determine the sulfur content. For lower carbon samples, such as the red oak and CPO, ASTM D5291 was used to determine the carbon, hydrogen and nitrogen content, while ASTM D1552 was used to determine the sulfur content. Weight percent oxygen for each sample was determined by subtracting the weight percentages of carbon, hydrogen, nitrogen, sulfur, and ash from 100 percent. The precision of this instrument is shown in Table 6 for each element. RSD and ppm stand for relative standard deviation and parts per million, respectively. For carbon, hydrogen, and nitrogen, either the ppm or RSD error can be used. For sulfur, the error that is the largest should be chosen.

Table 6: Precision of Leco CHNS analyzer

Element	Precision	
	ppm	RSD
Carbon	25	0.5%
Hydrogen	100	1.0%
Nitrogen	40	0.5%
Sulfur	5	<1%

Indirect tensile strength. Indirect tensile strength is a measure of the force a sample can handle before deformation occurs. An Enerpac 10 ton manual hydraulic press equipped

with an Omega digital pressure gauge was used to measure indirect tensile strength. For this test, a pellet was set on its side between a base plate and the hydraulic cylinder piston. The side placement allowed for the pellet to be tested in its weakest orientation. Once the pellet was in place, the hydraulic pump handle was depressed one full stroke. The maximum force experienced by the digital pressure gauge was recorded as the indirect tensile strength.



Figure 17: Indirect tensile strength test before (left) and after (right)

Impact resistance. Impact resistance is a measure of a sample's ability to withstand an impact. Referencing ASTM D440 (Drop Shatter Test for Coal), three separate pellets were dropped from a height of 6 feet onto a hard steel slab. Each pellet was repeatedly dropped until it fractured into pieces that each weighed less than half the original mass of the pellet. The impact resistance index (IRI) was calculated using Equation 2.

$$\text{IRI} = \frac{\text{Number of Drops}}{\text{Number of Fractured Pieces}} \times 100 \quad \text{Equation 2}$$

Abrasion resistance. Abrasion resistance, or durability, simulates coal handling equipment by determining how many fines are produced after tumbling a product in a rotating drum for a given length of time. Referencing ASTM D441 (Tumbler Test for Coal) and ASAE S269.2 (Durability for Cubes, Pellets, & Crumbles), 10 pellets from each experiment were rotated for 25 minutes in a 7" diameter by 8" length steel jar equipped with lifter shelves, see Figure 18. After the tumbling was completed, the remaining pellets were

passed through a sieve with 19 mm openings. The abrasion resistance was calculated using Equation 3. Since each abrasion test required 10 pellets, the test was performed once per experiment.

$$\text{Abrasion Resistance} = \frac{\text{Mass of Pellets after Tumbling}}{\text{Mass of Pellets before Tumbling}} \times 100 \quad \text{Equation 3}$$



Figure 18: Abrasion test apparatus

Mass density. For each experiment, the mass density of three random pellets was determined by measuring the mass and height of each pellet. The mass was measured with a Mettler Toledo ML4002E precision balance. A digital caliper was used to measure the height. The diameter of each pellet was assumed to be one inch unless otherwise noted.

Particle density. In contrast with mass density, the particle density excludes the void spaces between particles in a sample. A Quantachrome Instruments gas pycnometer was used to determine the particle density of three pellets per experimental run. The pycnometer operates on the basis of Boyle's law. After a sample is inserted into a cell of known volume, the pycnometer uses a reference volume and the pressure difference between the reference and sample cells to determine the sample volume. The particle density is then calculated using the sample volume and a user specified mass. The repeatability of this instrument is $< \pm 0.01\%$ for the 135 cm^3 sample cells.

Bulk density. Bulk density for both the pellets and the coal was measured. A sufficient quantity of sample was inserted into a glass beaker and the volume was recorded. The mass was recorded as the gross weight of sample with beaker minus the weight of the beaker.

Ash fusibility. Ash fusibility is a measure of the tendency of ash to melt at various temperatures. Since this test could not be completed in house, samples of both coal and pellets were sent to Standard Laboratories for analysis.

CHAPTER 4. RESULTS AND DISCUSSION

Statistical models were fit to the data collected using the analysis techniques discussed in Section 3.4. Only the statistically significant models will be discussed in this chapter; all of the fitted models are listed in Appendix C. Excerpts from the experimental data and from literature are presented alongside the statistical models when appropriate.

4.1 Higher heating value

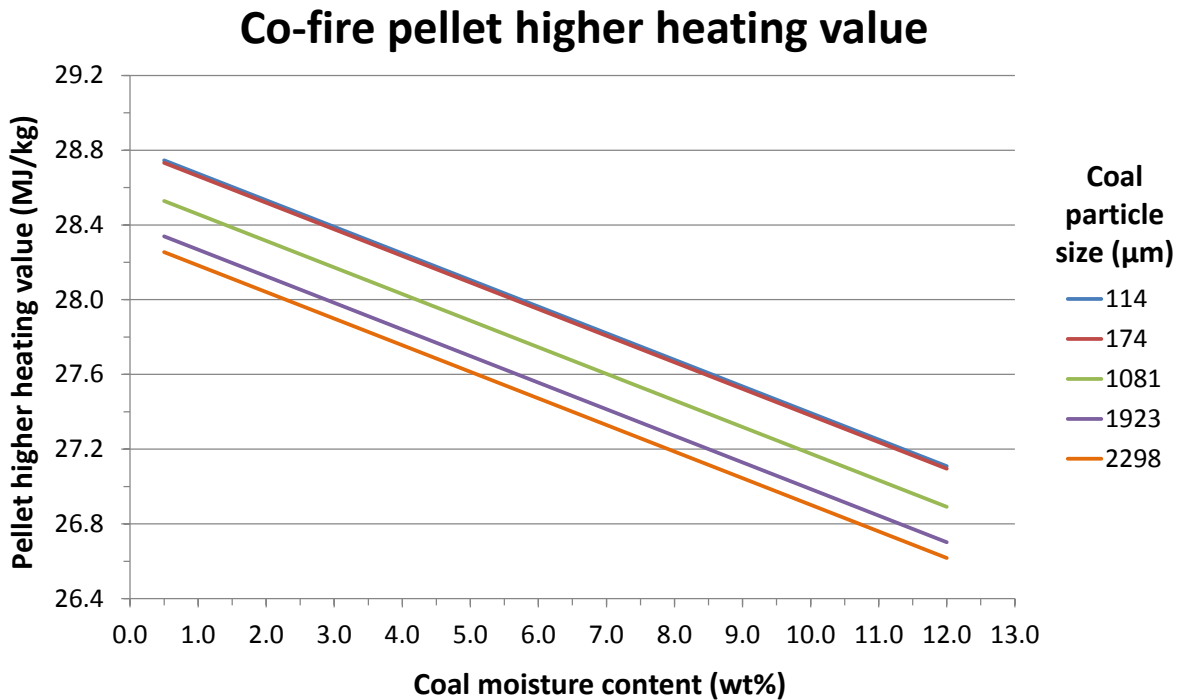
A full RSM model was fit to the pellet heating value data to yield an R^2 value of 0.83. The reduced model had an R^2 value of 0.77 and a statistically significant p-value less than 0.0001. Terms which were statistically significant in the reduced model are shaded in Table 7. The non-significant terms shown were included since they increased the accuracy of the reduced model.

Table 7: Pellet heating value reduced model summary

Term	Coefficient	P-value	Significance
Intercept (β_0)	28.587	<.0001	YES
Particle (x_1)	-2.250E-04	0.005	YES
Moisture (x_2)	-1.424E-01	<.0001	YES
Binder (x_3)	2.571E-02	0.393	NO
Cure (x_4)	1.870E-03	0.807	NO
Binder x Cure (x_3x_4)	-4.100E-04	0.091	NO
Cure x Cure (x_4x_4)	4.134E-05	0.057	NO

After the reduced model was developed, the predicted data was plotted to determine the effect of the experimental factors on the heating value response. Besides the intercept, coal moisture content (x_2) was the most significant term (p-value <0.0001) and is plotted against coal particle size (x_1) in Figure 19. This graph suggests that the heating value of the pellets increases as the coal moisture content decreases. Since the pellets were produced on a mass basis, lower coal moisture contents increase the amount of combustible material in the pellets, thereby increasing the heating value. It should be noted that the higher heating value (HHV) by definition negates the influence of moisture (enthalpy of vaporization) in a sample

by cooling the combustion products to a liquid state. If the enthalpy of water vaporization is included in the equation, then the lower heating value (LHV) results. In this case, all of the samples were tested using the HHV method, so the effect of coal moisture on heating value is valid. In addition to the effect of coal moisture, increasing coal particle sizes appear to lower the heating value of a pellet. This result would be expected if the bomb calorimeter did not completely burn the larger coal particles. However, the bomb calorimeter completely burned all samples, regardless of particle size. With respect to calorimeter precision, only the steps between the center point particle size of 1081 μm and the 174/1923 μm sizes are significant.

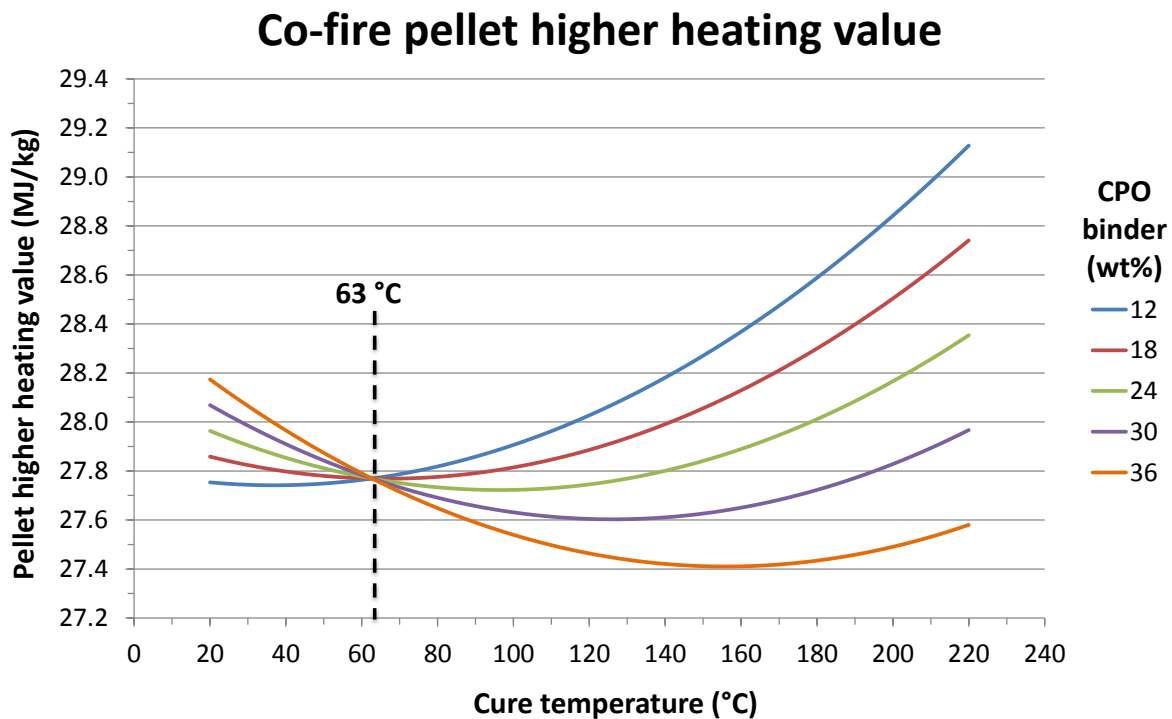


Fixed conditions: CPO binder fraction at 24 wt %, cure temperature at 120°C

Figure 19: Modeled pellet higher heating value with respect to coal moisture content and coal particle size

Due to the “cure x binder” interaction term, the effect of cure temperature on heating value depends largely on the CPO binder fraction. Figure 20 suggests that this effect revolves around a critical cure temperature of 63°C. Below that temperature, the steps between binder fractions are within calorimeter precision. In addition, experimental data below 70°C is based on only one axial experiment at 20°C. Therefore, conclusions drawn from the model below 63°C are considered insignificant. In contrast, inferences drawn above 63°C are valid.

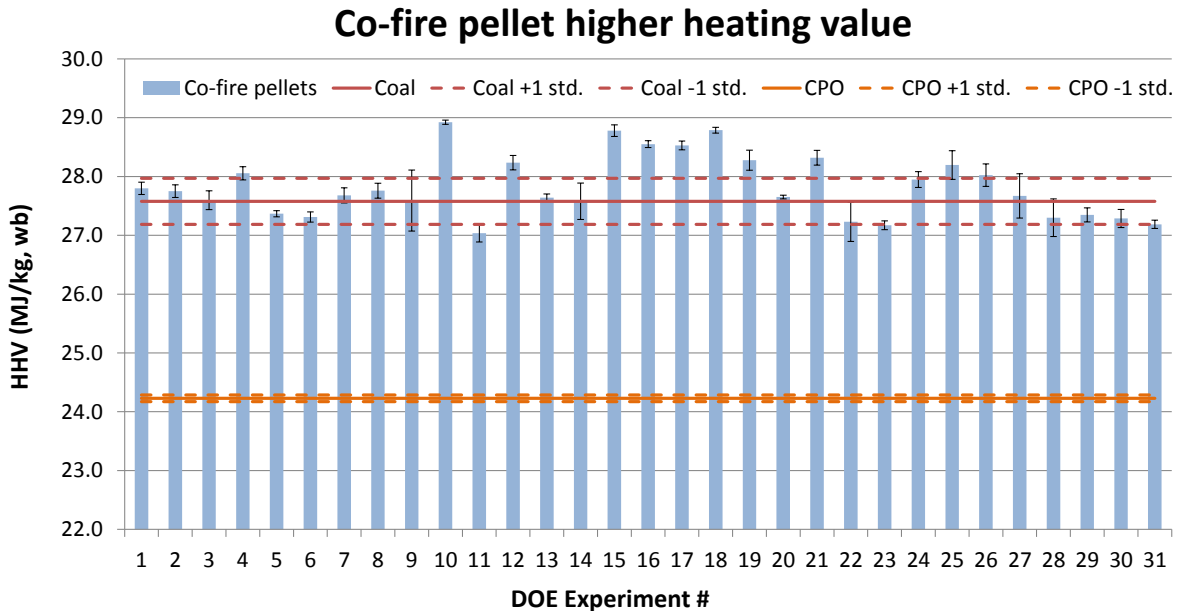
Here the heating value increases with higher cure temperatures, with the exception of the highest CPO fraction (36 wt%). This increase in heating value can possibly be attributed to a loss of moisture in the pellets at higher cure temperatures, as will be discussed in Section 4.2.1. In addition to cure temperature, larger CPO binder fractions appear to decrease the heating value. This effect is expected since the CPO has a lower higher heating value than the coal, 24.2 vs. 27.6 MJ/kg, respectively.



Fixed conditions: coal particle size at 1081 μm , coal moisture content at 6 wt%

Figure 20: Modeled pellet higher heating value with respect to cure temperature and CPO binder fraction

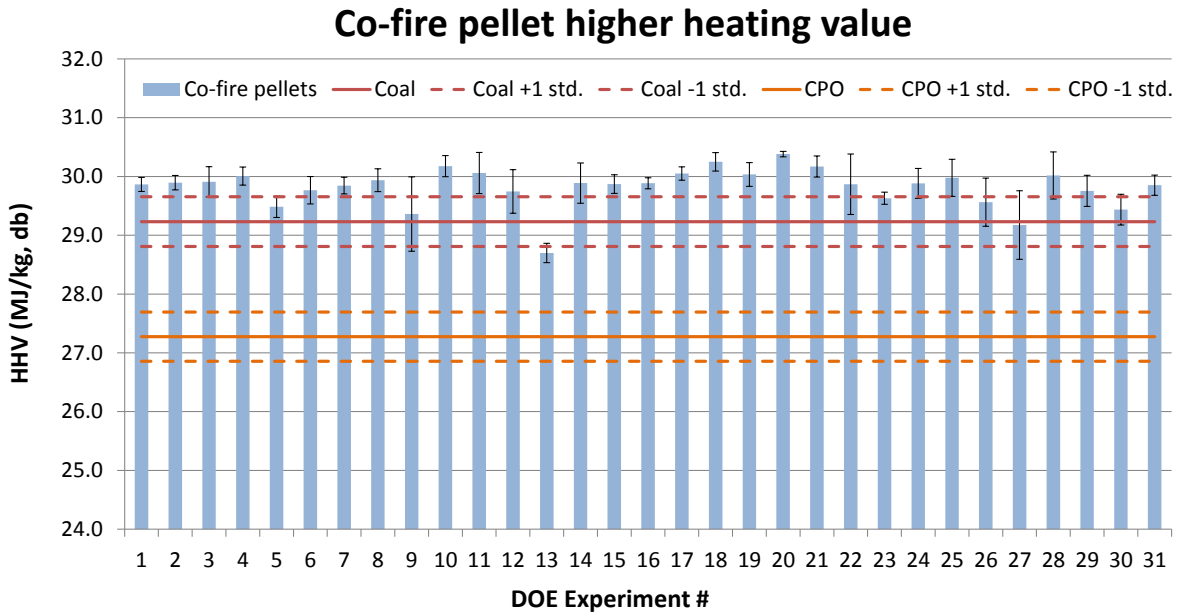
The experimental heating value data exhibits an interesting phenomenon. As shown in Figure 21, the pellet heating values (blue bars) congregate around the heating value of the coal (solid red line). In fact, a few of the pellet heating values even surpass the first standard deviation of the coal (dashed red line). Since each pellet is a mixture of coal and CPO which have differing heating values, the resulting pellet heating value should lie between those two heating values. As shown in the Figure 21, the experimental results indicate otherwise.



Note: Solid horizontal red and orange lines correspond with the average coal and CPO higher heating values, the corresponding horizontal dashed lines represent the 1st standard deviation

Figure 21: Pellet higher heating values on a wet basis sorted by experiment number

In order to further investigate the pellet heating value phenomenon on a consistent basis, the pellet, coal, and CPO heating values were converted to a dry basis using ASTM D3180, and are shown in Figure 22. The moisture value used in the ASTM calculation for the pellets includes contributions from both the coal and CPO, as measured by a thermogravimetric analyzer. After dry basis conversion, the heating values appear more uniform across the spread of experiments. In addition, a greater number of pellet heating values exceed the heating value of the coal. This effect echoes an earlier conclusion that the heating value of a pellet increases as the coal moisture content decreases (Figure 19).



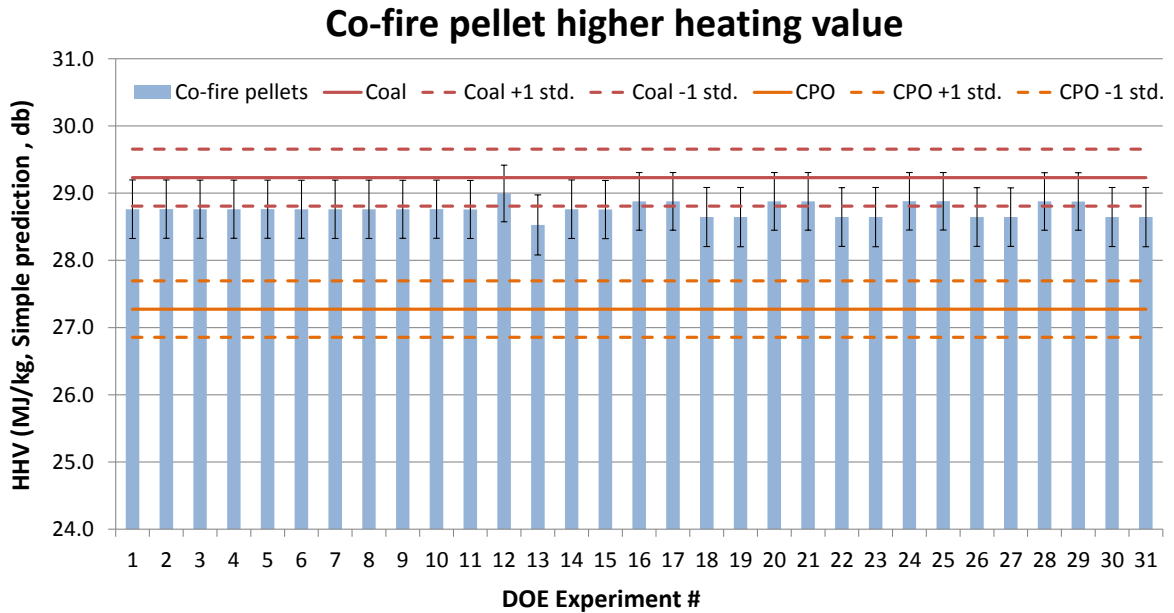
Note: Solid horizontal red and orange lines correspond with the average coal and CPO higher heating values, the corresponding horizontal dashed lines represent the 1st standard deviation

Figure 22: Pellet higher heating values on an ASTM dry basis sorted by experiment number

In addition to analyzing the pellet heating values on a dry basis, a predicted pellet heating value was calculated using Equation 4. In this equation, the heating value (dry basis) of the CPO and coal is multiplied by the respective mass fractions of the coal and CPO in the pellet and then added together to yield a “simple” predicted higher heating value.

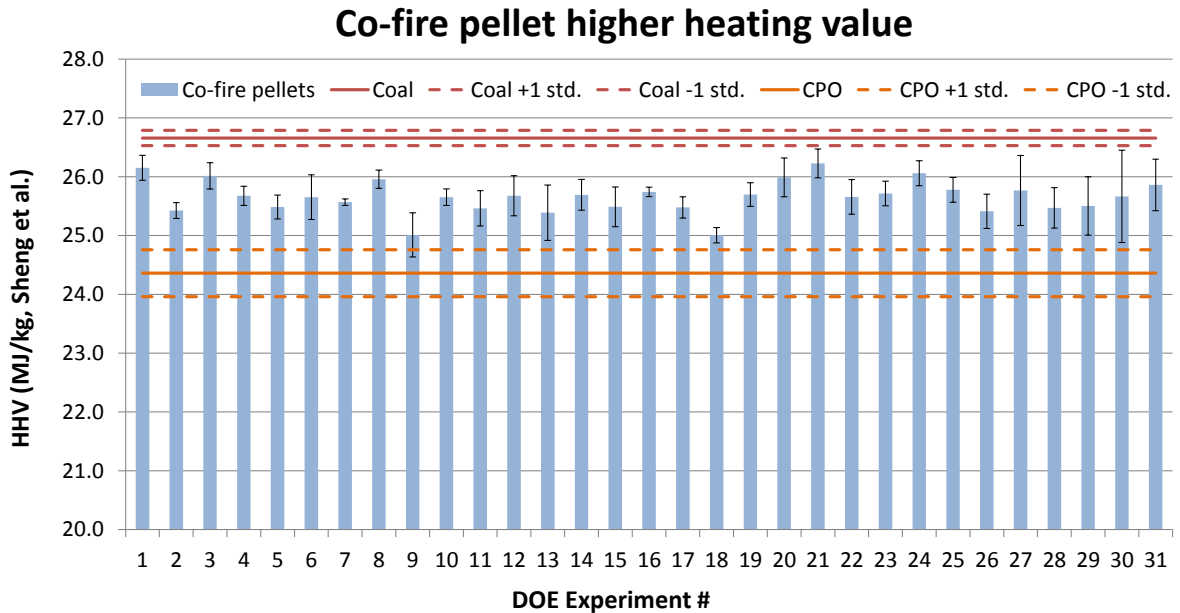
$$HHV_{Pellet} = Fraction_{CPO} \times HHV_{CPO} + Fraction_{Coal} \times HHV_{Coal} \quad \text{Equation 4}$$

The simple predicted pellet higher heating values shown in Figure 23 are expected. Even though the pellet HHV error bars cross the coal heating value for a few of the experiments, the pellet heating values do not exceed the first standard deviation of the coal, as is seen in Figure 22.



Note: Solid horizontal red and orange lines correspond with the average coal and CPO higher heating values, the corresponding horizontal dashed lines represent the 1st standard deviation

Figure 23: Predicted pellet higher heating values



Note: Solid horizontal red and orange lines correspond with the average coal and CPO higher heating values, the corresponding horizontal dashed lines represent the 1st standard deviation

Figure 24: Pellet higher heating values predicted by the correlation developed by Sheng et al. [35]

In addition to the simple prediction, a correlation developed by Sheng et al. was utilized to predict pellet heating values [35]. They note that a heating value correlation based on the ultimate analysis (dry basis) of a fuel is the most accurate approach. The equation developed by Sheng et al. is shown in Equation 5 where C, H, O correspond with the respective elemental carbon, hydrogen, and oxygen contents of the pellets on a dry basis. While the Sheng et al. correlation was developed for biomass fuels, its use in predicting the heating value of coal appears to be more accurate than dedicated coal correlations surveyed by Majumder et al. [36]. Therefore, it can be correctly used to predict the heating value of the pellets.

$$HHV = -1.3675 + 0.3137C + 0.7009H + 0.0318O \quad \text{Equation 5}$$

The predicted higher heating values for the pellets, coal and CPO are shown in Figure 24. Similar to Figure 23, the heating values of the pellets land almost exactly between the heating values of the coal and CPO, as expected. Therefore, the predicted heating values of the pellets from both the simple correlation and the Sheng et al. correlation are lower than the values determined with the bomb calorimeter. Since simple manipulations of the heating value data did not yield any concrete conclusions, additional analytical tests were subsequently performed to investigate the pellet heating value abnormality.

A Fourier transform infrared spectrometer (FTIR) is used to identify chemical bonds in a sample by associating them with a specific infrared wavelength. After the bonds are identified, they can be used to estimate what types of chemical compounds are present. In this case, the pellets, coal, and CPO were analyzed to determine if any newly formed compounds were present in the pellets that were not detected in the coal or CPO. These new compounds could possibly account for the additional bond energies needed to achieve the higher than predicted heating values seen in the pellets. However, this hypothesis was invalidated as no other peaks (compounds) were present in the pellets other than those that were also identified in the coal and CPO (Figure 25). Literature was surveyed to help identify the peaks [37–43]. Suggested compounds for each of the major peaks are shown in the figure.

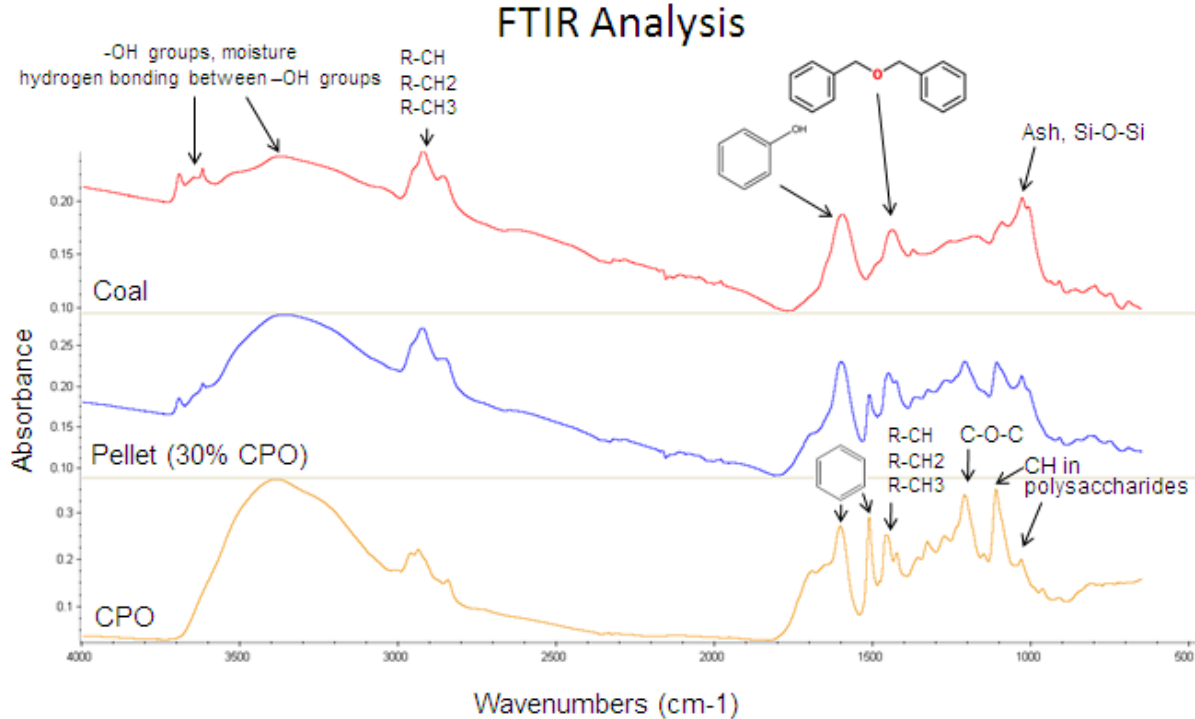
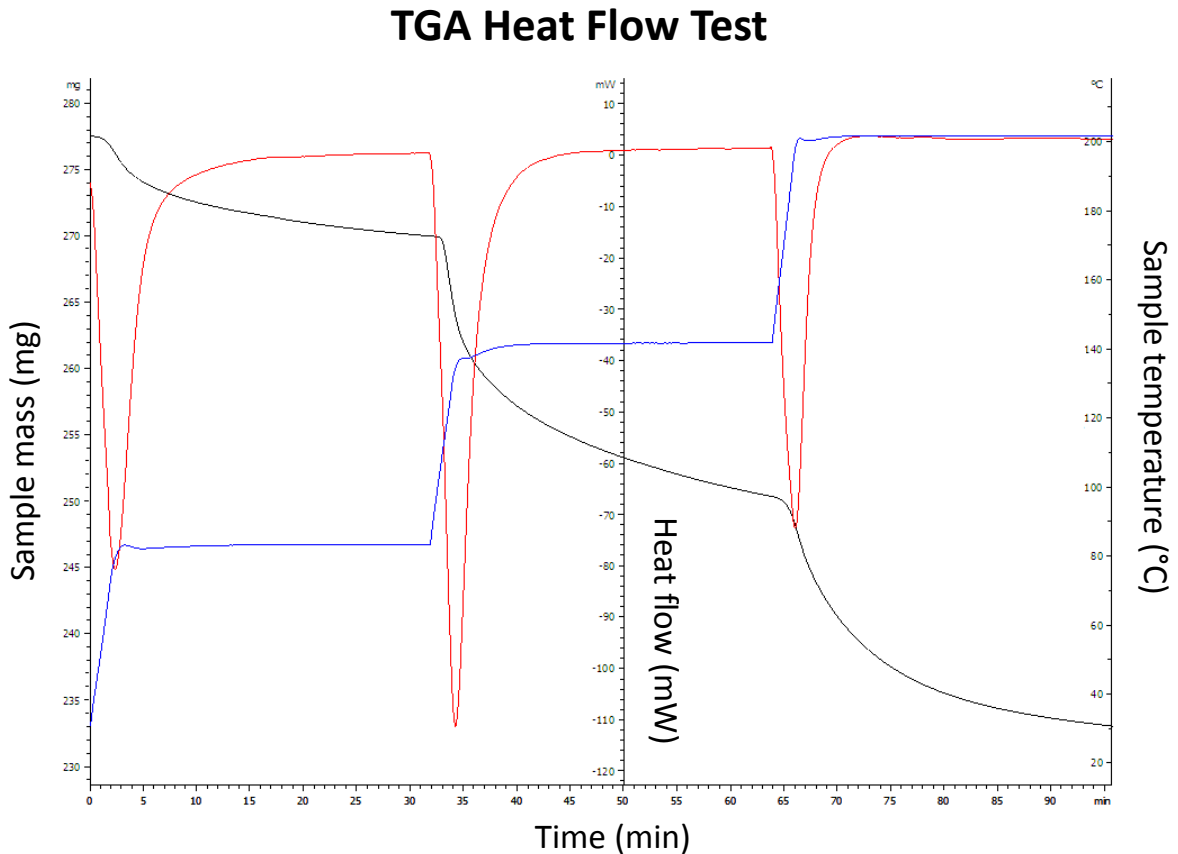


Figure 25: FTIR analysis of the coal, pellets, and CPO

In addition to the FTIR analysis, a heat flow test was conducted using a TGA equipped with a differential scanning calorimeter (DSC). The DSC could detect if any endothermic reactions were taking place during the mixing of the hot CPO (80°C) and ambient temperature coal prior to pelletization. If endothermic reactions were evident, then they could explain the higher than predicted heating values experienced by the pellets. In order to test this hypothesis, cold CPO and coal were mixed together and then inserted into the TGA. As shown in Figure 26, the CPO-coal mixture did not experience any additional heat flow (red line) other than that which was required to bring the mixture to the tested temperatures of 80, 140, and 200°C (blue line). Each of the “dips” in the heat flow correspond with the heat required to bring the mixture up to each of the tested temperatures. Other than those “dips”, no other heat flow events were recorded. Therefore, it was concluded that no endothermic reactions were taking place during the mixing of the hot CPO and ambient temperature coal. With regard to the sample mass (black line) in Figure 27, it is evident that the mass decreases throughout the test. Similar to the conclusion for the heating

value model, this loss of mass can be attributed to a drying out of the coal, and also a loss of volatiles at the higher test temperatures.



Note: Black, red, & blue lines correspond with sample mass, heat flow, and temperature, respectively. Positive heat flow is exothermic.

Figure 26: Heat flow test of a coal - CPO mixture using a thermogravimetric analyzer

A few conclusions can be drawn from the pellet heating value analysis. In contrast to raw biomass, the co-fire pellets have approximately the same heating value as the parent coal. This feature allows utilities to burn the pellets without a loss in boiler capacity. On a theoretical basis, a high pellet HHV can be theoretically achieved through the combination of low moisture coal and CPO, small coal particles, and low CPO binder fractions. A curing treatment is not necessary since it appears to only remove moisture from the pellets. As discussed, the pellets achieved a higher HHV than predicted by both the simple correlation and the Sheng et al. correlation. Analytical tests were performed to determine the

mechanisms that could possibly account for this irregularity. No concrete conclusions have been made at this point. It is recommended that this heating value phenomenon be explored in the future since any further investigation on this topic is out of the scope of this thesis.

4.2 Proximate analysis

4.2.1 Moisture

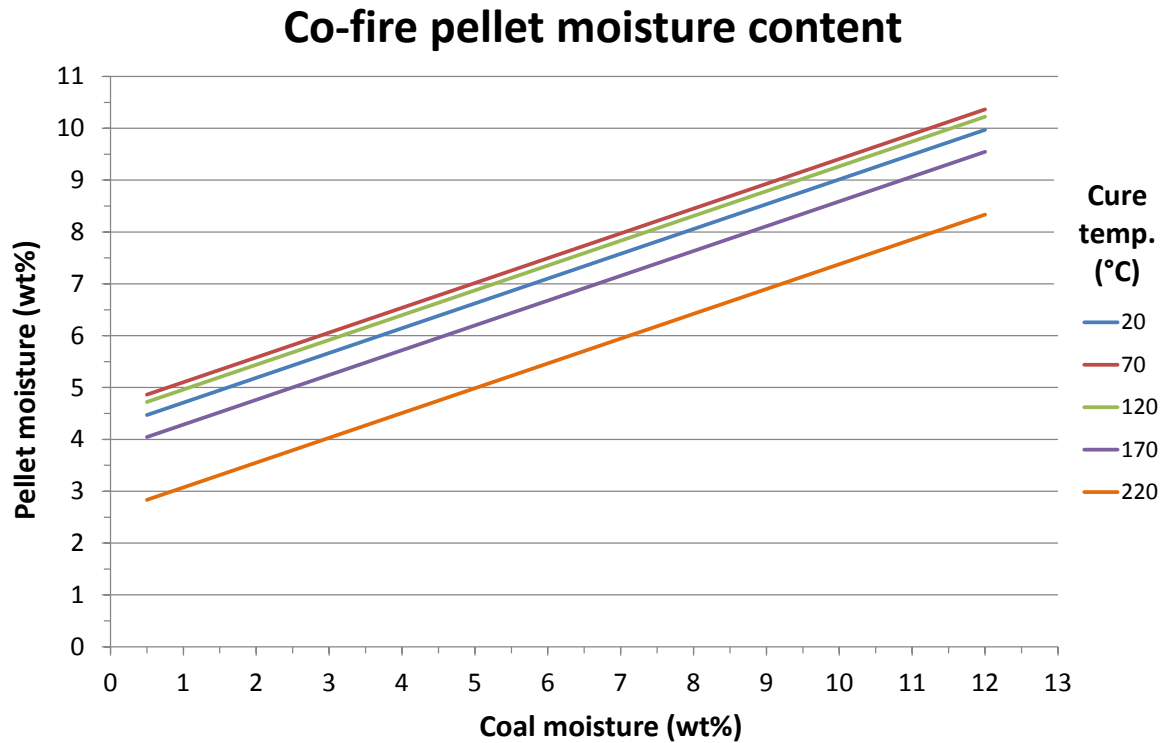
The full RSM model for co-fire pellet moisture was statistically significant with an R^2 value of 0.82. The reduced model was also statistically significant with an R^2 value of 0.80 and a p-value of less than 0.0001. Terms which were statistically significant in the reduced model are shaded in Table 8. The non-significant terms shown were included since they increased the accuracy of the reduced model. Coal moisture content (x_2) was the most significant term in the model with a p-value less than 0.0001. CPO binder fraction (x_3) was also a significant term with a p-value of 0.008. Both of these terms are expected to be significant since moisture in the pellets can theoretically only be derived from the coal and CPO.

Table 8: Pellet moisture content reduced model summary

Term	Coefficient	P-value	Significance
Intercept (β_0)	-3.630	0.3417	NO
Particle (x_1)	1.881E-03	0.085	NO
Moisture (x_2)	4.783E-01	<.0001	YES
Binder (x_3)	7.050E-01	0.008	YES
Cure (x_4)	-1.160E-02	0.635	NO
Particle x Binder (x_1x_3)	-7.400E-05	0.095	NO
Binder x Cure (x_3x_4)	1.213E-03	0.116	NO
Binder x Binder (x_3x_3)	-1.646E-02	0.002	YES
Cure x Cure (x_4x_4)	-1.070E-04	0.118	NO

As Figure 27 suggests, pellet moisture content is proportional to coal moisture content. That is, as the coal moisture content increases, the pellet moisture content increases as well. In fact, the coal moisture content is generally equal to the resulting pellet moisture content, as might be expected since the coal constitutes a large portion of the pellet's mass.

In contrast with coal moisture, increasing cure temperatures appear to decrease the pellet moisture, undoubtedly through the evaporation of water at the higher temperatures. An exception to this observation is the cure temperature of 20°C, which can be disregarded since it is based on only one experiment.



Fixed conditions: coal particle size at 1081 μm , CPO binder fraction at 24 wt%

Figure 27: Modeled pellet moisture content with respect to coal moisture content and cure temperature

Similar to coal moisture, the CPO binder plays a large role in the pellet moisture as indicated by the significant CPO binder first and second order terms. These significant terms are a result of the relatively high CPO moisture content (16.0 wt%) when compared with the coal. In the model, the CPO binder fraction and coal particle size effects appear to revolve around a focal point of 25.4 wt% CPO binder (Figure 28). For binder fractions up to 25.4 wt%, pellet moisture increases with higher binder fractions, as is expected. After 25.4 wt% however, pellet moisture decreases with higher CPO binder fractions. As there is no physical explanation for this effect, the prediction after 25.4 wt% will be attributed to model error.

Coal particle size is not a significant model term, and its influence on pellet moisture will not be discussed.

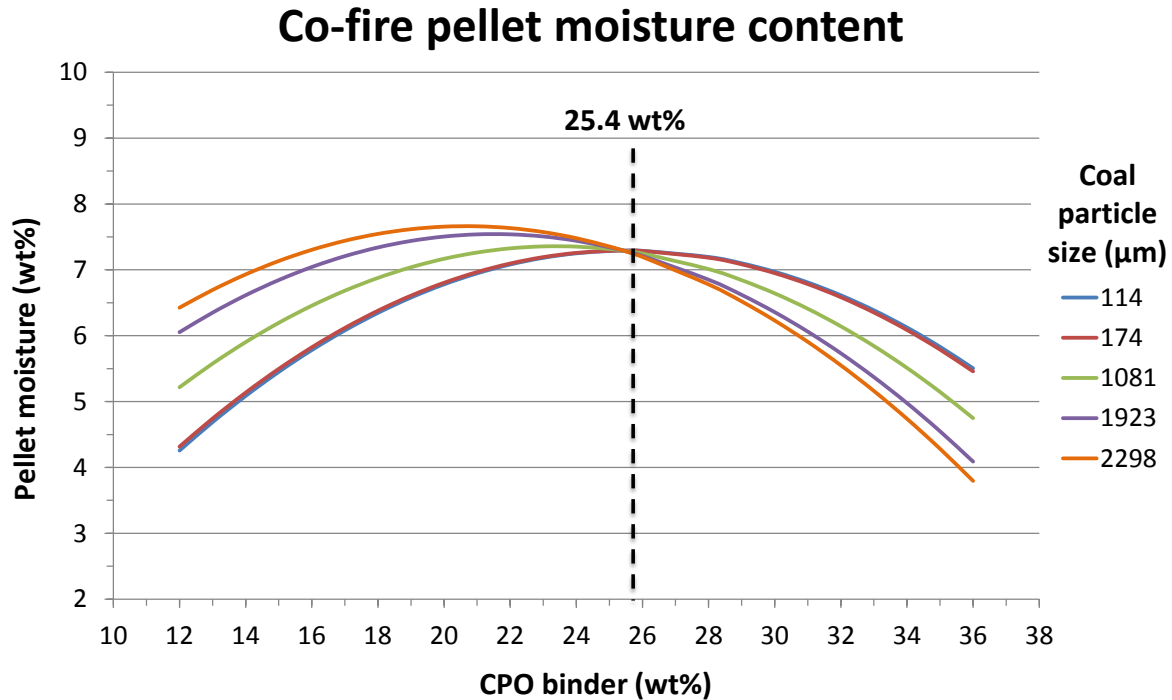


Figure 28: Modeled pellet moisture content with respect to CPO binder fraction and coal particle size

4.2.2 Volatiles

The reduced model for co-fire pellet volatile content was statistically significant with an R^2 value of 0.89 and a p-value of less than 0.0001. The lack-of-fit (LOF) test was also significant with a p-value of 0.0496, which implies that another model might fit the data better. However, the LOF p-value rounds up to the 95% confidence interval limit of 0.05, so the reduced model is assumed to be a good fit. As shown in Table 9, most of the terms were significant in the reduced model. All four of the first order terms have negative coefficients, meaning that they are inversely proportional to volatile content.

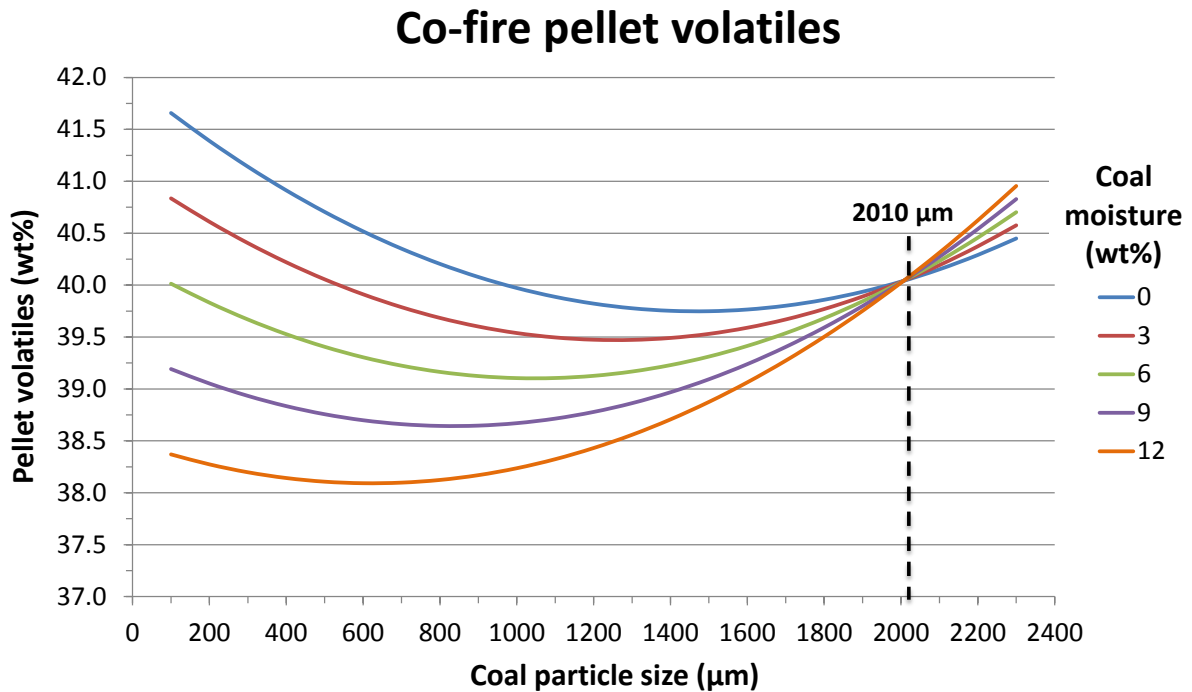
The volatile content reduced model had critical points that were mostly within the experimental design space. Critical points represent the condition at which the first derivative of the statistical model is equal to zero. For the volatile model, the critical points

2006 μm , 1.75 wt%, 11.6 wt%, and 119°C correspond with the coal particle size, coal moisture content, CPO binder fraction, and cure temperature factors, respectively. For this particular combination of critical points, the predicted pellet volatile content is 37.9 wt%.

Table 9: Pellet volatile content reduced model summary

Term	Coefficient	P-value	Significance
Intercept (β_0)	48.317	<.0001	YES
Particle (x_1)	-5.589E-03	<.0001	YES
Moisture (x_2)	-2.884E-01	0.002	YES
Binder (x_3)	-5.448E-01	0.005	YES
Cure (x_4)	-2.439E-02	0.064	NO
Particle x Moisture (x_1x_2)	1.437E-04	0.038	YES
Particle x Binder (x_1x_3)	1.082E-04	0.003	YES
Particle x Particle (x_1x_1)	1.018E-06	0.002	YES
Binder x Binder (x_3x_3)	1.415E-02	0.001	YES
Cure x Cure (x_4x_4)	1.028E-04	0.055	NO

The critical coal particle size is demonstrated in Figure 29. For particle sizes larger than 2010 μm , the volatiles model is considered insignificant since the steps between coal moisture levels are borderline on TGA precision. In addition, the model is prone to error in this region since it is based on one experiment at 2298 μm . Below 2010 μm , the model is significant and its prediction is influenced heavily by the significant particle x moisture interaction term. For lower coal moisture contents, pellet volatiles increase as coal particles decrease in size. This effect slowly changes as the coal moisture content increases to culminate in the prediction that volatiles mostly decrease for decreasing particle sizes at high coal moisture contents. The fact that coal moisture has a significant effect on the volatiles indicates that not all the pellet moisture is being driven off during the first stage of TGA analysis at 105°C. With regard to coal particle size, it is expected that smaller coal particles would increase the pellet volatiles since smaller particles have more surface area by which the coal volatiles can escape.

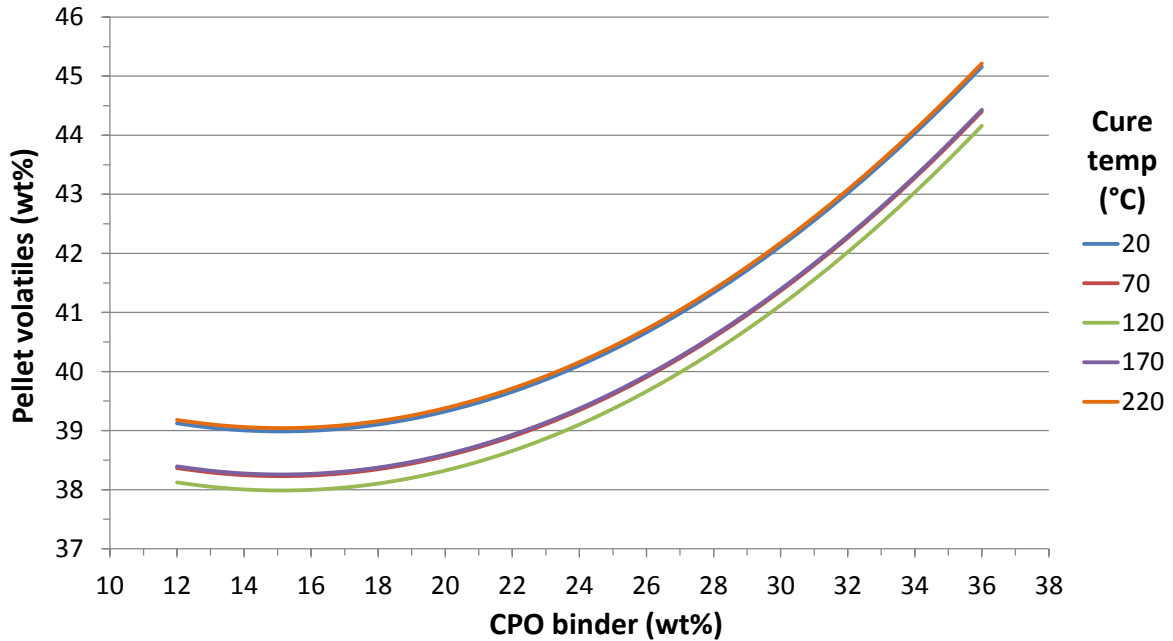


Fixed conditions: CPO binder fraction at 24 wt %, cure temperature at 120°C

Figure 29: Modeled pellet volatile content with respect to coal particle size and coal moisture content

As shown in Figure 30, CPO binder fraction also plays a significant role in pellet volatile content. After the critical binder fraction of 12.5 wt%, pellet volatiles increase steadily as the CPO binder fraction increases. This prediction is realistic since the volatile content of the CPO is twice that of the coal, 65.4 vs. 33.6 wt%, respectively. In contrast with CPO binder fraction, the cure temperature does not have a clear effect on the volatile content. Theoretically, higher cure temperatures should drive off pellet volatiles. This hypothesis is not supported by the model. During pellet production however, higher cure temperatures, especially 220°C, did appear to drive off volatiles since the oven atmosphere was “smoky” after the curing treatment.

Co-fire pellet volatiles



Fixed conditions: coal particle size at 1081 μm , coal moisture content at 6 wt%

Figure 30: Modeled pellet volatile content with respect to CPO binder fraction and cure temperature

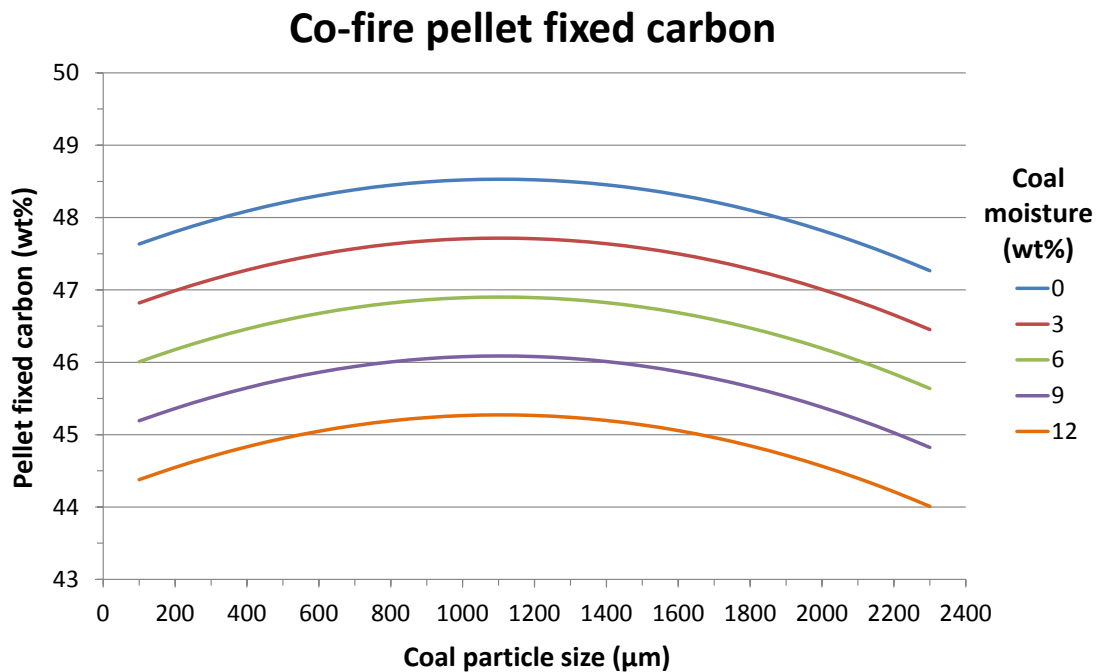
4.2.3 Fixed carbon

The reduced model for co-fire pellet fixed carbon content was statistically significant with an R^2 value of 0.81 and a p-value of less than 0.0001. All the terms were significant in this model. Other than the intercept, coal moisture content (x_2) and CPO binder fraction (x_3) were the most significant terms in the model with p-values less than 0.0001.

Table 10: Pellet fixed carbon content reduced model summary

Term	Coefficient	P-value	Significance
Intercept (β_0)	51.304	<.0001	YES
Particle (x_1)	1.957E-03	0.008	YES
Moisture (x_2)	-2.714E-01	<.0001	YES
Binder (x_3)	-1.931E-01	<.0001	YES
Cure (x_4)	6.483E-03	0.036	YES
Particle x Particle (x_1x_1)	-8.854E-07	0.008	YES

As shown in Figure 31, coal particle size does appear to have a slight impact on fixed carbon yield. This effect is not expected and is attributed to model error. Since central composite designs fit a line to five points, some curvature is expected, even if it is not realistic. In contrast, coal moisture content has a clear impact on the pellet fixed carbon yield. Decreasing coal moisture increases the amount of fixed carbon. If moisture was not driven off prior to the fixed carbon analysis, this effect would be expected since moisture displaces mass in the pellet, and is not a carbonaceous compound. However, the first step in the ASTM standard used in the proximate analysis is to heat the sample to 105°C in a nitrogen environment so that moisture is driven off from the sample. The fact that coal moisture has an impact on fixed carbon means that the pellet moisture is not being driven off completely during the moisture or volatiles stages of the proximate analysis.



Fixed conditions: CPO binder fraction at 24 wt %, cure temperature at 120°C

Figure 31: Modeled pellet fixed carbon content with respect to coal particle size and coal moisture content

CPO binder fraction has a meaningful impact on fixed carbon, as is indicated the large coefficient for the single order term. In Figure 32, increasing CPO fractions directly decrease the pellet fixed carbon content. This prediction is valid since the CPO has a lower

fixed carbon content than the coal, 23.4 versus 51.9 wt%, respectively. Unlike the volatile model, cure temperature has a clear effect on fixed carbon yield, effectively increasing the fixed carbon as cure temperatures increase. One explanation for this prediction is that at higher cure temperatures, CPO in the pellets is polymerizing, and possibly converting the volatiles into fixed carbon. However, this hypothesis is not clearly supported by the volatiles model as the volatiles should decrease for increasing cure temperatures (see Figure 30). In addition, the steps between the cure temperature factor levels are very small, and may be considered meaningless for industrial scale applications.

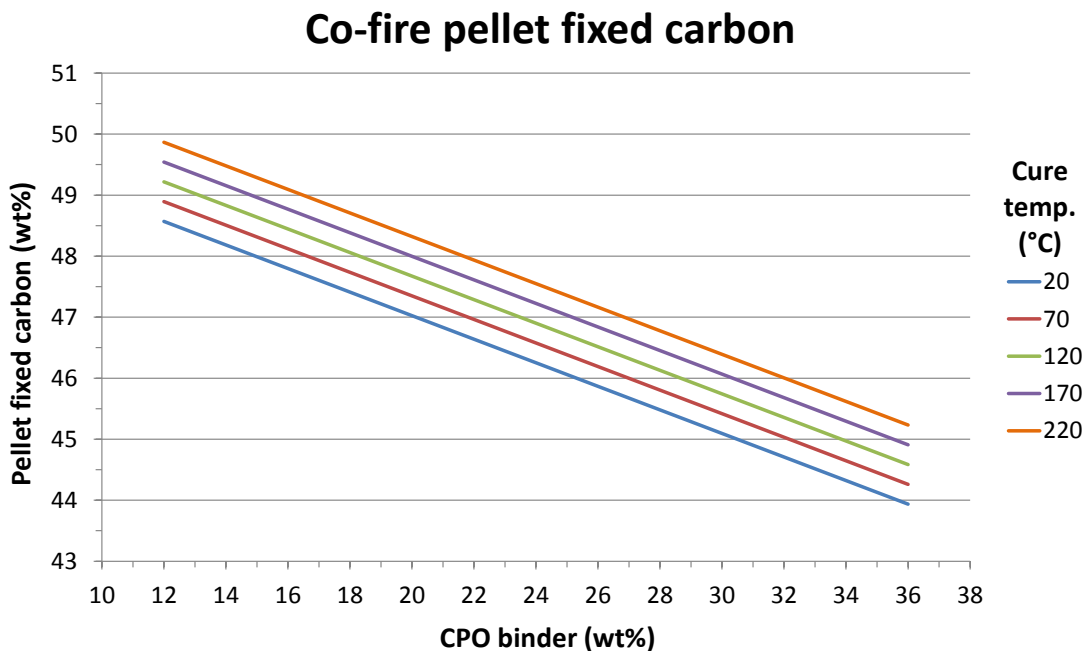


Figure 32: Modeled pellet fixed carbon content with respect to CPO binder fraction and cure temperature.

4.2.4 Ash

The full model for co-fire pellet ash content was not statistically significant, and had a low R^2 value of 0.63 when compared with the previously discussed models. In contrast, the reduced model for ash content was statistically significant with a p-value of 0.0041, and a low R^2 value of 0.60. Since the R^2 value is somewhat low, the reduced model will only be used drawing for general conclusions. Significant terms in the reduced model are shown in

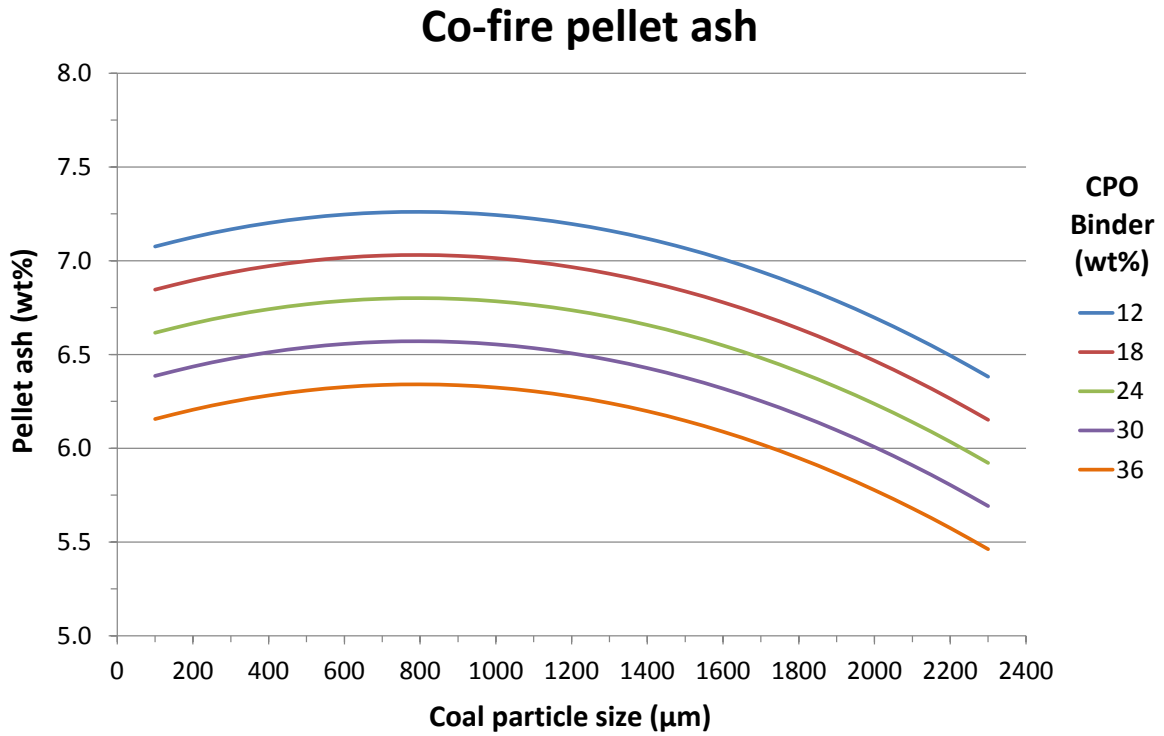
Table 11 as shaded. The non-significant terms shown were included since they increased the accuracy of the reduced model. Other than the intercept, coal particle size (x_1) and CPO binder fraction (x_3) were the most significant terms in the model.

Table 11: Pellet ash content reduced model summary

Term	Coefficient	P-value	Significance
Intercept (β_0)	8.5364	<.0001	YES
Particle (x_1)	1.037E-03	0.030	YES
Moisture (x_2)	-2.621E-01	0.069	NO
Binder (x_3)	-3.833E-02	0.011	YES
Cure (x_4)	-6.167E-03	0.171	NO
Particle x Moisture (x_1x_2)	-7.087E-05	0.079	NO
Moisture x Cure (x_2x_4)	1.267E-03	0.073	NO
Particle x Particle (x_1x_1)	-3.863E-07	0.035	YES
Moisture x Moisture (x_2x_2)	9.532E-03	0.262	NO

The effect of coal particle size and CPO binder fraction can be viewed in Figure 33. Generally, increasing coal particle sizes decrease ash content. This effect is minimal since the average change is ± 0.5 wt%. Ash content is tied closer to coal type and rank rather than particle size. Similarly to coal particle size, increasing CPO binder fractions decrease pellet ash content. This effect, while minimal, is expected due to the low ash content of CPO.

The small changes between factors levels for the ash content are echoed in the experimental data. As shown in Figure 34, ash content is not statistically significant from one CPO binder fraction to the next. The ash content averaged over all 31 experiments was 6.73 ± 0.98 wt%. In contrast, the average ash content of the parent coal was 8.84 ± 1.77 wt% and the ash content for the CPO was 0.05 ± 0.03 wt%. The CPO ash content is approximately zero since almost all of the ash resulting from the pyrolysis process is captured with the biochar. Therefore, any ash present in the pellets is derived from the coal. This is particularly evident in the fact that the averaged pellet ash content is approximately 23.9 wt% less than the coal, which directly corresponds with the center point CPO binder fraction of 24 wt%.



Fixed conditions: coal moisture content at 6 wt%, cure temperature at 120°C

Figure 33: Modeled pellet ash content with respect to coal particle size and CPO binder fraction

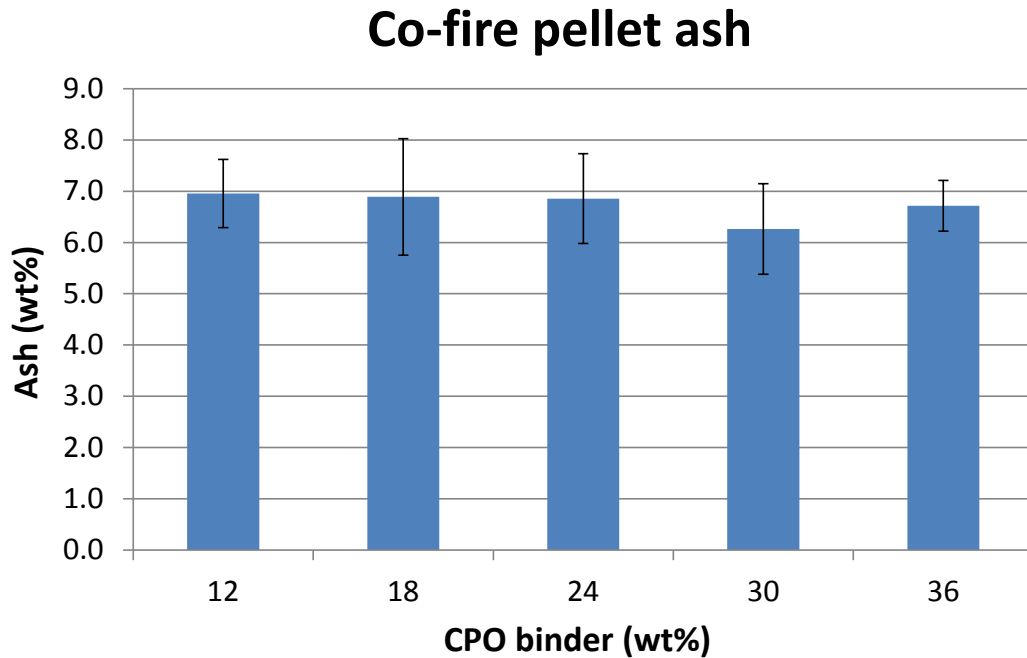


Figure 34: Pellet ash content with respect to CPO binder fraction

4.3 Ultimate Analysis

Statistical models for both elemental carbon and sulfur are discussed in this section. Hydrogen, nitrogen, and oxygen models are not discussed since they had very low R^2 values, and were not statistically significant. All model summaries can be referenced in Appendix C.

4.3.1 Carbon

The reduced elemental carbon model had a rather low R^2 value of 0.65, but it was statistically significant with a p-value of 0.0004. Significant terms are shown in Table 12 as shaded. The non-significant terms shown were included since they increased the accuracy of the reduced model. Apart from the intercept, CPO binder fraction (x_3) and cure temperature (x_4) were the most significant terms.

Table 12: Pellet elemental carbon content reduced model summary

Term	Coefficient	P-value	Significance
Intercept (β_0)	76.816	<.0001	YES
Particle (x_1)	-1.407E-03	0.245	NO
Moisture (x_2)	-8.139E-02	0.467	NO
Binder (x_3)	-5.445E-01	0.026	YES
Cure (x_4)	8.958E-03	0.023	YES
Particle x Moisture (x_1x_2)	-1.540E-04	0.086	NO
Particle x Binder (x_1x_3)	7.904E-05	0.079	NO
Binder x Binder (x_3x_3)	7.842E-03	0.104	NO

Due to the particle x binder interaction term, the influence of the CPO binder fraction on elemental carbon depends on the coal particle size. The effect of both CPO binder fraction and coal particle size appears to revolve around a focal point of 29.5 wt% CPO binder (see Figure 35). Similar to what was discussed for previous models, the prediction above 30 wt% CPO is based on only one experiment at 36 wt%, and will therefore be disregarded. Below 29.5 wt%, increasing CPO binder fractions decrease the elemental carbon content. The exception is for the 2298 μm particle size which experiences a local minimum. Is it expected that pellet elemental carbon should decrease with increasing CPO binder fractions since the elemental carbon content of CPO is half that of coal, 23.4 vs. 51.9

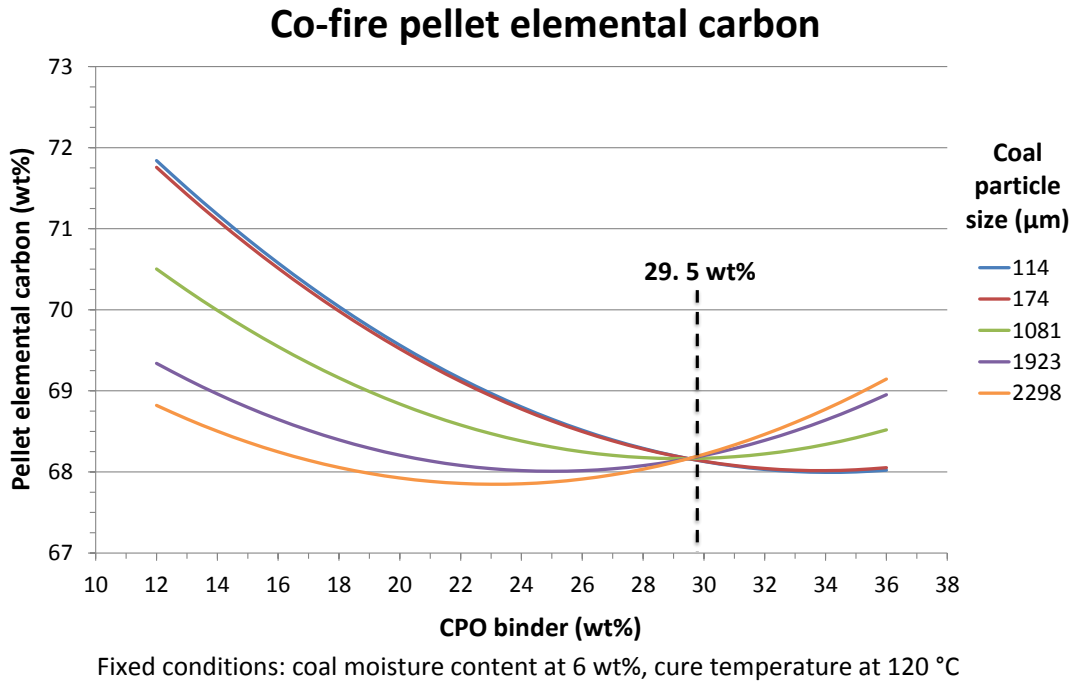


Figure 35: Modeled pellet elemental carbon content with respect to CPO binder fraction and coal particle size

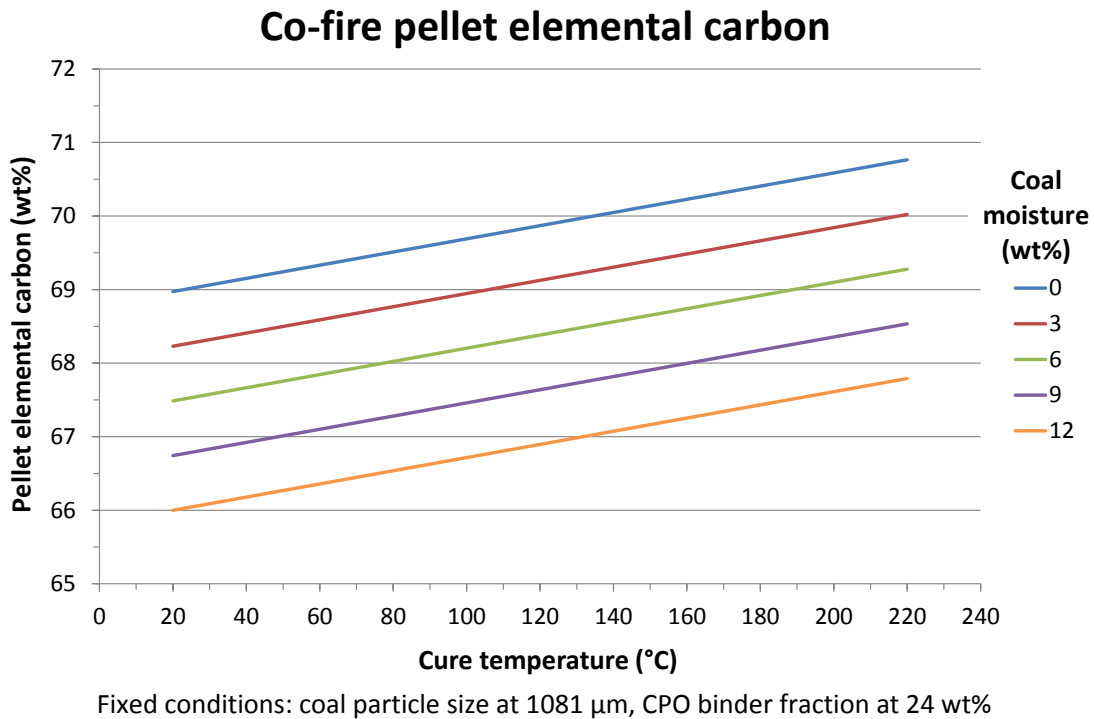


Figure 36: Modeled pellet elemental carbon content with respect to cure temperature and coal moisture content

wt%, respectively. With regard to coal particle size, elemental carbon appears to decrease as particle sizes increase. Since the CHN instrument combusts samples in order to analyze carbon content, the larger coal particles are likely not burning completely, thus yielding the effect seen in Figure 35.

As shown in Figure 36, increasing cure temperatures appear to increase elemental carbon in the pellets. This effect is attributed to model error since higher cure temperatures cannot create or destroy elemental carbon. In contrast, decreasing coal moisture directly increases elemental carbon. This effect is similar to that seen for heating value as moisture displaces mass in the pellet and does not contain any elemental carbon.

4.3.2 Sulfur

The reduced elemental sulfur model had a low R^2 value of 0.66 and a p-value less than 0.0001, making the model statistically significant. As shown in Table 13, terms which were statistically significant are shown as shaded. The non-significant terms shown were included since they increased the accuracy of the reduced model. CPO binder fraction (x_3) was the most significant 1st order term with a p-value of 0.024.

Table 13: Pellet elemental sulfur content reduced model summary

Term	Coefficient	P-value	Significance
Intercept (β_0)	2.321	<.0001	YES
Particle (x_1)	2.024E-04	0.242	NO
Moisture (x_2)	-4.652E-02	0.218	NO
Binder (x_3)	-2.118E-02	0.024	YES
Cure (x_4)	7.417E-04	0.219	NO
Particle x Binder (x_1x_3)	-9.441E-06	0.181	NO
Moisture x Moisture (x_2x_2)	3.333E-03	0.270	NO

Sulfur content is an important factor in solid fuel selection due to hazardous emissions associated with sulfur. Theoretically, the pellet sulfur content should decrease as the CPO binder fraction increases, since the CPO is very low in sulfur compared with the coal, 0.002 vs. 2.33 wt%, respectively. The very low sulfur content of CPO can be traced

back to the pyrolyzed red oak biomass, which is naturally low in sulfur (0.01 wt%). In Figure 37, the sulfur content does decrease with increasing CPO binder fractions, as expected. Coal moisture does not clearly effect sulfur content, as is predicted by the insignificant model term (p-value = 0.218).

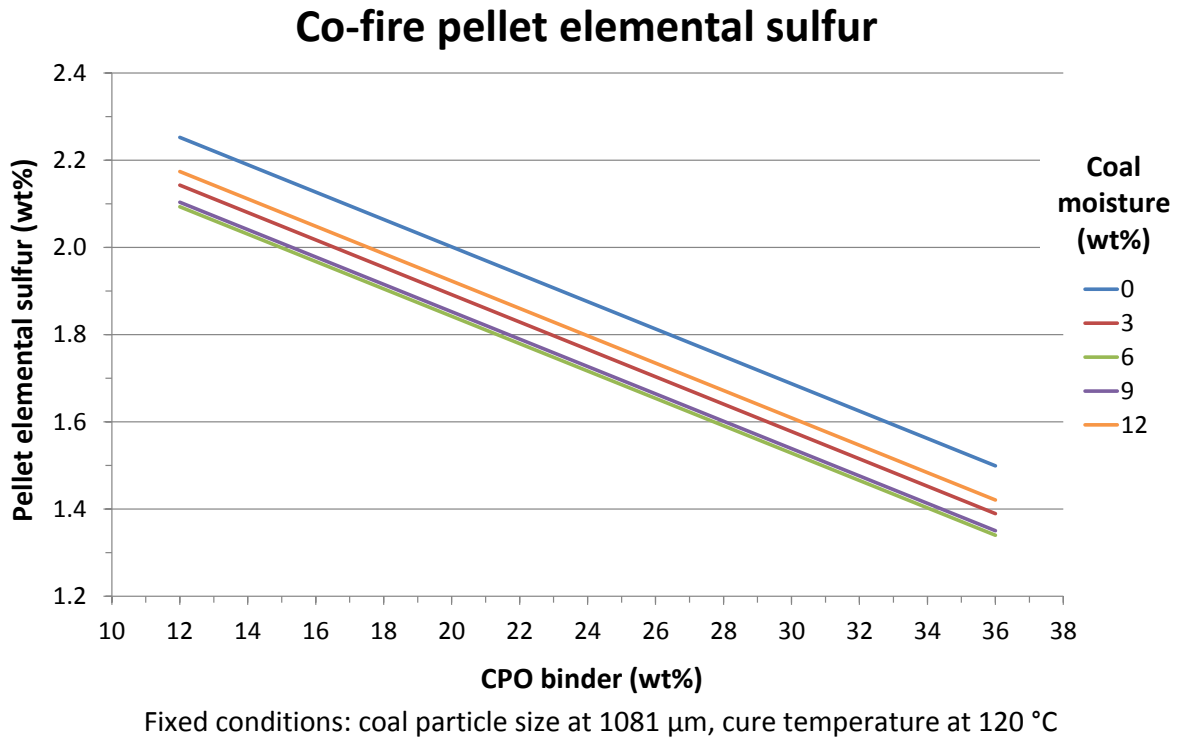


Figure 37: Modeled pellet elemental sulfur content with respect to CPO binder fraction and coal moisture content

4.4 Durability

4.4.1 Indirect tensile strength

The full statistical model for indirect tensile strength had a low R^2 value of 0.50, and was not statistically significant. While the reduced model was significant (p-value = 0.0408), it also had a very low R^2 value of 0.44. The model summary is shown in Table 14 as a reference for drawing general conclusions, and should not be used to predict specific values. The first and second order moisture content terms were significant in the reduced model. The negative first order moisture term coefficient suggests that increasing coal moisture leads

to a decrease in indirect tensile strength. However, this observation is not linear and depends on the quadratic moisture term.

Table 14: Pellet indirect tensile strength reduced model summary

Term	Coefficient	P-value	Significance
Intercept (β_0)	1165.464	0.0007	YES
Particle (x_1)	1.521E-01	0.405	NO
Moisture (x_2)	-146.846	0.006	YES
Binder (x_3)	-6.778	0.300	NO
Cure (x_4)	-6.638	0.066	NO
Particle x Particle (x_1x_1)	-9.727E-05	0.237	NO
Moisture x Moisture (x_2x_2)	12.913	0.003	YES
Cure x Cure (x_4x_4)	2.864E-02	0.052	NO

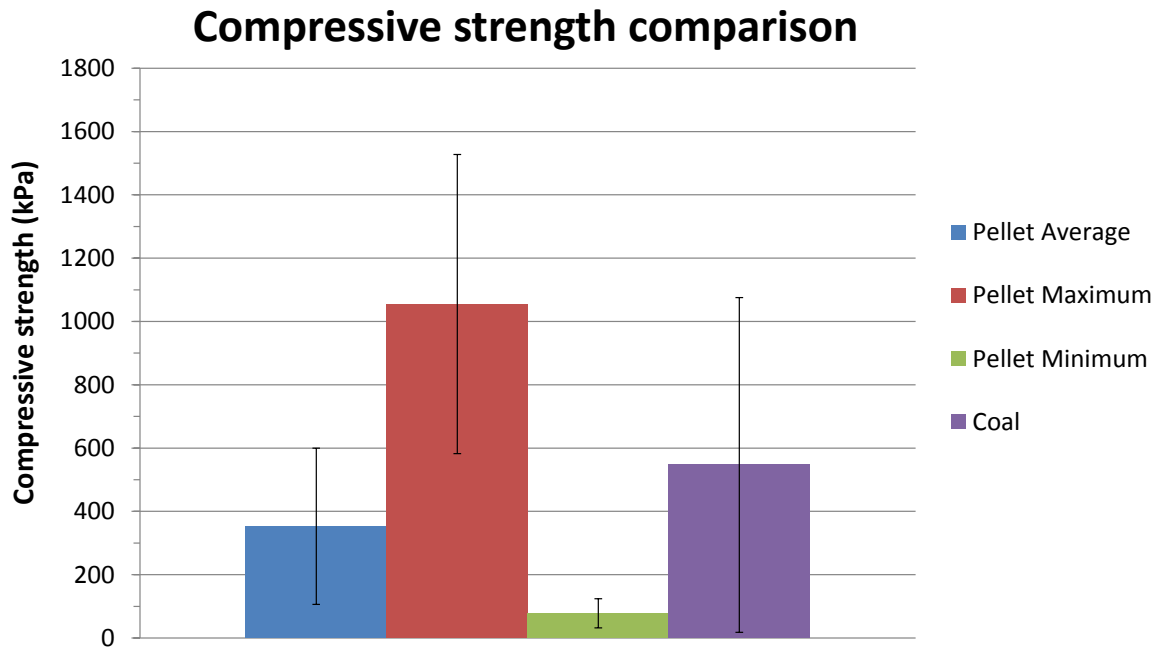


Figure 38: Indirect tensile strength comparison

Like the statistical model, the indirect tensile strength experimental data is generally not significant between experiments. As shown in Figure 38, the large standard deviation of

the coal indirect tensile strength encompasses both the pellet maximum and minimum error bars. Therefore, no statistically significant conclusions can be drawn for comparison of the pellets and the parent coal. The use of non-standard indirect tensile strength testing equipment may have contributed to the large variances shown in the data. However, Kaliyan et al. note that repeatability problems in indirect tensile strengths tests have been reported by many researchers [44]. Therefore, other strength tests may be more appropriate for testing the co-fire pellets.

4.4.2 Impact resistance

Like the indirect tensile strength analysis, the impact tests were prone to large variances across the spread of experiments. The full statistical model for impact resistance had a very low R^2 value of 0.48, and was not statistically significant. One reason for the poor model fit is that the result of the impact resistance test was limited to 1000. This is because some of the pellets were malleable enough to be dropped many times past the limit of 10 drops without experiencing fracture. This test limit is evident in the residuals vs. predicted plot (Figure 39). In the figure, a line of predicted points is apparent. A residuals plot with randomized data points is desired for the linear model assumption.

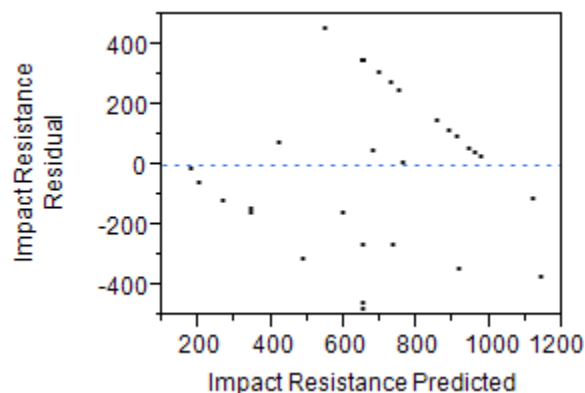


Figure 39: Impact resistance statistical model residuals vs. predicted values

A summary of the impact resistance experimental data is shown in Figure 40. A significant conclusion that can be drawn from the figure is that the averaged pellet impact resistance is greater than the parent coal. The reason for this is likely due to the presence of the CPO binder in the pellets. Pellets with higher CPO binder fractions typically had higher

impact resistance values. Pellets with low CPO binder fractions typically scored lower on the impact resistance test due to the brittle nature of the parent coal. Like the statistical model, variances across the 31 experiments were large as is evident by the large error bars on the averaged pellet data in Figure 40. The large variances are possibly due to the small sample size of 90 g (3 pellets) used for each experiment. The ASTM D440 drop shatter test for coal specifies that a sample size of 50 lbs (22.7 kg) be used [45].

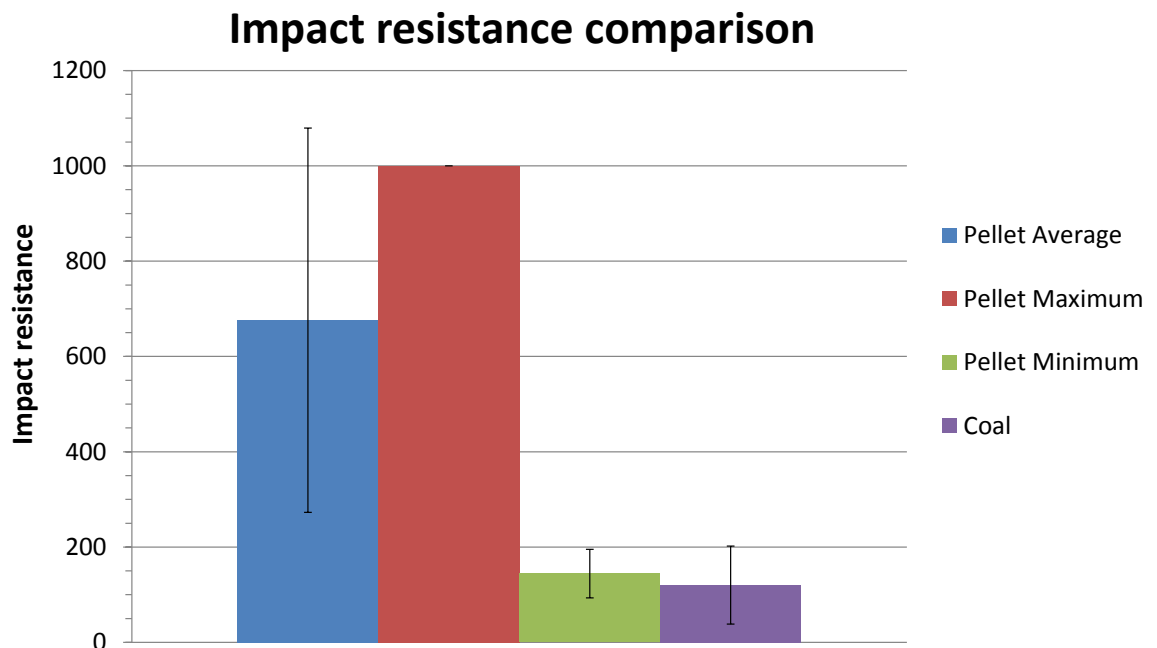


Figure 40: Impact resistance comparison

4.4.3 Abrasion resistance

The abrasion resistance statistical model was not statistically significant, and had an extremely low R^2 value of 0.36. Similar to the impact resistance model, the assumption of a linear model was rejected after examining the residuals vs. predicted plot in Figure 41. Instead of the preferred randomized points, a pattern is definitely apparent in the figure.

As shown in Figure 42, the averaged pellet abrasion resistance is higher than that of the parent coal. However, this comparison is borderline significant as evidenced by the large error bars for the pellet average. Due to the large quantity of pellets required for each test, only one test was performed per experiment. Therefore, no error bars are shown for the

pellet minimum or maximum abrasion resistance. Similar to impact resistance, CPO binder fraction plays possibly the largest role in pellet abrasion resistance due to its ability to bind the coal particles together. Over the entire 31 experiment spectrum, pellets with higher CPO binder fractions generally performed better in the abrasion test. In addition, pellets from 18 of the 31 experiments meet the minimum durability index of 95 as specified by the Pellet Fuels Institute [46].

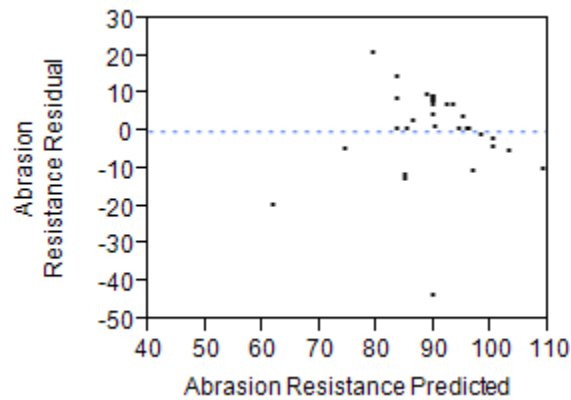


Figure 41: Abrasion resistance statistical model residuals vs. predicted values

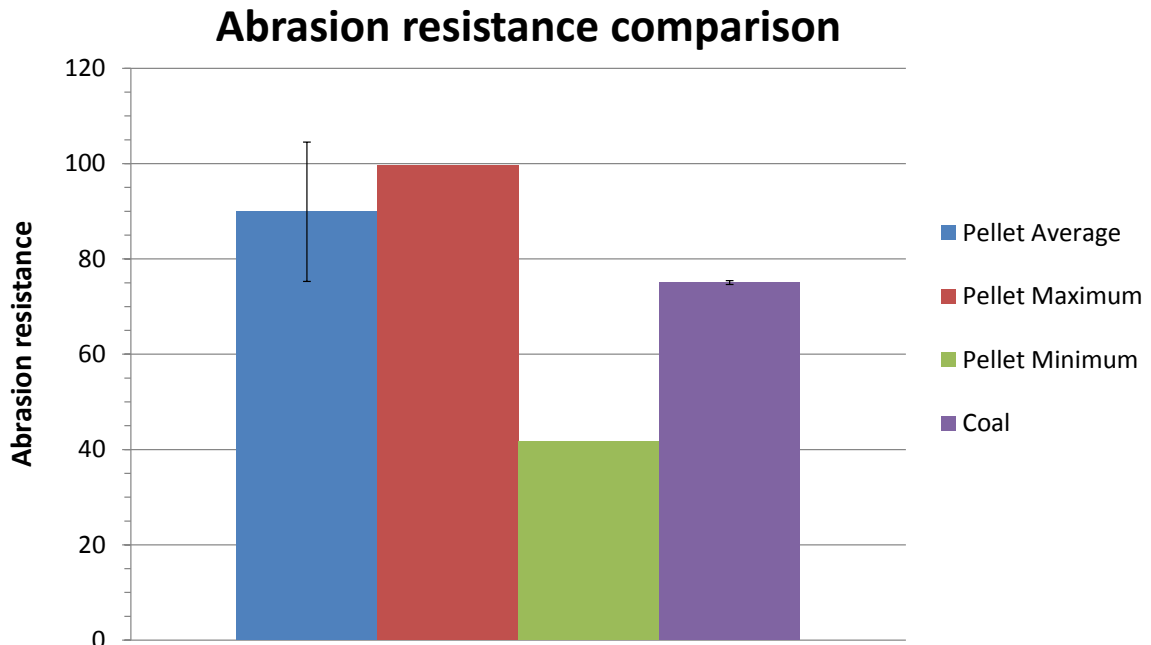


Figure 42: Abrasion resistance comparison

4.5 Other analysis

4.5.1 Density

The statistical model for pellet mass density was not significant, and can be referenced in Appendix C. Pellet mass densities ranged from 0.93 to 1.39 g/cm³, with an averaged value of 1.21 ± 0.09 g/cm³. This average density is close to the 1.2 g/cm³ achieved by a comparable laboratory scale pellet press surveyed by Kaliyan et al. [44].

Unlike for mass density, the reduced model for particle density was statistically significant (p-value < 0.0001) with an R² value of 0.80. However, the lack-of-fit test was also significant, which means a different model may fit the data better. Nonetheless, general conclusions can still be made from the reduced model. Terms which were statistically significant are shown in Table 15 as shaded. The non-significant terms shown were included since they increased the accuracy of the reduced model. CPO binder fraction (x_3) was the most significant term with a p-value less than 0.0001.

Table 15: Pellet particle density reduced model summary

Term	Coefficient	P-value	Significance
Intercept (β_0)	1.357	<.0001	YES
Particle (x_1)	-6.012E-05	0.025	YES
Moisture (x_2)	1.912E-02	0.0003	YES
Binder (x_3)	-4.194E-03	<.0001	YES
Cure (x_4)	8.885E-04	0.003	YES
Particle x Cure (x_1x_4)	-2.314E-07	0.070	NO
Moisture x Cure (x_2x_4)	-9.917E-05	0.010	YES
Particle x Particle (x_1x_1)	3.384E-08	0.001	YES

As shown in Figure 43, increasing CPO binder fractions decrease the particle density of the pellets. In practice, the CPO binder should increase the particle density since the CPO is non-porous and fills the void spaces between and inside of the coal particles. In addition, the CPO has a higher mass density than the coal, 1.22 vs. 0.81 g/cm³, respectively. In contrast with the CPO binder, increasing coal moisture contents increase particle density. This effect is expected since the added moisture fills the voids between coal particles.

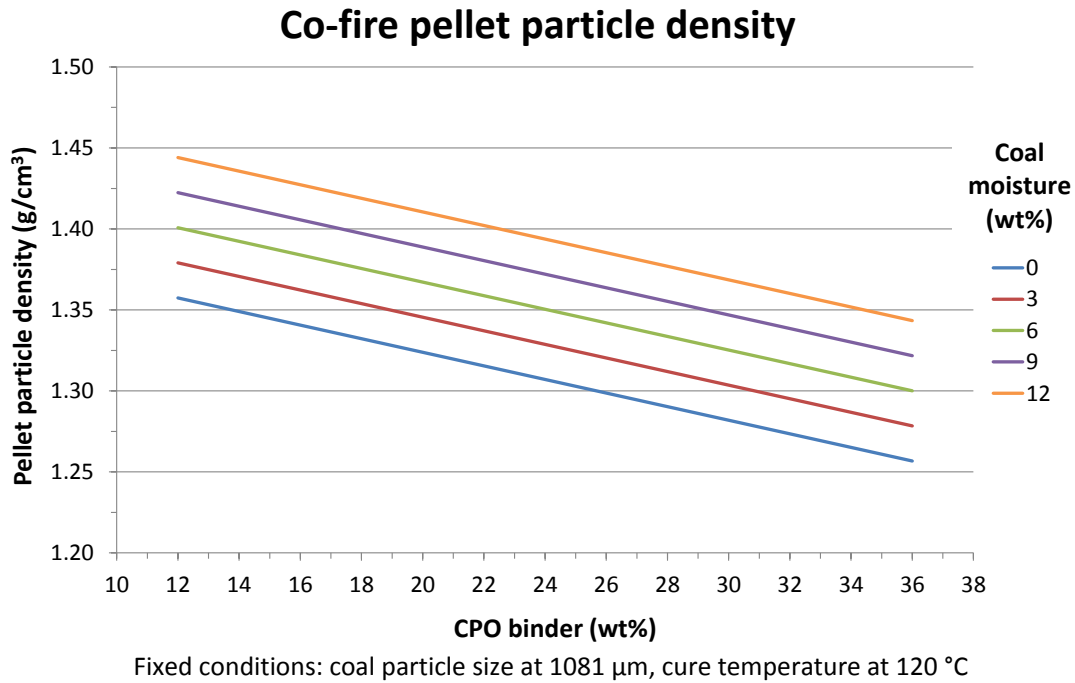


Figure 43: Modeled pellet particle density with respect to CPO binder fraction and coal moisture content

Both coal particle size and cure temperature appear to revolve around a focal point at 1270 μm in Figure 44. Below 1270 μm , particle density increases with higher cure temperatures and smaller coal particle sizes. In contrast after 1270 μm , particle density increases with lower cure temperatures, and larger particle sizes. As previously mentioned, the LOF test was significant for this model, so the focal point of 1270 μm is most likely due to an adequate fit of the model to the experimental data. With regard to the experimental data, an important conclusion that can be made is that the pellet particle density is generally higher than the corresponding mass density for any given experiment. This is expected since the particle density negates the effect of void spaces on the sample volume.

In contrast with mass and particle densities, the parent coal had a bulk density roughly twice that of the pellets, 969 vs. 471 kg/m^3 . This large disparity is due to the well-defined shape and size of the co-fire pellets. The coal is comprised of many different particle sizes which pack more efficiently than the large pellets. For commercial applications, a smaller pellet shape may be used in order to produce a bulk density that is competitive with coal.

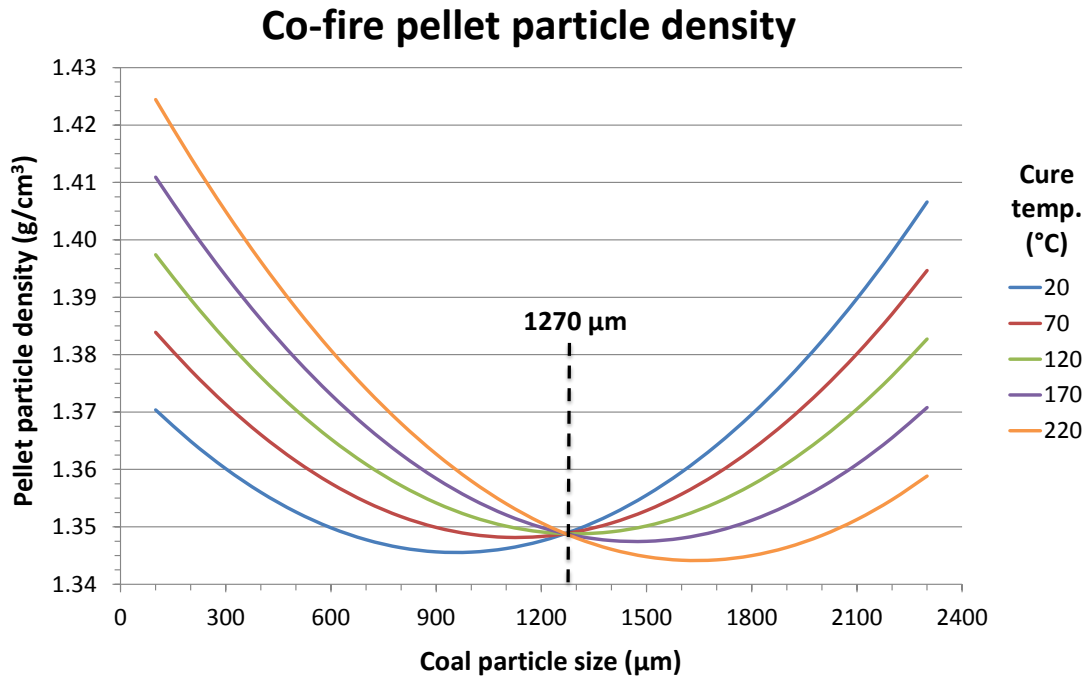


Figure 44: Modeled pellet particle density with respect to coal particle size and cure temperature

4.5.2 Ash fusibility

An ash fusibility test measures the tendency of ash to melt at different temperatures. This analysis is important for biomass fuels as they are known to produce low-melting point ash compounds which foul and corrode boiler surfaces. Figure 45 shows the test points used in the ash fusibility analysis. “IT”, “ST”, “HT”, and “FT” correspond with initial, softening, hemispherical, and fluid temperatures, respectively.

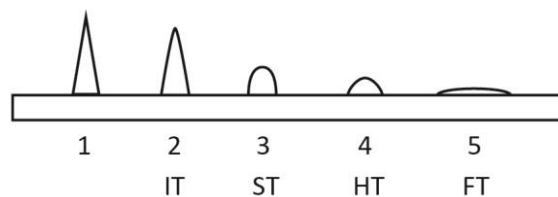


Figure 45: Ash fusibility test points

Pellets from the center point experiments (Exp. 1-7) were utilized for this analysis. As shown in Figure 46, the pellet ash withstood a higher temperature for first three test

stages. The coal ash withstood a higher temperature for the final stage. A significant conclusion that can be drawn from the figure is that the pellet ash melting temperatures are very similar to that of the parent coal, and can be expected to perform similarly during combustion in an industrial scale boiler.

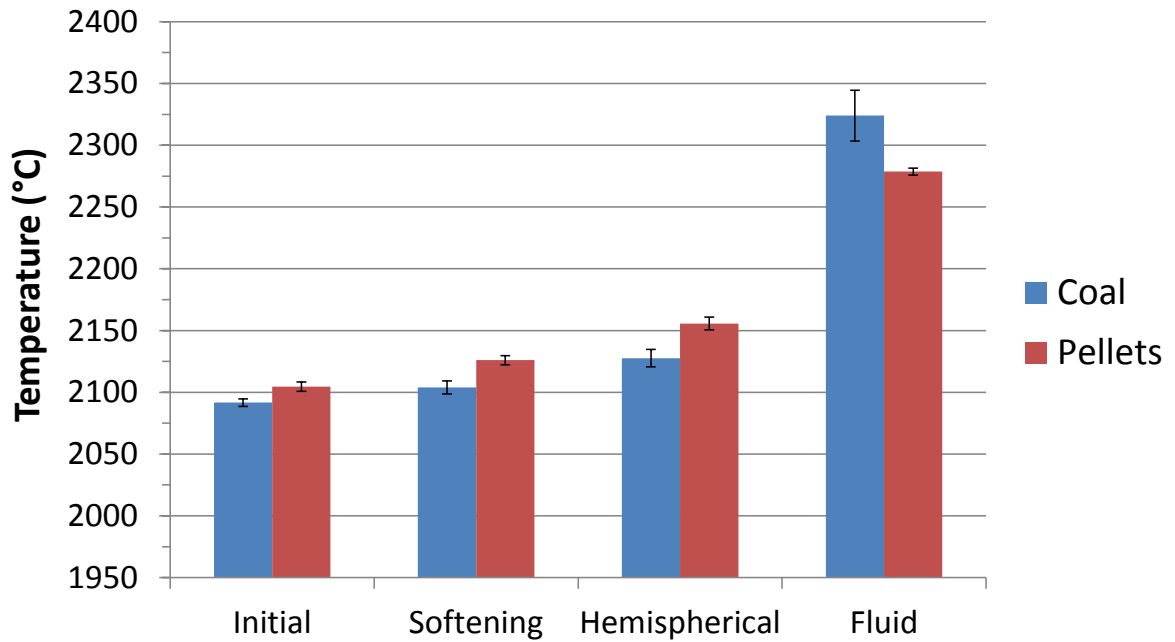


Figure 46: Ash fusibility comparison for coal and co-fire pellets

CHAPTER 5. CONCLUSIONS

5.1 Experimental Conclusions

The concept of a co-fire pellet has been demonstrated. A statistical design of experiments was successfully performed in order to evaluate the pellets in terms of coal particle size, coal moisture content, CPO binder fraction, and cure temperature. Statistical models were fit to the experimental data.

Pellet heating values are maximized for small coal particles, low coal moisture contents, high cure temperatures, and low CPO binder fractions. Higher cure temperatures increase the heating value by removing moisture from the pellet. Decreasing CPO binder fractions increase the heating value of a pellet due to the lower heating value of the CPO compared to the parent coal. In the experimental data, the pellet heating values closely resemble the parent coal heating value, even though the simple correlation and a correlation by Sheng et al. predict the heating values should land between that of the coal and the CPO [35]. Analytical tests were conducted to determine the mechanism behind this heating value abnormality; no concrete conclusions have been made at this point. Since the heating value of the pellets is approximately equal to the heating value of the parent coal, utilities can combust the co-fire pellets without any loss in boiler steam output.

In terms of proximate analysis, pellet moisture decreases for increasing coal moisture and cure temperatures, as is expected. Higher CPO binder fractions increase volatiles due to the higher volatile content of the CPO. With regard to fixed carbon, increasing CPO binder fractions decrease fixed carbon due to the low fixed carbon content of the CPO. Pellet ash decreases for larger CPO binder fractions, owing to the very low ash content of the CPO. The extremely low ash content of the CPO binder allows for a reduction in pellet ash that is directly related to the CPO binder fraction. In addition, the use of the co-fire pellets in place of conventional coal allows for a reduction in boiler ash that is again proportional to the CPO binder fraction. In contrast with biomass co-firing, the co-fire pellets do not contain any alkali metals that are known to corrode and foul boilers. During the production of the pellets, the alkali metals from the pyrolyzed biomass are captured with the biochar.

In terms of the pellet elemental analysis, increasing coal moisture decreases elemental carbon, as is expected. Pellet sulfur content decreases for increasing CPO binder fractions due to the naturally low sulfur content of the pyrolyzed biomass. The low pellet sulfur content can help utilities reduce sulfur emissions.

Significant conclusions cannot be drawn from the indirect tensile strengths tests. The impact resistance of the pellets was higher than the parent coal due to the impact absorbing nature of the CPO. The pellets also were more abrasion resistant than the coal, again owing to the adhesive nature of the CPO. Increasing CPO binder fractions generally lead to better impact and abrasion resistance. The low significance of the strength and durability tests is likely due to the small sample size used during analysis.

Pellet particle density was higher than the respective mass density. Increasing coal moisture led to an increase in particle density, while higher CPO binder fractions decreased the particle density. Ash fusibility temperatures were approximately the same for both the pellets and parent coal.

Overall, the CPO binder fraction has the largest impact on the production and properties of the pellets. In contrast, the pellet curing process was determined to be an unnecessary treatment. Co-fire pellets can be used to reduce power plant coal consumption due to the renewable CPO binder fraction and the similar heating value of the pellets compared to the parent coal. In addition, the partially renewable nature of the co-fire pellets can possibly satisfy renewable portfolio standard requirements for individual states. Finally, the co-fire pellets could be used to meet any future carbon emission limits since the biomass derived CPO fraction in the pellets has a low net CO₂ cycle compared to the parent coal.

5.2 Future Work

Future work regarding the pellets could include a number of items. The pellet higher heating values should be further investigated to determine why they are higher than predicted. An alkali metals analysis should be conducted on the pellets in order to determine the relative concentrations of metals known to contribute to boiler fouling and corrosion. A combustion test should be conducted in order to compare the gas and particulate emissions of the pellets with the parent coal. The combustion test could be especially useful for an electrical utility in determining whether the pellets will meet environmental regulations.

In the design of experiments, the cure temperature factor was used to simulate accelerated pellet aging as it has been noticed that the pellets attain increased strength and durability over time. A series of tests could be therefore conducted to investigate the mechanism behind the pellet aging process. The use of the coal-CPO mixture (prior to pelletization) in boilers could be investigated as an alternative to the pelletized form. The elimination of the pelletization step might improve the economic viability of the coal-CPO mixture for use as a solid fuel. Finally, a techno-economic analysis should be conducted to help electrical utilities compare the coal-CPO fuel with other boiler fuels.

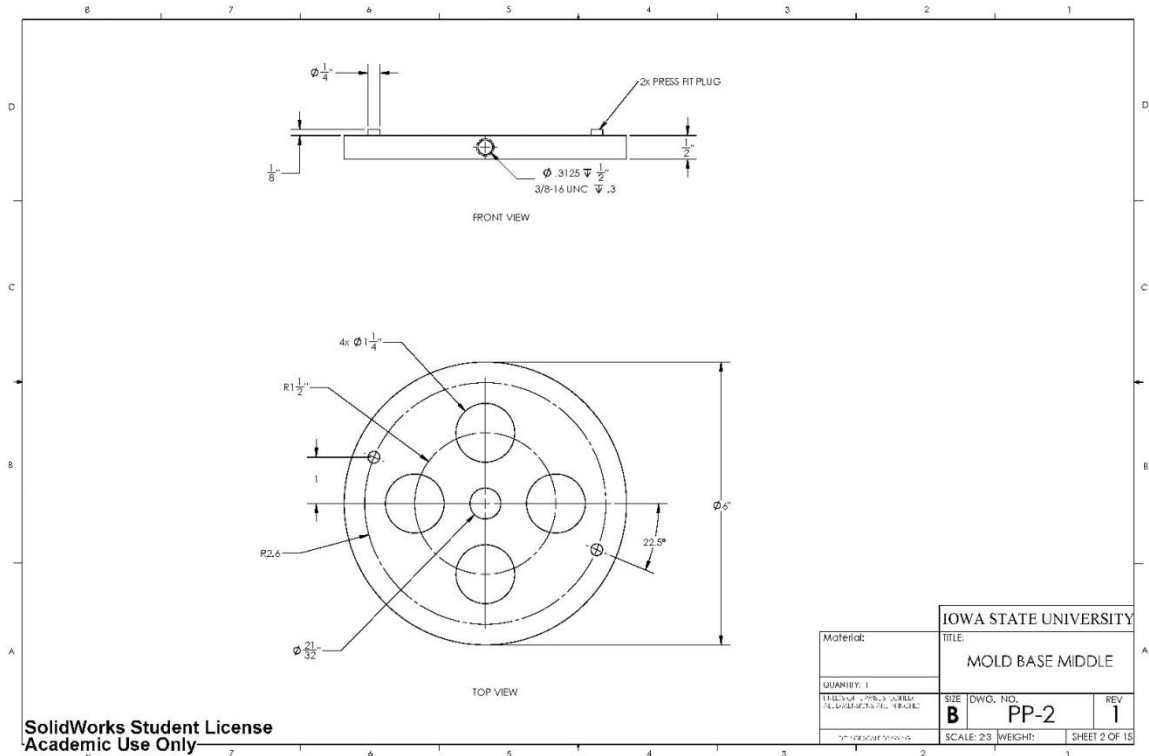
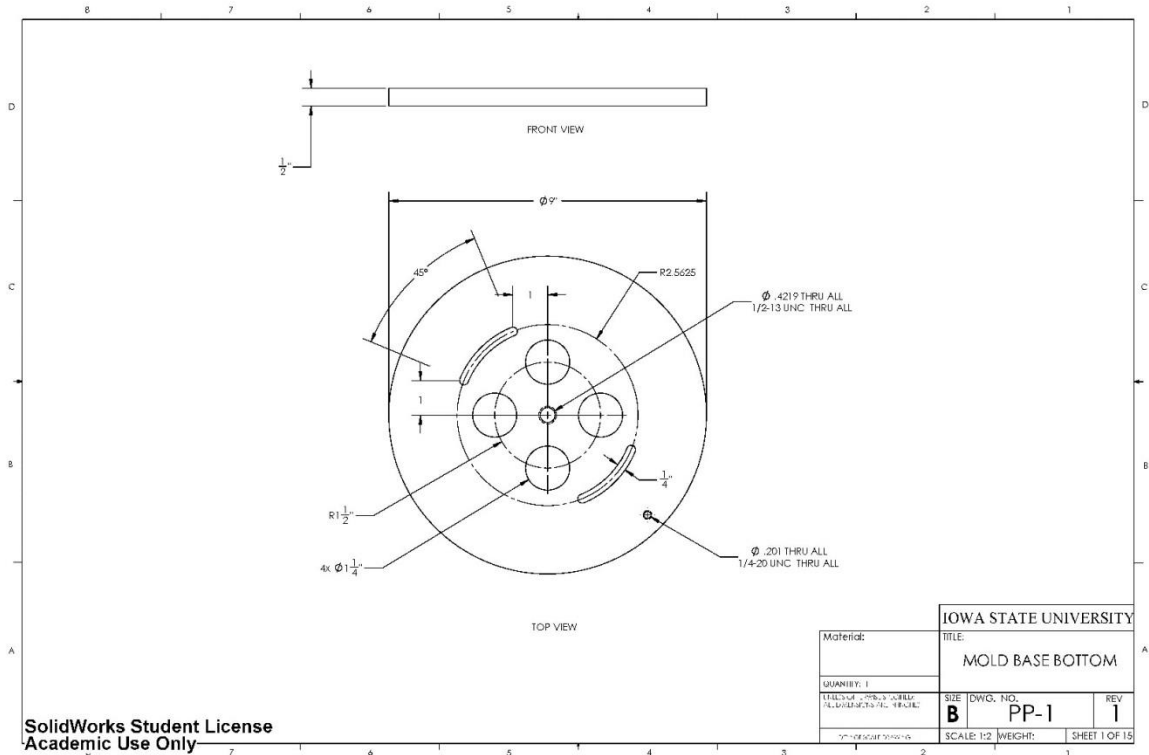
BIBLIOGRAPHY

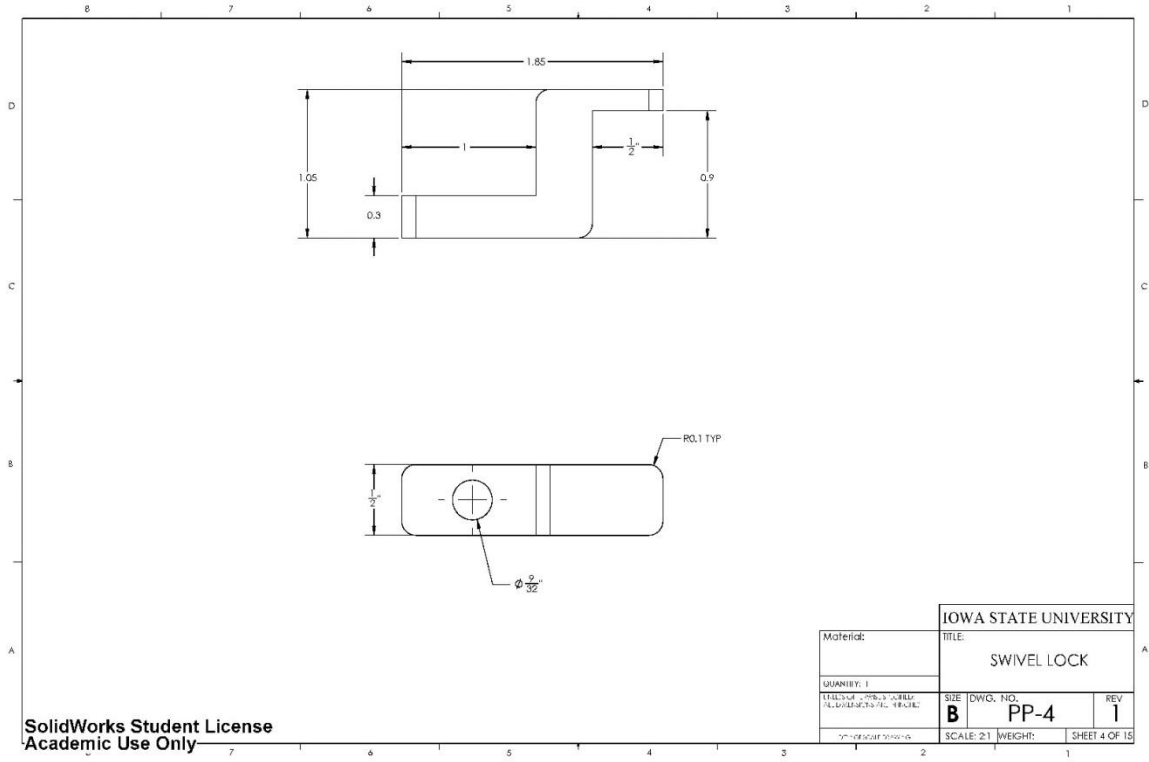
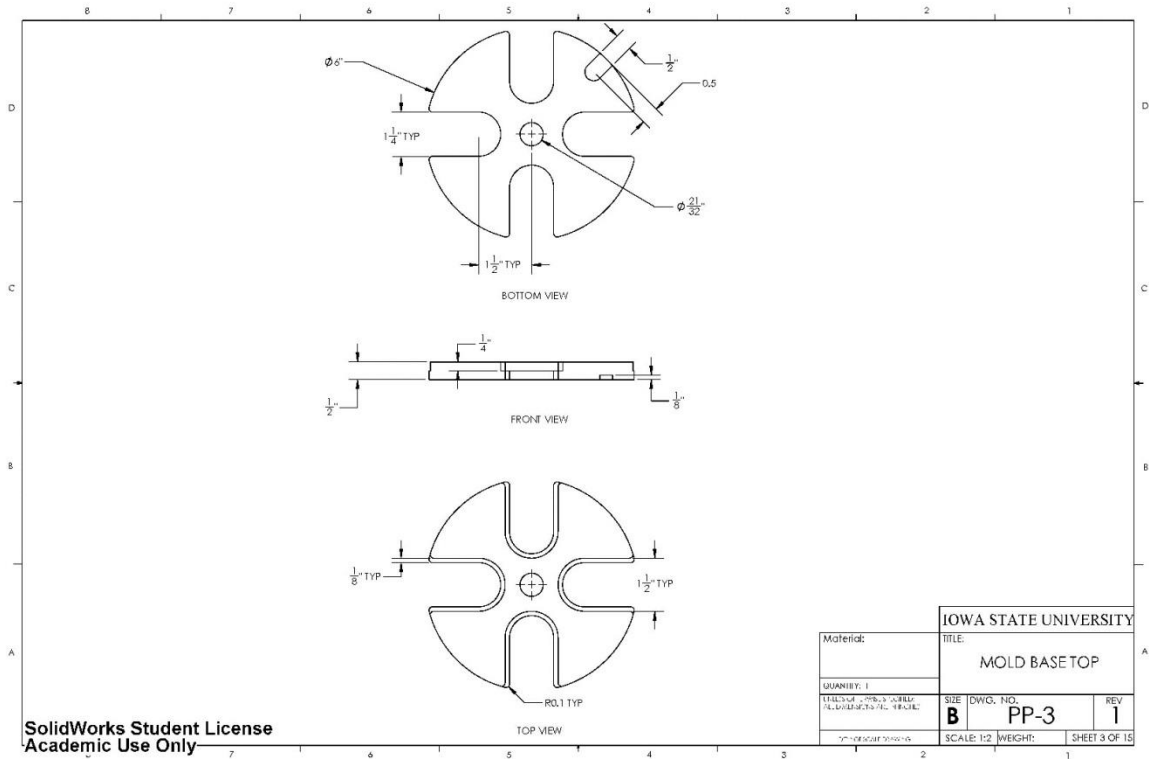
- [1] U.S. Energy Information Administration, 2011, International Energy Outlook 2011.
- [2] United Nations, 2011, World Population Prospects: The 2010 Revision.
- [3] U.S. Environmental Protection Agency, 2013, “Mercury and Air Toxics Standards” [Online]. Available: <http://www.epa.gov/airquality/powerplanttoxics/actions.html>.
- [4] U.S. Environmental Protection Agency, 2013, “National Ambient Air Quality Standards” [Online]. Available: <http://epa.gov/air/criteria.html>.
- [5] U.S. Environmental Protection Agency, 2013, “Interstate Air Pollution Transport” [Online]. Available: <http://www.epa.gov/airtransport/>.
- [6] U.S. Environmental Protection Agency, 2013, Proposed Carbon Pollution Standard for New Power Plants.
- [7] Yin H., and Powers N., 2010, “Do state renewable portfolio standards promote in-state renewable generation?,” *Energy Policy*, **38**(2), pp. 1140–1149.
- [8] Wisler R., Namovicz C., Gielecki M., and Smith R., 2007, “The experience with renewable portfolio standards in the United States,” *The Electricity Journal*.
- [9] Noguee A., Deyette J., and Clemmer S., 2007, “The Projected Impacts of a National Renewable Portfolio Standard,” *The Electricity Journal*, **20**(4), pp. 33–47.
- [10] Barbose G., *Renewables Portfolio Standards in the United States: A Status Update*.
- [11] Basu P., Butler J., and Leon M., 2011, “Biomass co-firing options on the emission reduction and electricity generation costs in coal-fired power plants,” *Renewable energy*, **36**(1), pp. 282–288.
- [12] Brown R., *Biorenewable Resources: Engineering New Products from Agriculture*. 2003, Iowa State Press.
- [13] Khan A., and Jong W. De, 2009, “Biomass combustion in fluidized bed boilers: Potential problems and remedies,” *Fuel processing technology*, **90**(1), pp. 21–50.
- [14] Yin C., Rosendahl L., and Kær S., 2008, “Grate-firing of biomass for heat and power production,” *Progress in Energy and Combustion ...*, **34**(6), pp. 725–754.
- [15] Grammelis P., 2010, *Solid Biofuels for Energy: A Lower Greenhouse Gas Alternative*, Springer London, London.
- [16] Stevens C., and Brown R., 2011, *Thermochemical processing of biomass: Conversion into fuels, chemicals and power*.
- [17] Zbogar A., Frandsen F. J., Jensen P. A., and Glarborg P., 2005, “Heat transfer in ash deposits: A modelling tool-box,” *Progress in Energy and Combustion Science*, **31**(5-6), pp. 371–421.
- [18] Wang S., Llamazos E., Baxter L., and Fonseca F., 2008, “Durability of biomass fly ash concrete: Freezing and thawing and rapid chloride permeability tests,” *Fuel*, **87**(3), pp. 359–364.
- [19] Tumuluru J., and Wright C., 2011, “A review of biomass densification systems to develop uniform feedstock commodities for bioenergy application,” *Biofuels, Bioproducts ...*, pp. 683–707.
- [20] Food and Agriculture Organization of the United Nations, 2013, “Feed Milling Processes” [Online]. Available: <http://www.fao.org/docrep/X5738E/x5738e0j.htm>.
- [21] Bergman P., and Boersma A., 2005, “Torrefaction for biomass co-firing in existing coal-fired power stations,” ... Research Centre of the ..., (July).

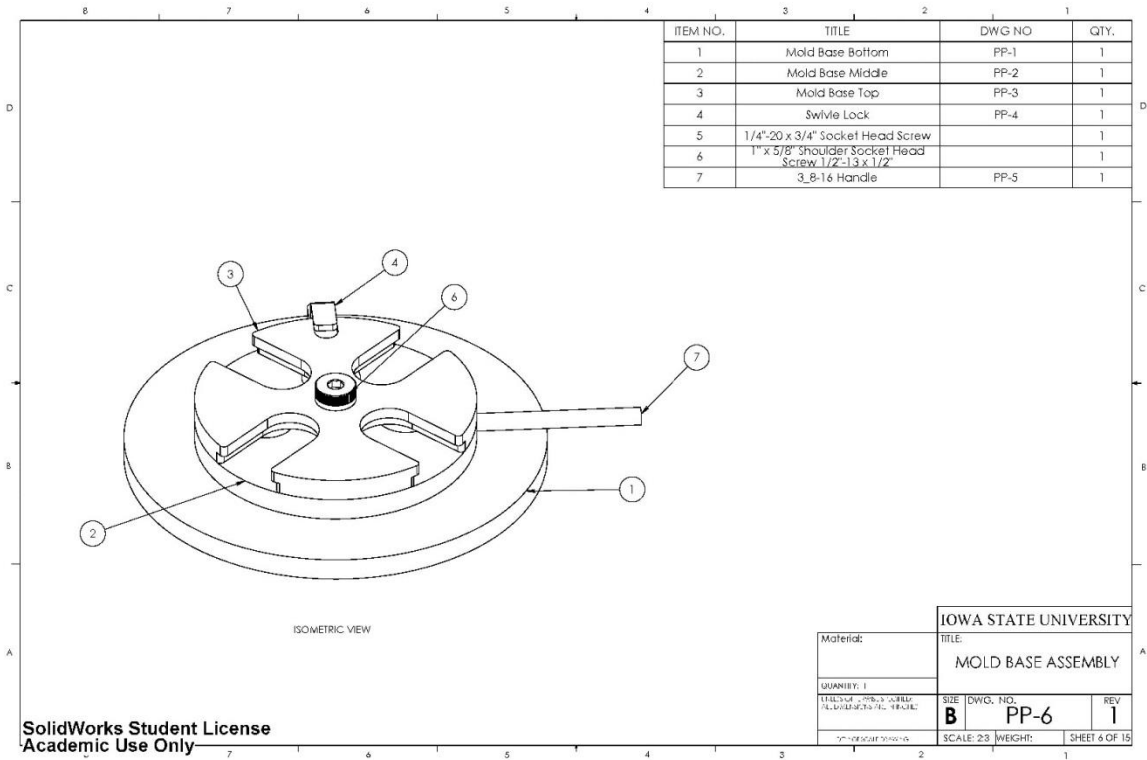
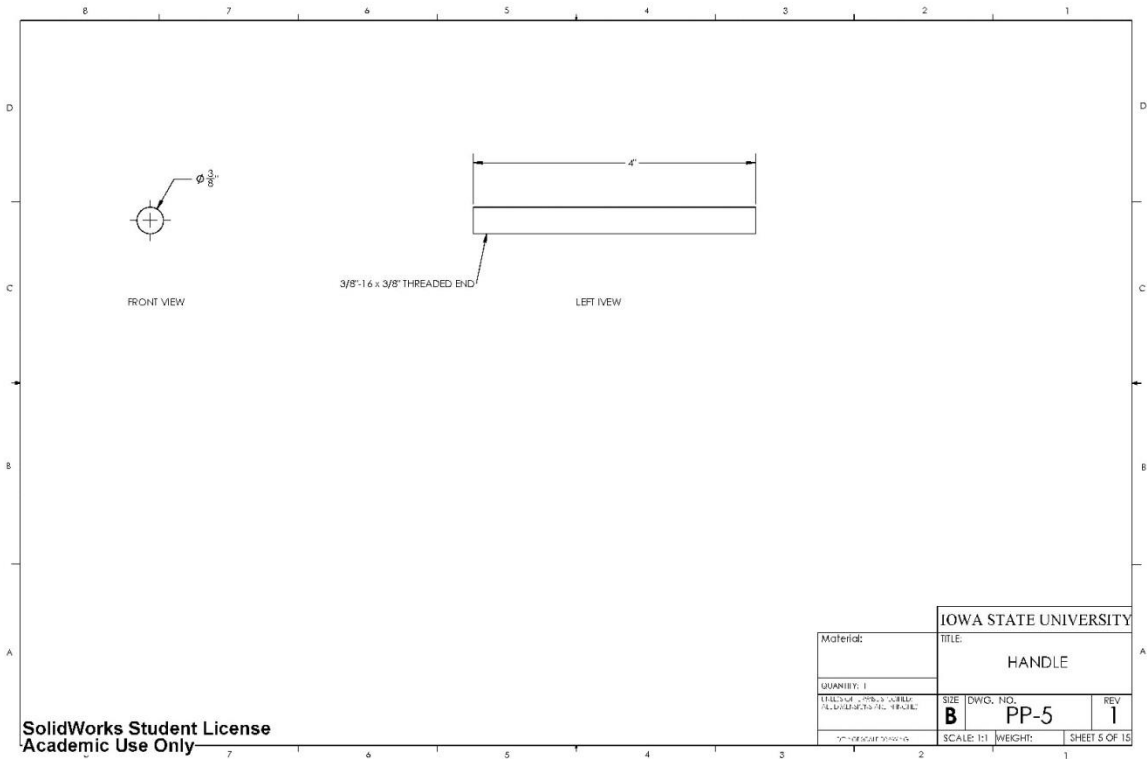
- [22] Bergman P., 2005, "Combined torrefaction and pelletisation," The TOP process, (July).
- [23] Friend A. J., 2012, "'Co-fire pellets' for emissions reduction and renewable energy generation," *Energy-Tech*, pp. 6–10.
- [24] Rover M. R., Johnston P. A., Smith R. G., and Brown R. C., 2013, "Sugar and Phenolic Oligomer Recovery from the Heavy Ends of Fractionated Bio-oil," Under Internal Review.
- [25] Peralta J., Raouf M., Tang S., and Williams R., 2012, "Bio-Renewable Asphalt Modifiers and Asphalt Substitutes," *Sustainable Bioenergy and ...*, pp. 89–115.
- [26] Alonso M., and Valdés A., 2002, "Coal recovery from fines cleaning wastes by agglomeration with colza oil: a contribution to the environment and energy preservation," *Fuel processing ...*, **75**, pp. 85–95.
- [27] Sastry K., 1991, "Pelletization of fine coals."
- [28] Kuehl R., 2000, *Design of experiments: statistical principles of research design and analysis*, Duxbury/Thomson Learning.
- [29] Rekab K., and Shaikh M., 2005, *Statistical design of experiments with engineering applications*.
- [30] Ellens C., 2009, "Design, optimization and evaluation of a free-fall biomass fast pyrolysis reactor and its products."
- [31] Pollard A. S., Rover M. R., and Brown R. C., 2011, "Characterization of bio-oil recovered as stage fractions with unique chemical and physical properties," *Journal of Analytical and Applied ...*, **93**, pp. 129–138.
- [32] Rover M. R., "The Effect of Pyrolysis Temperature on Recovery of Bio-Oil as Distinctive Stage Fractions," *Journal of Analytical and Applied Pyrolysis*.
- [33] Brown T., and Zhang Y., 2012, "Techno- • economic analysis of biobased chemicals production via integrated catalytic processing," *Biofuels, Bioproducts and ...*, pp. 73–87.
- [34] Library4science, 2013, "Reduction of the Sample to Analytical Size" [Online]. Available: [http://www.chromatography-online.org/quant/Sample Collection, Transport and Storage/Reduction of the Sample to Analytical Size.html](http://www.chromatography-online.org/quant/Sample%20Collection,%20Transport%20and%20Storage/Reduction%20of%20the%20Sample%20to%20Analytical%20Size.html).
- [35] Sheng C., and Azevedo J. L. T., 2005, "Estimating the higher heating value of biomass fuels from basic analysis data," *Biomass and Bioenergy*, **28**(5), pp. 499–507.
- [36] Majumder a, Jain R., Banerjee P., and Barnwal J., 2008, "Development of a new proximate analysis based correlation to predict calorific value of coal," *Fuel*, **87**(13–14), pp. 3077–3081.
- [37] Scholze B., and Meier D., 2001, "Characterization of the water-insoluble fraction from pyrolysis oil (pyrolytic lignin). Part I. PY–GC/MS, FTIR, and functional groups," *Journal of Analytical and Applied Pyrolysis*.
- [38] Li J., Wang C., and Yang Z., 2010, "Production and separation of phenols from biomass-derived bio-petroleum," *Journal of Analytical and Applied Pyrolysis*.
- [39] Mansouri N. El, and Salvadó J., 2007, "Analytical methods for determining functional groups in various technical lignins," *Industrial Crops and Products*.
- [40] Sahoo S., and SeydibeyoÄŸlu M., 2011, "Characterization of industrial lignins for their utilization in future value added applications," *Biomass and Bioenergy*.

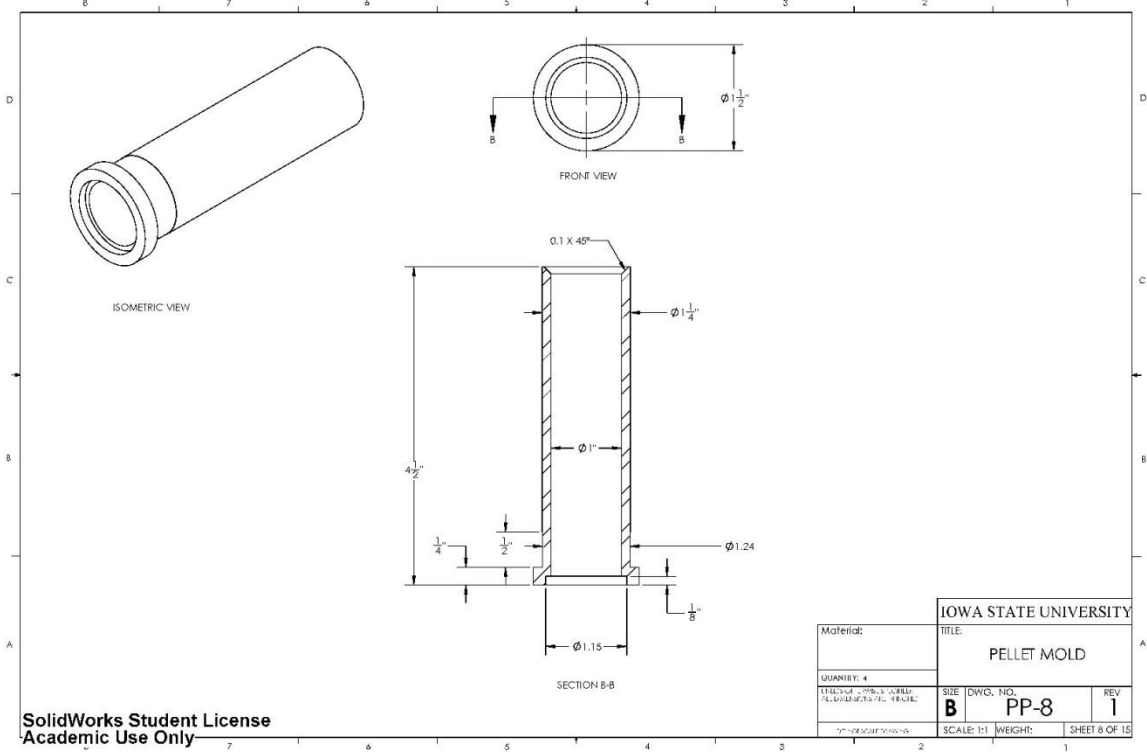
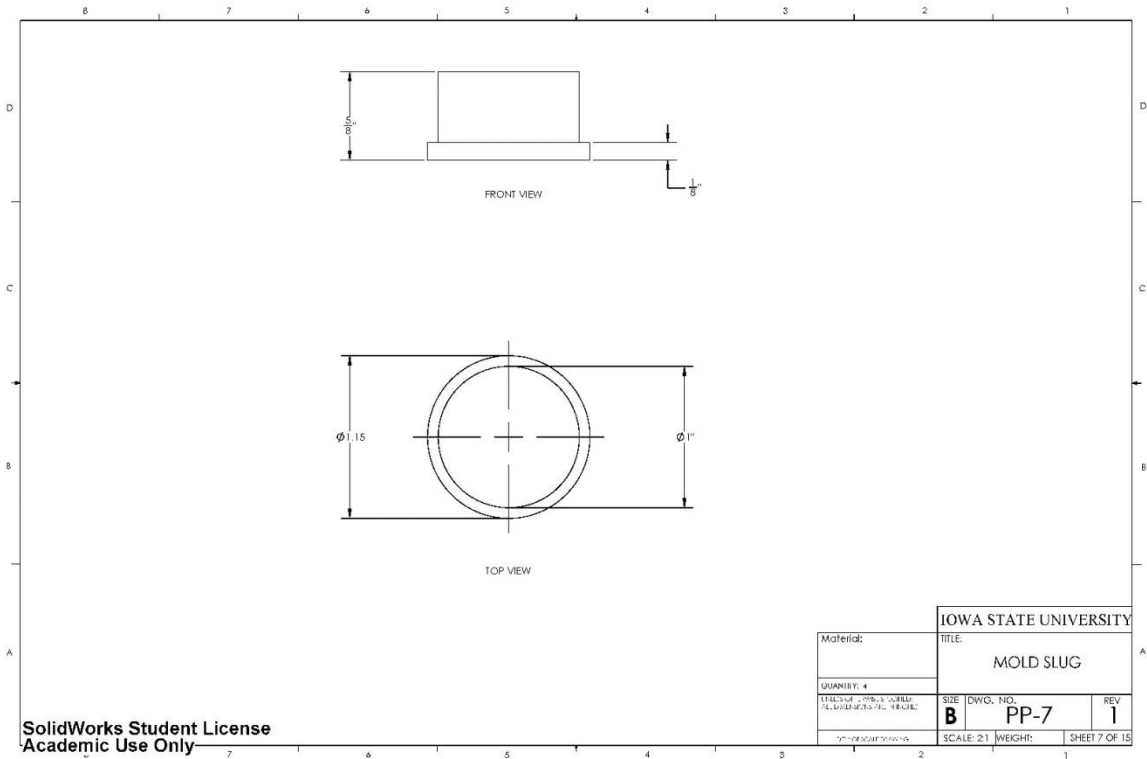
- [41] Kizgut S., Baran Y., and Cuhadaroglu D., 2003, “Reactivity and characterisation of various rank Turkish bituminous coal chars,” *Journal of thermal analysis and*
- [42] Cooke N., Fuller O., and Gaikwad R., 1986, “FT-ir spectroscopic analysis of coals and coal extracts,” *Fuel*.
- [43] Solomon P., and Carangelo R., 1988, “FT-ir analysis of coal: 2. Aliphatic and aromatic hydrogen concentration,” *Fuel*.
- [44] Kaliyan N., and Vance Morey R., 2009, “Factors affecting strength and durability of densified biomass products,” *Biomass and Bioenergy*, **33**(3), pp. 337–359.
- [45] American Standards for Testing of Materials, 2007, D440: Standard Test Method of Drop Shatter Test for Coal.
- [46] Pellet Fuels Institute, 2011, Standard Specification for Residential/Commercial Densified Fuel.

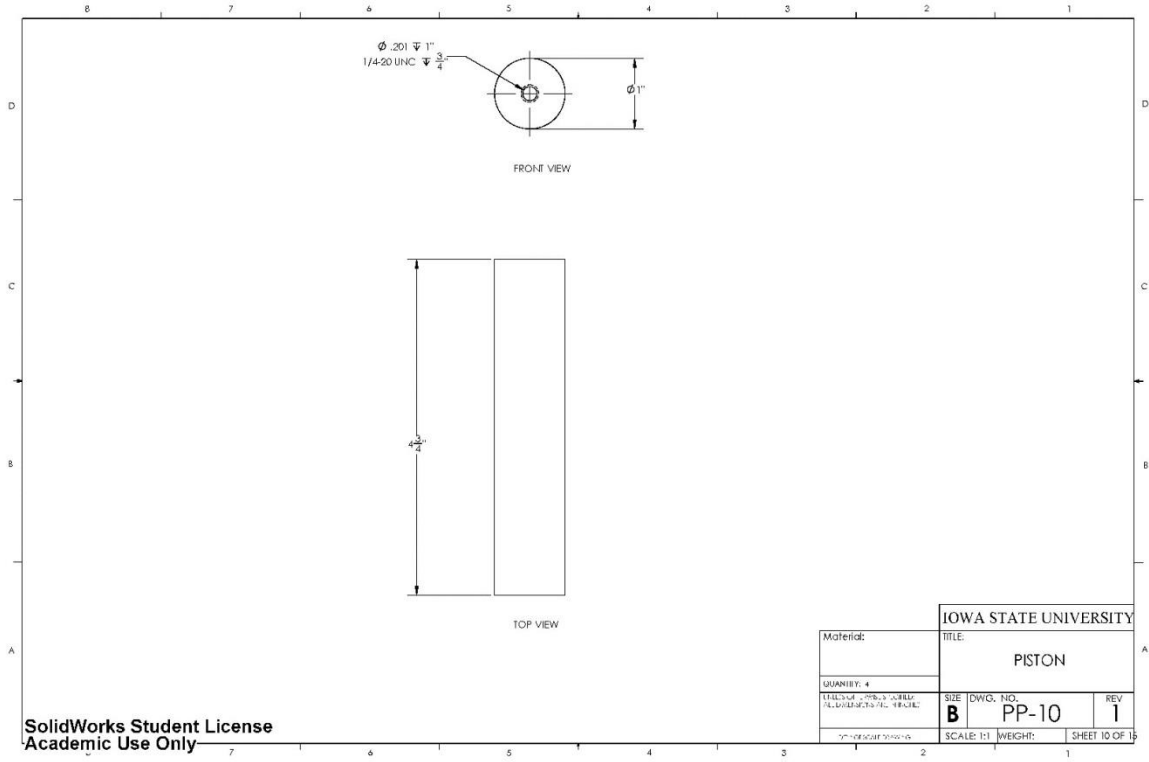
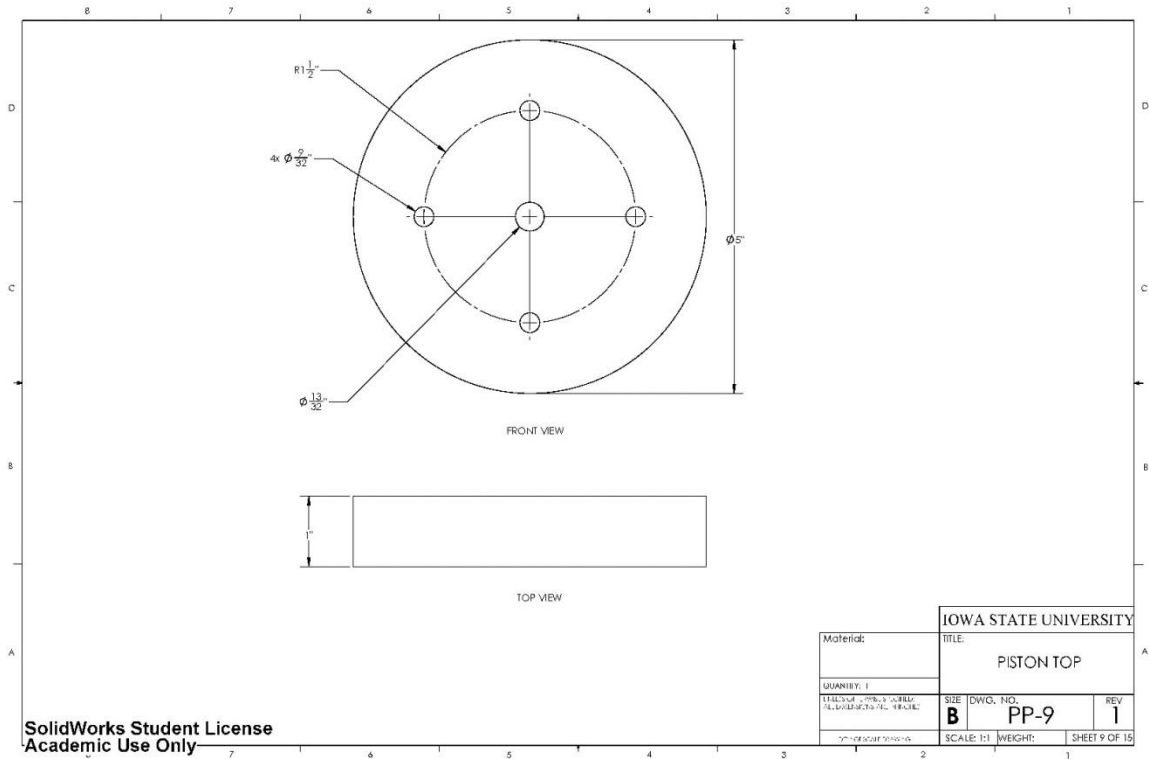
APPENDIX A: PELLET MOLD DRAWINGS

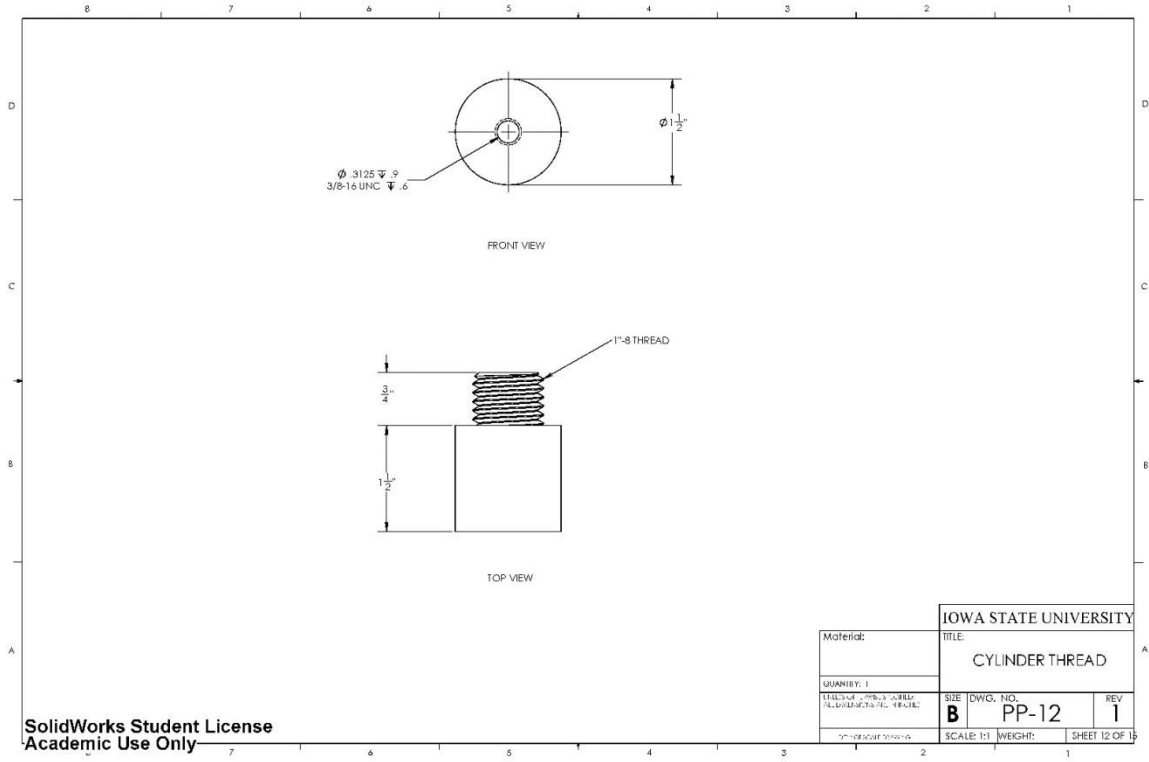
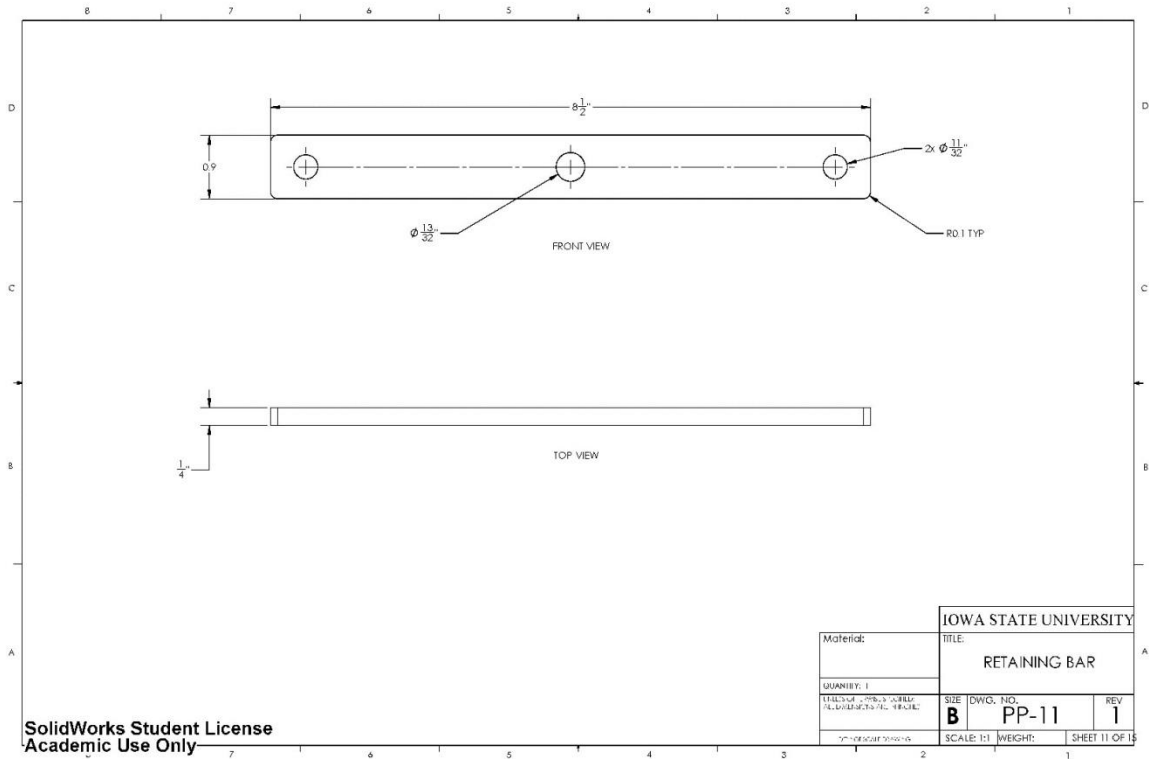




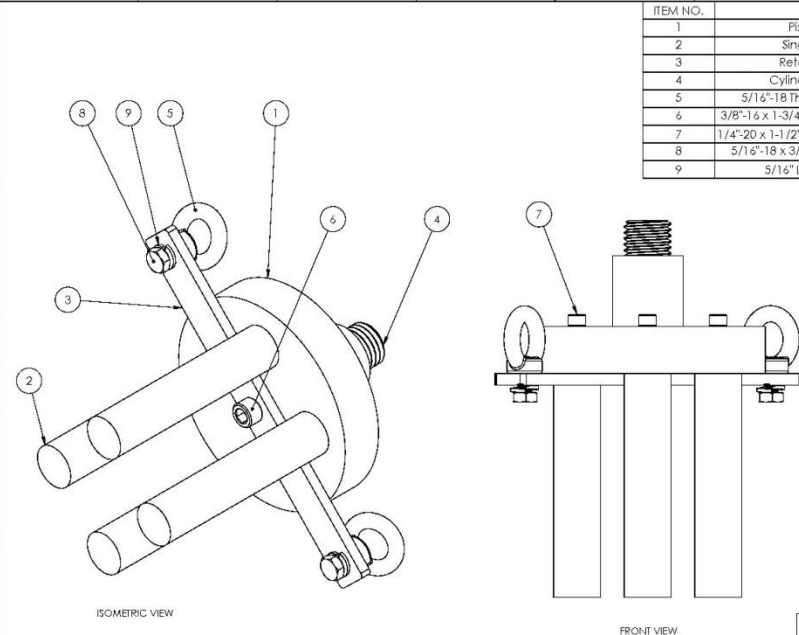








ITEM NO.	TITLE	DWG NO	QTY.
1	Piston Top	PP-9	1
2	Single Piston	PP-10	4
3	Retaining Bar	PP-11	1
4	Cylinder Threads	PP-12	1
5	5/16"-18 Threaded Eye Nut		2
6	3/8"-16 x 1-3/4" Socket Cap Screw		1
7	1/4"-20 x 1-1/2" Socket Head Screw		4
8	5/16"-18 x 3/4" Hex Cap Screw		2
9	5/16" Lock Washer		2



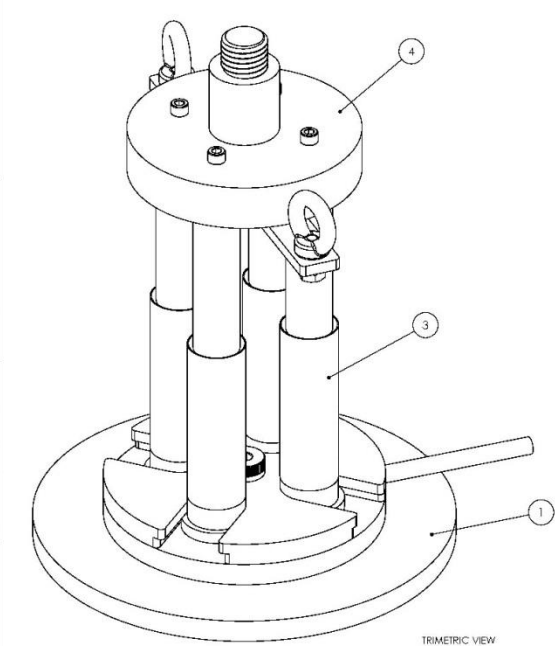
ISOMETRIC VIEW

FRONT VIEW

IOWA STATE UNIVERSITY			
TITLE: PISTON ASSEMBLY			
MATERIAL:	SIZE: B	DWG. NO: PP-13	REV: 1
QUANTITY: 1	SCALE: 2:1	WEIGHT:	SHEET 13 OF 15

SolidWorks Student License
Academic Use Only

ITEM NO.	TITLE	DWG NO	QTY.
1	Mold Base	PP-6	1
2	Mold Slug	PP-7	4
3	Single Mold	PP-8	4
4	Piston Assembly	PP-13	1
5	Top Ram	PP-14	4



TRIMETRIC VIEW

IOWA STATE UNIVERSITY			
TITLE: PELLET PRESS ASSEMBLY			
MATERIAL:	SIZE: B	DWG. NO: PP-15	REV: 1
QUANTITY: 1	SCALE: 2:1	WEIGHT:	SHEET 15 OF 15

SolidWorks Student License
Academic Use Only

APPENDIX B: EXPERIMENTAL DATA**Coal particle size distributions**

Sieve mesh number	Sieve size opening (μm)	Cumulative percentage of sample retained on each sieve (sorted by coal distribution)					As received
		$-\alpha$	-1	0	1	$+\alpha$	
--	25000	--	--	--	--	--	8.80
--	19000	--	--	--	--	--	18.37
--	13300	--	--	--	--	--	32.59
--	9432	--	--	--	--	--	50.89
3.5	5600	--	--	--	--	9.42	66.13
4	4750	--	--	--	--	18.98	--
6	3350	--	--	--	10.34	35.53	73.88
8	2360	--	--	--	38.54	49.06	--
10	2000	--	--	14.65	--	59.08	--
12	1680	--	--	27.13	56.44	67.92	--
14	1400	--	--	37.25	--	--	--
16	1180	--	--	46.03	68.46	--	85.72
20	850	--	--	59.25	75.34	--	--
35	500	--	--	72.47	83.31	82.33	--
50	300	--	19.75	--	--	--	--
60	250	--	28.03	--	--	--	--
80	180	4.54	45.53	--	--	--	--
100	150	28.67	68.16	90.54	93.99	--	--
120	125	39.56	82.52	--	--	--	--
140	106	57.90	93.29	--	--	--	--
170	90	75.66	--	--	--	--	--
200	75	87.71	96.05	--	--	--	--
230	63	99.14	--	--	--	--	--
Pan	--	100	100	100	100	100	100

Higher heating value

Exp. ID	Run ID	HHV Avg. (MJ/kg)	HHV Std. (MJ/kg)
1	20	27.80	0.105
2	16	27.75	0.107
3	24	27.60	0.160
4	15	28.06	0.112
5	22	27.37	0.053
6	13	27.31	0.086
7	9	27.68	0.128
8	14	27.76	0.126
9	31	27.59	0.518
10	17	28.92	0.037
11	5	27.04	0.150
12	29	28.23	0.123
13	18	27.64	0.063
14	25	27.58	0.311
15	12	28.78	0.100
16	26	28.55	0.059
17	3	28.53	0.075
18	11	28.79	0.050
19	10	28.28	0.171
20	4	27.65	0.030
21	30	28.32	0.125
22	28	27.23	0.333
23	27	27.17	0.074
24	8	27.95	0.135
25	7	28.20	0.243
26	23	28.02	0.191
27	6	27.67	0.377
28	2	27.30	0.319
29	1	27.35	0.120
30	21	27.29	0.154
31	19	27.19	0.071
Coal		27.58	0.392
Red Oak		18.43	0.130
Cyclone 1 Biochar		26.69	0.771
Cyclone 2 Biochar		25.78	1.535
CPO		24.23	0.058

Proximate analysis

Exp. ID	Run ID	Fixed				Fixed			
		Moisture Average (wt%)	Volatiles Average (wt%)	Carbon Average (wt%)	Ash Average (wt%)	Moisture Std. Dev. (wt%)	Volatiles Std. Dev. (wt%)	Carbon Std. Dev. (wt%)	Ash Std. Dev. (wt%)
1	20	6.91	39.52	47.31	6.26	0.124	0.256	0.593	0.313
2	16	7.17	38.81	46.67	7.36	0.129	0.166	0.697	0.842
3	24	7.74	40.00	45.56	6.71	0.589	0.595	0.710	0.722
4	15	6.50	39.13	47.04	7.33	0.306	0.472	0.669	0.970
5	22	7.18	39.07	47.06	6.69	0.541	0.590	0.754	0.929
6	13	8.25	39.21	46.33	6.21	0.657	0.605	0.466	0.827
7	9	7.26	39.47	46.91	6.37	0.097	0.376	0.433	0.218
8	14	7.28	39.49	46.68	6.55	0.431	0.213	0.238	0.018
9	31	6.03	41.30	46.28	6.39	0.995	2.940	0.470	1.839
10	17	4.15	39.86	48.64	7.35	0.559	0.728	0.612	0.837
11	5	10.05	37.10	45.75	7.09	0.920	0.367	0.876	0.375
12	29	5.08	38.56	49.40	6.96	1.104	1.787	0.720	0.667
13	18	3.69	43.89	45.70	6.72	0.508	0.724	0.778	0.495
14	25	7.72	39.66	45.72	6.90	0.182	0.516	0.212	0.678
15	12	3.65	40.77	48.38	7.20	0.389	0.574	0.440	1.144
16	26	4.46	40.72	47.53	7.28	0.230	0.309	0.524	0.015
17	3	5.06	40.72	47.16	7.06	0.261	0.318	0.254	0.590
18	11	4.83	42.69	45.97	6.51	0.463	0.058	0.405	0.001
19	10	5.85	41.23	46.45	6.47	0.272	0.169	0.242	0.329
20	4	8.99	38.71	45.88	6.42	0.097	0.652	0.575	0.191
21	30	6.13	38.59	47.74	7.55	0.373	0.217	0.025	0.203
22	28	8.83	40.91	44.08	6.18	1.108	0.243	0.996	0.091
23	27	8.30	41.95	43.36	6.39	0.198	0.348	0.201	0.239
24	8	6.48	37.94	48.21	7.38	0.656	1.154	1.126	1.628
25	7	5.94	38.52	48.97	6.57	0.566	0.681	0.843	0.985
26	23	5.21	42.24	46.05	6.50	1.143	1.011	0.913	1.235
27	6	5.16	42.94	45.29	6.61	1.389	1.046	0.897	1.282
28	2	9.05	39.27	46.04	5.64	0.578	0.305	0.351	0.530
29	1	8.10	37.78	47.42	6.71	0.712	0.631	0.985	0.786
30	21	7.30	43.32	43.76	5.62	0.634	0.653	1.359	0.444
31	19	8.93	42.19	43.59	5.29	0.471	0.234	0.355	0.872
Coal		5.66	33.62	51.89	8.84	0.272	1.558	1.327	1.767
Red Oak		6.24	76.02	17.49	0.25	0.034	0.179	0.142	0.044
Cyclone 1 Biochar		1.67	13.98	63.20	21.15	0.052	0.225	2.307	2.219
Cyclone 2 Biochar		2.43	22.48	62.62	12.47	0.047	0.673	1.651	2.323
CPO		11.17	65.42	23.36	0.05	1.349	1.058	0.398	0.029

Ultimate analysis

Exp. ID	Run ID	C Avg.	H2 Avg.	N2 Avg.	S Avg.	O2 Avg.	C Std.	H2 Std.	N2 Std.	S Std.	O2 Std.
		(wt%)	(wt%)	(wt%)	(wt%)	(wt%)	Dev.	Dev.	Dev.	Dev.	Dev.
1	20	69.86	5.630	1.161	1.565	15.52	0.588	0.0805	0.0160	0.0217	0.665
2	16	67.51	5.610	1.103	1.803	16.58	0.369	0.0457	0.0162	0.1124	0.178
3	24	68.74	5.730	1.131	1.722	15.97	0.462	0.0604	0.0501	0.0637	0.574
4	15	68.76	5.591	1.119	1.780	15.42	0.414	0.0479	0.0156	0.0566	0.408
5	22	67.70	5.564	1.113	1.574	17.36	0.424	0.0619	0.0178	0.0038	0.384
6	13	67.95	5.370	1.088	1.602	18.62	0.928	0.1579	0.0664	0.0223	0.385
7	9	67.84	5.594	1.212	1.597	17.39	0.133	0.0285	0.0121	0.0924	0.154
8	14	69.35	5.497	1.127	1.828	15.78	0.315	0.0238	0.0050	0.1564	0.318
9	31	66.31	5.743	0.997	1.585	18.97	0.828	0.0996	0.0555	0.0956	0.943
10	17	70.21	5.527	1.213	1.755	13.90	0.076	0.0319	0.0035	0.0770	0.166
11	5	66.86	5.227	1.170	1.779	17.87	0.484	0.0429	0.0126	0.0568	0.594
12	29	69.75	5.509	1.214	1.816	14.75	0.608	0.0320	0.0013	0.0166	0.651
13	18	69.46	5.502	1.032	1.568	16.25	1.347	0.1597	0.1128	0.0448	1.087
14	25	68.09	5.571	1.074	1.533	16.63	0.689	0.1386	0.0296	0.0328	0.568
15	12	70.23	5.421	1.132	1.936	13.66	0.981	0.0712	0.0599	0.0811	0.482
16	26	70.35	5.518	1.175	1.867	13.81	0.155	0.0369	0.0106	0.0322	0.205
17	3	69.51	5.369	1.252	2.133	14.45	0.503	0.0396	0.0217	0.0472	0.366
18	11	67.22	5.651	1.185	1.630	17.81	0.191	0.0360	0.0193	0.0373	0.174
19	10	69.40	5.459	1.094	1.649	16.03	0.526	0.0962	0.0903	0.0424	0.274
20	4	68.86	5.343	1.222	2.090	16.07	0.947	0.0414	0.0181	0.0280	1.033
21	30	71.16	5.462	1.244	1.840	12.75	0.661	0.0494	0.0192	0.0420	0.700
22	28	66.44	5.897	0.945	1.534	19.00	0.163	0.0765	0.0232	0.0819	0.073
23	27	67.78	5.563	0.969	1.541	17.56	0.513	0.1326	0.0240	0.0246	0.446
24	8	70.55	5.406	1.306	2.181	13.18	0.382	0.0190	0.0186	0.0424	0.362
25	7	69.90	5.365	1.243	2.154	15.01	0.455	0.0260	0.0191	0.4223	0.429
26	23	68.03	5.785	1.004	1.483	17.20	0.209	0.0777	0.0126	0.0301	0.110
27	6	69.54	5.662	1.123	1.408	15.73	1.436	0.1305	0.0534	0.2531	1.297
28	2	66.71	5.478	1.168	1.903	19.10	0.883	0.0565	0.0489	0.0950	0.883
29	1	67.78	5.359	1.183	2.084	16.91	1.337	0.0663	0.0075	0.0916	1.341
30	21	67.64	5.755	1.075	1.533	18.38	2.223	0.1714	0.1050	0.1902	2.439
31	19	67.20	5.796	0.993	1.477	19.09	1.180	0.1228	0.1123	0.0784	1.248
Coal		73.42	5.204	1.510	2.334	11.44	0.319	0.0224	0.0124	0.4154	0.379
Red Oak		46.97	6.406	0.200	0.010	40.15	0.644	0.1493	0.0315	0.0054	0.772
Cyclone 1 Biochar		70.48	2.610	0.262	0.006	20.39	0.532	0.0188	0.0214	0.0018	0.571
Cyclone 2 Biochar		74.99	3.382	0.318	0.010	15.04	2.382	0.1147	0.0099	0.0009	2.486
CPO		58.94	6.666	0.336	0.002	27.80	0.532	0.1786	0.0498	0.0009	0.577

Strength and durability tests

Exp. ID	Run ID	Indirect Tensile Strength Average (kPa)	Indirect Tensile Strength Std. Dev. (kPa)	Impact Resistance Average	Impact Resistance Std. Dev.	Abrasion Resistance
1	20	161	4.0	1000	0.00	99.2
2	16	175	26.1	1000	0.00	99.1
3	24	584	443	170	125.3	45.9
4	15	136	21.1	189	139.8	94.4
5	22	147	8.0	1000	0.00	96.8
6	13	285	22.2	1000	0.00	98.5
7	9	237	34.7	383	534.6	98.3
8	14	216	87.6	467	462.6	85.7
9	31	437	81.7	767	404.1	97.8
10	17	584	176	194	122.9	84.4
11	5	1055	472	492	454.4	91.4
12	29	384	190	1000	0.00	71.9
13	18	179	31.6	1000	0.00	98.3
14	25	627	54.7	147	89.11	89.3
15	12	655	71.7	722	481.1	97.0
16	26	319	38.0	1000	0.00	95.6
17	3	722	55.3	432	492.96	86.0
18	11	565	287	167	57.74	92.3
19	10	177	94.1	1000	0.00	98.4
20	4	453	78.4	567	404.1	96.0
21	30	147	28.7	1000	0.00	99.6
22	28	388	50.8	1000	0.00	97.8
23	27	427	108	767	404.1	98.8
24	8	225	10.5	1000	0.00	98.9
25	7	333	31.1	1000	0.00	99.5
26	23	78	45.9	144	50.92	41.7
27	6	301	17.4	1000	0.00	95.0
28	2	287	38.0	1000	0.00	99.6
29	1	338	126	172	85.53	73.1
30	21	113	71.8	178	19.25	70.0
31	19	209	32.6	1000	0.00	97.2
Coal		547	529	120	81.87	75.1

Mass and particle densities

Exp. ID	Run ID	Mass Density Average (g/cm ³)	Mass Density Std. Dev. (g/cm ³)	Particle Density Average (g/cm ³)	Particle Density Std. Dev. (g/cm ³)
1	20	1.22	0.01	1.341	0.004
2	16	1.25	0.00	1.360	0.007
3	24	1.09	0.03	1.350	0.011
4	15	1.20	0.02	1.341	0.003
5	22	1.25	0.01	1.345	0.006
6	13	1.23	0.01	1.365	0.010
7	9	1.24	0.01	1.332	0.004
8	14	1.20	0.00	1.418	0.012
9	31	1.25	0.01	1.350	0.010
10	17	1.17	0.01	1.295	0.003
11	5	1.25	0.01	1.382	0.017
12	29	0.93	0.01	1.394	0.010
13	18	1.27	0.00	1.323	0.002
14	25	1.18	0.03	1.370	0.013
15	12	1.26	0.01	1.326	0.004
16	26	1.27	0.01	1.373	0.007
17	3	1.22	0.00	1.443	0.006
18	11	1.29	0.01	1.287	0.010
19	10	1.27	0.01	1.389	0.005
20	4	1.28	0.00	1.461	0.005
21	30	1.27	0.01	1.424	0.010
22	28	1.28	0.00	1.362	0.013
23	27	1.25	0.00	1.379	0.013
24	8	1.27	0.01	1.359	0.006
25	7	1.27	0.00	1.352	0.008
26	23	1.10	0.00	1.316	0.003
27	6	1.22	0.00	1.343	0.003
28	2	1.27	0.01	1.428	0.007
29	1	1.17	0.01	1.426	0.011
30	21	1.15	0.02	1.376	0.010
31	19	1.39	0.07	1.352	0.012

APPENDIX C: STATISTICAL MODELS

Pellet heating value full model

Summary of Fit

Rsquare	0.834
RSquare Adj	0.689
Root Mean Square Error	0.293
Mean of Response	27.83

Analysis of Variance

Source	DF	Sum of Squares	Mean Square	F Ratio	Model Test	
					Prob > F	Significance
Model	14	6.9051	0.4932	5.744	0.0007	YES
Error	16	1.3739	0.0859			
C. Total	30	8.2790				

Lack Of Fit

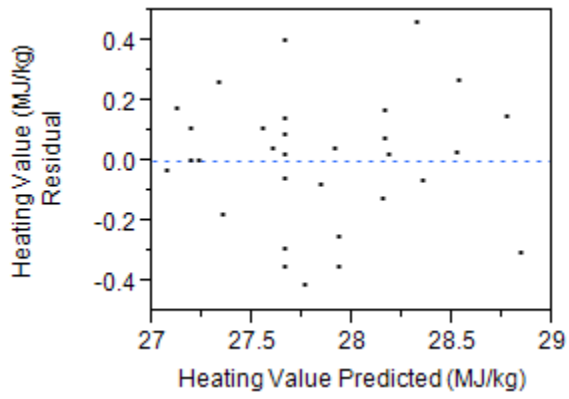
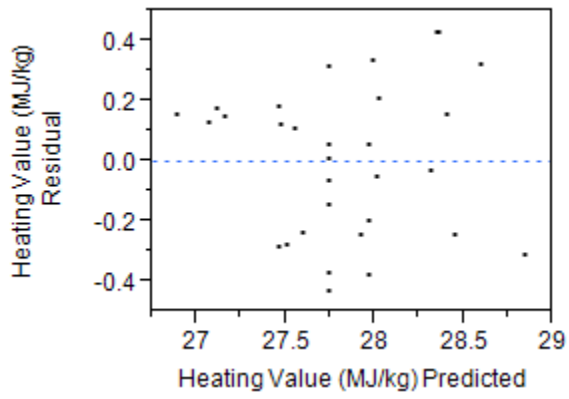
Source	DF	Sum of Squares	Mean Square	F Ratio	Lack of Fit Test	
					Prob > F	Significance
Lack Of Fit	10	0.9759	0.0976	1.471	0.3296	NO
Pure Error	6	0.3979	0.0663			
Total Error	16	1.3739		Max RSq	0.9519	

Terms

Source	Estimate	DF	Sum of Squares	F Ratio	Term Test	
					Prob > F	Significance
Particle (x_1)	-5.2100E-04	1	0.0899	1.0465	0.322	NO
Moisture (x_2)	-2.0957E-01	1	0.1928	2.2449	0.154	NO
Binder (x_3)	-3.1670E-02	1	0.0121	0.1415	0.712	NO
Cure (x_4)	-1.9820E-03	1	0.0045	0.0523	0.822	NO
Particle x Moisture (x_1x_2)	2.5175E-05	1	0.0698	0.8132	0.381	NO
Particle x Binder (x_1x_3)	1.1289E-05	1	0.0562	0.6540	0.431	NO
Moisture x Binder (x_2x_3)	-4.4100E-03	1	0.1008	1.1740	0.295	NO
Particle x Cure (x_1x_4)	-2.4240E-07	1	0.0018	0.0209	0.887	NO
Moisture x Cure (x_2x_4)	4.9580E-04	1	0.0885	1.0307	0.325	NO
Binder x Cure (x_3x_4)	-4.1000E-04	1	0.2426	2.8248	0.112	NO
Particle x Particle (x_1x_1)	-4.3880E-08	1	0.0105	0.1225	0.731	NO
Moisture x Moisture (x_2x_2)	7.2398E-03	1	0.1219	1.4194	0.251	NO
Binder x Binder (x_3x_3)	1.4975E-03	1	0.0834	0.9716	0.339	NO
Cure x Cure (x_4x_4)	4.6063E-05	1	0.3807	4.4337	0.051	NO

Intercept

Source	Estimate	t Ratio	Intercept Test	
			Prob> t	Significance
Intercept (β)	29.7820	20.37	<.0001	YES

Residuals for pellet heating value full model**Residuals for pellet heating value reduced model**

Pellet heating value reduced model**Summary of Fit**

Rsquare	0.773
RSquare Adj	0.716
Root Mean Square Error	0.280
Mean of Response	27.83

Analysis of Variance

Source	DF	Sum of Squares	Mean Square	F Ratio	Model Test	
					Prob > F	Significance
Model	6	6.3985	1.0664	13.611	<.0001	YES
Error	24	1.8804	0.0784			
C. Total	30	8.2790				

Lack Of Fit

Source	DF	Sum of Squares	Mean Square	F Ratio	Lack of Fit Test	
					Prob > F	Significance
Lack Of Fit	18	1.4825	0.0824	1.242	0.4212	NO
Pure Error	6	0.3979	0.0663			
Total Error	24	1.8804		Max RSq	0.9519	

Terms

Source	Estimate	DF	Sum of Squares	F Ratio	Term Test	
					Prob > F	Significance
Particle (x_1)	-2.2500E-04	1	0.7444	9.5014	0.005	YES
Moisture (x_2)	-1.4236E-01	1	4.3776	55.872	<.0001	YES
Binder (x_3)	2.5708E-02	1	0.0592	0.7560	0.393	NO
Cure (x_4)	1.8698E-03	1	0.0048	0.0611	0.807	NO
Binder x Cure (x_3x_4)	-4.1000E-04	1	0.2426	3.0958	0.091	NO
Cure x Cure (x_4x_4)	4.1341E-05	1	0.3142	4.0100	0.057	NO

Intercept

Source	Estimate	t Ratio	Intercept Test	
			Prob> t	Significance
Intercept (β)	28.5869	36.61	<.0001	YES

Reduced Model F-Test

Model	SSE	MSE	DF	F_{calc}	$H_0: F_{calc} > F_{0.05, df1, df2}$	
					$F_{0.05, df1, df2}$	Reject H_0 ?
Full	1.3739	0.0859	14	0.7374	2.6987	NO
Reduced	1.8804		6			

Pellet moisture full model**Summary of Fit**

Rsquare	0.824
RSquare Adj	0.670
Root Mean Square Error	0.981
Mean of Response	6.686

Analysis of Variance

Source	DF	Sum of Squares	Mean Square	F Ratio	Model Test	
					Prob > F	Significance
Model	14	72.0883	5.14916	5.349	0.001	YES
Error	16	15.4024	0.96265			
C. Total	30	87.4907				

Lack Of Fit

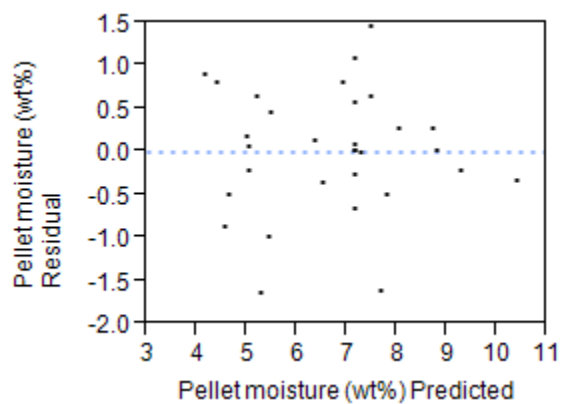
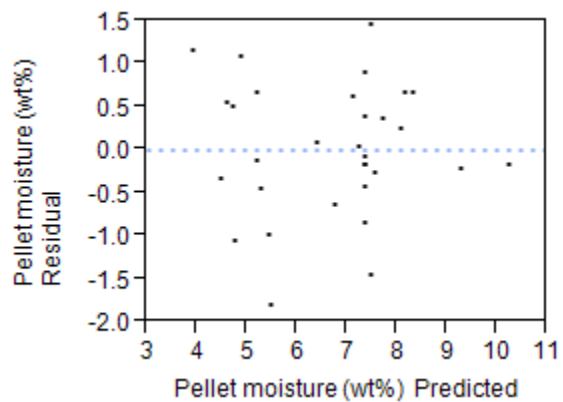
Source	DF	Sum of Squares	Mean Square	F Ratio	Lack of Fit Test	
					Prob > F	Significance
Lack Of Fit	10	13.4825	1.3483	4.213	0.046	YES
Pure Error	6	1.9199	0.3200			
Total Error	16	15.4024		Max RSq	0.9781	

Terms

Source	Estimate	DF	Sum of Squares	F Ratio	Term Test	
					Prob > F	Significance
Particle (x_1)	1.2855E-03	1	0.5470	0.568	0.462	NO
Moisture (x_2)	4.2144E-01	1	0.7795	0.810	0.382	NO
Binder (x_3)	6.6326E-01	1	5.3273	5.534	0.032	YES
Cure (x_4)	-4.8250E-03	1	0.0266	0.028	0.870	NO
Particle x Moisture (x_1x_2)	-3.4480E-05	1	0.1310	0.136	0.717	NO
Particle x Binder (x_1x_3)	-7.4000E-05	1	2.4102	2.504	0.133	NO
Moisture x Binder (x_2x_3)	6.8750E-03	1	0.2450	0.255	0.621	NO
Particle x Cure (x_1x_4)	2.4000E-06	1	0.1761	0.183	0.675	NO
Moisture x Cure (x_2x_4)	-1.5580E-03	1	0.8742	0.908	0.355	NO
Binder x Cure (x_3x_4)	1.2125E-03	1	2.1170	2.199	0.158	NO
Particle x Particle (x_1x_1)	2.4020E-07	1	0.3151	0.327	0.575	NO
Moisture x Moisture (x_2x_2)	9.6182E-03	1	0.2151	0.224	0.643	NO
Binder x Binder (x_3x_3)	-1.6450E-02	1	10.0673	10.458	0.005	YES
Cure x Cure (x_4x_4)	-1.0700E-04	1	2.0494	2.129	0.164	NO

Intercept

Source	Estimate	t Ratio	Intercept Test	
			Prob> t	Significance
Intercept (β)	-3.2273	-0.66	0.519	NO

Residuals for pellet moisture full model**Residuals for pellet moisture reduced model**

Pellet moisture reduced model**Summary of Fit**

Rsquare	0.801
RSquare Adj	0.729
Root Mean Square Error	0.890
Mean of Response	6.686

Analysis of Variance

Source	DF	Sum of Squares	Mean Square	F Ratio	Model Test	
					Prob > F	Significance
Model	8	70.0836	8.76045	11.072	<.0001	YES
Error	22	17.4071	0.79123			
C. Total	30	87.4907				

Lack Of Fit

Source	DF	Sum of Squares	Mean Square	F Ratio	Lack of Fit Test	
					Prob > F	Significance
Lack Of Fit	16	15.4872	0.9679	3.025	0.089	NO
Pure Error	6	1.9199	0.3200			
Total Error	22	17.4071		Max RSq	0.9781	

Terms

Source	Estimate	DF	Sum of Squares	F Ratio	Term Test	
					Prob > F	Significance
Particle (x_1)	1.8812E-03	1	2.5733	3.252	0.085	NO
Moisture (x_2)	4.7833E-01	1	49.4214	62.461	<.0001	YES
Binder (x_3)	7.0498E-01	1	6.6606	8.418	0.008	YES
Cure (x_4)	-1.1599E-02	1	0.1837	0.232	0.635	NO
Particle x Binder (x_1x_3)	-7.4000E-05	1	2.4102	3.046	0.095	NO
Binder x Cure (x_3x_4)	1.2125E-03	1	2.1170	2.676	0.116	NO
Binder x Binder (x_3x_3)	-1.6459E-02	1	10.2471	12.951	0.002	YES
Cure x Cure (x_4x_4)	-1.0700E-04	1	2.0890	2.640	0.118	NO

Intercept

Source	Estimate	Intercept Test		
		t Ratio	Prob> t	Significance
Intercept (β)	-3.6296	-0.97	0.3417	NO

Reduced Model F-Test

Model	SSE	MSE	DF	F_{calc}	$H_0: F_{calc} > F_{0.05, df1, df2}$	
					$F_{0.05, df1, df2}$	Reject H_0 ?
Full	15.4024	0.9627	14	0.3471	2.8477	NO
Reduced	17.4071		8			

Pellet volatiles full model**Summary of Fit**

Rsquare	0.913
RSquare Adj	0.836
Root Mean Square Error	0.705
Mean of Response	40.179

Analysis of Variance

Source	DF	Sum of Squares	Mean Square	F Ratio	Model Test	
					Prob > F	Significance
Model	14	82.9606	5.9258	11.922	<.0001	YES
Error	16	7.9529	0.4971			
C. Total	30	90.9136				

Lack Of Fit

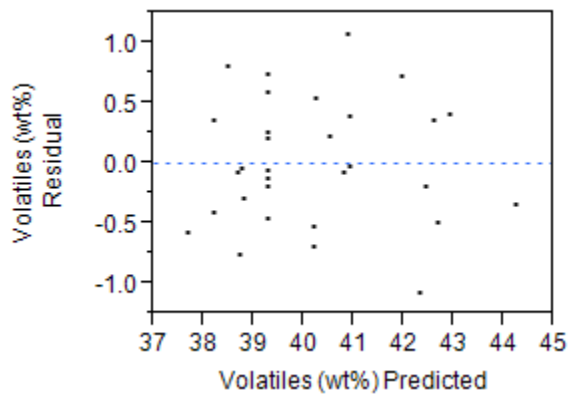
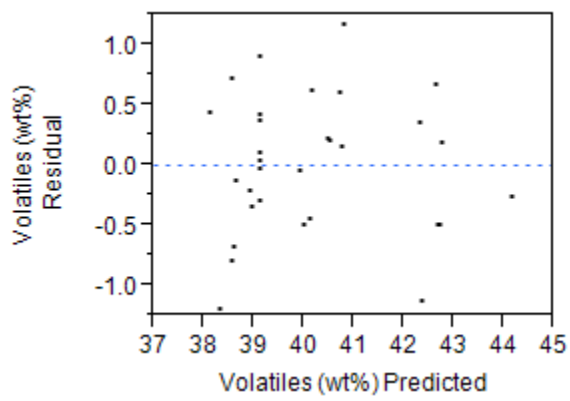
Source	DF	Sum of Squares	Mean Square	F Ratio	Lack of Fit Test	
					Prob > F	Significance
Lack Of Fit	10	7.0574	0.7057	4.728	0.0352	YES
Pure Error	6	0.8956	0.1493			
Total Error	16	7.9529		Max RSq	0.9901	

Terms

Source	Estimate	DF	Sum of Squares	F Ratio	Term Test	
					Prob > F	Significance
Particle (x_1)	-5.5520E-03	1	10.2026	20.526	0.0003	YES
Moisture (x_2)	-1.8467E-01	1	0.1497	0.301	0.591	NO
Binder (x_3)	-5.8105E-01	1	4.0886	8.226	0.011	YES
Cure (x_4)	-1.8450E-02	1	0.3893	0.783	0.389	NO
Particle x Moisture (x_1x_2)	1.4370E-04	1	2.2762	4.579	0.048	YES
Particle x Binder (x_1x_3)	1.0820E-04	1	5.1638	10.389	0.005	YES
Moisture x Binder (x_2x_3)	9.7917E-03	1	0.4970	1.000	0.332	NO
Particle x Cure (x_1x_4)	-1.0310E-06	1	0.0325	0.066	0.801	NO
Moisture x Cure (x_2x_4)	-6.3300E-04	1	0.1444	0.291	0.597	NO
Binder x Cure (x_3x_4)	3.7500E-05	1	0.0020	0.004	0.950	NO
Particle x Particle (x_1x_1)	1.0561E-06	1	6.0908	12.254	0.003	YES
Moisture x Moisture (x_2x_2)	-2.1892E-02	1	1.1144	2.242	0.154	NO
Binder x Binder (x_3x_3)	1.3590E-02	1	6.8708	13.823	0.002	YES
Cure x Cure (x_4x_4)	9.4688E-05	1	1.6087	3.236	0.091	NO

Intercept

Source	Estimate	t Ratio	Intercept Test	
			Prob> t	Significance
Intercept (β)	48.2337	13.71	<.0001	YES

Residuals for pellet volatiles full model**Residuals for pellet volatiles reduced model**

Pellet volatiles reduced model**Summary of Fit**

Rsquare	0.893
RSquare Adj	0.847
Root Mean Square Error	0.681
Mean of Response	40.179

Analysis of Variance

Source	DF	Sum of Squares	Mean Square	F Ratio	Model Test	
					Prob > F	Significance
Model	9	81.1702	9.0189	19.439	<.0001	YES
Error	21	9.7434	0.4640			
C. Total	30	90.9136				

Lack Of Fit

Source	DF	Sum of Squares	Mean Square	F Ratio	Lack of Fit Test	
					Prob > F	Significance
Lack Of Fit	15	8.8478	0.5899	3.952	0.0496	YES
Pure Error	6	0.8956	0.1493			
Total Error	21	9.7434		Max RSq	0.9901	

Terms

Source	Estimate	DF	Sum of Squares	F Ratio	Term Test	
					Prob > F	Significance
Particle (x_1)	-5.5890E-03	1	12.2775	26.462	<.0001	YES
Moisture (x_2)	-2.8838E-01	1	5.6132	12.098	0.002	YES
Binder (x_3)	-5.4483E-01	1	4.5684	9.846	0.005	YES
Cure (x_4)	-2.4388E-02	1	1.7792	3.835	0.064	NO
Particle x Moisture (x_1x_2)	1.4370E-04	1	2.2762	4.906	0.038	YES
Particle x Binder (x_1x_3)	1.0820E-04	1	5.1638	11.130	0.003	YES
Particle x Particle (x_1x_1)	1.0179E-06	1	5.6994	12.284	0.002	YES
Binder x Binder (x_3x_3)	1.4153E-02	1	7.5317	16.233	0.001	YES
Cure x Cure (x_4x_4)	1.0280E-04	1	1.9163	4.130	0.055	NO

Intercept

Source	Estimate	t Ratio	Intercept Test	
			Prob> t	Significance
Intercept (β)	48.3166	20.28	<.0001	YES

Reduced Model F-Test

Model	SSE	MSE	DF	F_{calc}	$H_0: F_{calc} > F_{0.05, df1, df2}$	
					$F_{0.05, df1, df2}$	Reject H_0 ?
Full	7.9529	0.4971	14	0.7204	2.9582	NO
Reduced	9.7434		9			

Pellet fixed carbon full model**Summary of Fit**

Rsquare	0.871
RSquare Adj	0.758
Root Mean Square Error	0.741
Mean of Response	46.482

Analysis of Variance

Source	DF	Sum of Squares	Mean Square	F Ratio	Model Test	
					Prob > F	Significance
Model	14	59.1396	4.2243	7.698	0.0001	YES
Error	16	8.7797	0.54873			
C. Total	30	67.9192				

Lack Of Fit

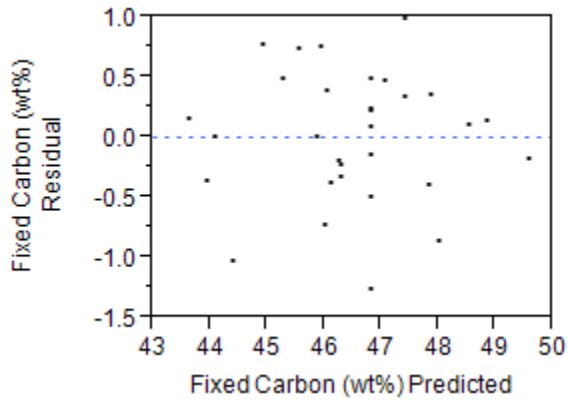
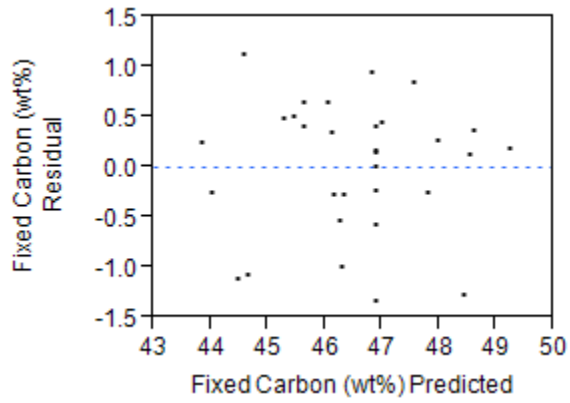
Source	DF	Sum of Squares	Mean Square	F Ratio	Lack of Fit Test	
					Prob > F	Significance
Lack Of Fit	10	6.6809	0.6681	1.910	0.2212	NO
Pure Error	6	2.0987	0.3498			
Total Error	16	8.7797		Max RSq	0.9691	

Terms

Source	Estimate	DF	Sum of Squares	F Ratio	Term Test	
					Prob > F	Significance
Particle (x_1)	3.2003E-03	1	3.3900	6.178	0.024	YES
Moisture (x_2)	-1.9154E-02	1	0.0016	0.003	0.958	NO
Binder (x_3)	-8.6322E-02	1	0.0902	0.164	0.691	NO
Cure (x_4)	2.6450E-02	1	0.8001	1.458	0.245	NO
Particle x Moisture (x_1x_2)	-3.8880E-05	1	0.1665	0.304	0.589	NO
Particle x Binder (x_1x_3)	-4.0850E-05	1	0.7352	1.340	0.264	NO
Moisture x Binder (x_2x_3)	-1.4514E-02	1	1.0920	1.990	0.178	NO
Particle x Cure (x_1x_4)	8.7630E-08	1	0.0002	0.000	0.984	NO
Moisture x Cure (x_2x_4)	9.3330E-04	1	0.3136	0.572	0.461	NO
Binder x Cure (x_3x_4)	-1.0000E-03	1	1.4400	2.624	0.125	NO
Particle x Particle (x_1x_1)	-9.0300E-07	1	4.4526	8.114	0.012	YES
Moisture x Moisture (x_2x_2)	2.1071E-03	1	0.0103	0.019	0.893	NO
Binder x Binder (x_3x_3)	2.9920E-03	1	0.3331	0.607	0.447	NO
Cure x Cure (x_4x_4)	-6.9150E-06	1	0.0086	0.016	0.902	NO

Intercept

Source	Estimate	t Ratio	Intercept Test	
			Prob> t	Significance
Intercept (β)	47.3316	12.81	<.0001	YES

Residuals for pellet fixed carbon full model**Residuals for pellet fixed carbon reduced model**

Pellet fixed carbon reduced model**Summary of Fit**

Rsquare	0.810
RSquare Adj	0.772
Root Mean Square Error	0.718
Mean of Response	46.482

Analysis of Variance

Source	DF	Sum of Squares	Mean Square	F Ratio	Model Test	
					Prob > F	Significance
Model	5	55.0323	11.0065	21.352	<.0001	YES
Error	25	12.8870	0.5155			
C. Total	30	67.9192				

Lack Of Fit

Source	DF	Sum of Squares	Mean Square	F Ratio	Lack of Fit Test	
					Prob > F	Significance
Lack Of Fit	19	10.7882	0.5678	1.623	0.285	NO
Pure Error	6	2.0987	0.3498			
Total Error	25	12.8870		Max RSq	0.9691	

Terms

Source	Estimate	DF	Sum of Squares	F Ratio	Term Test	
					Prob > F	Significance
Particle (x_1)	1.9572E-03	1	4.2561	8.257	0.008	YES
Moisture (x_2)	-2.7139E-01	1	15.9088	30.862	<.0001	YES
Binder (x_3)	-1.9306E-01	1	32.2017	62.470	<.0001	YES
Cure (x_4)	6.4833E-03	1	2.5220	4.893	0.036	YES
Particle x Particle (x_1x_1)	-8.8540E-07	1	4.3584	8.455	0.008	YES

Intercept

Source	Estimate	t Ratio	Intercept Test	
			Prob> t	Significance
Intercept (β)	51.3035	63.46	<.0001	YES

Reduced Model F-Test

Model	SSE	MSE	DF	F_{calc}	$H_0: F_{calc} > F_{0.05, df1, df2}$	
					$F_{0.05, df1, df2}$	Reject H_0 ?
Full	8.7797	0.5487	14	0.8317	2.6458	NO
Reduced	12.8870		5			

Pellet ash full model**Summary of Fit**

Rsquare	0.628
RSquare Adj	0.302
Root Mean Square Error	0.455
Mean of Response	6.654

Analysis of Variance

Source	DF	Sum of Squares	Mean Square	F Ratio	Model Test	
					Prob > F	Significance
Model	14	5.5819	0.3987	1.929	0.1041	NO
Error	16	3.3066	0.2067			
C. Total	30	8.8885				

Lack Of Fit

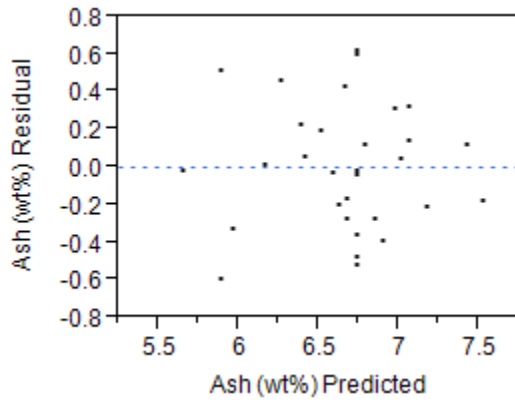
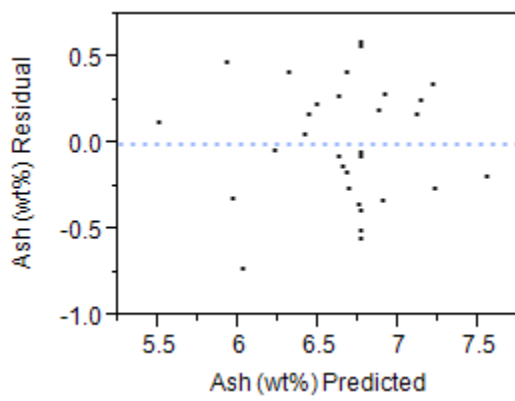
Source	DF	Sum of Squares	Mean Square	F Ratio	Lack of Fit Test	
					Prob > F	Significance
Lack Of Fit	10	1.9314	0.1931	0.843	0.6142	NO
Pure Error	6	1.3752	0.2292			
Total Error	16	3.3066		Max RSq	0.8453	

Terms

Source	Estimate	DF	Sum of Squares	F Ratio	Term Test	
					Prob > F	Significance
Particle (x_1)	1.0801E-03	1	0.3861	1.868	0.191	NO
Moisture (x_2)	-2.1402E-01	1	0.2010	0.973	0.339	NO
Binder (x_3)	5.8838E-03	1	0.0004	0.002	0.965	NO
Cure (x_4)	-3.0250E-03	1	0.0105	0.051	0.825	NO
Particle x Moisture (x_1x_2)	-7.0870E-05	1	0.5533	2.678	0.121	NO
Particle x Binder (x_1x_3)	6.3167E-06	1	0.0176	0.085	0.774	NO
Moisture x Binder (x_2x_3)	-2.2220E-03	1	0.0256	0.124	0.730	NO
Particle x Cure (x_1x_4)	-1.4840E-06	1	0.0674	0.326	0.576	NO
Moisture x Cure (x_2x_4)	1.2667E-03	1	0.5776	2.795	0.114	NO
Binder x Cure (x_3x_4)	-2.5400E-04	1	0.0930	0.450	0.512	NO
Particle x Particle (x_1x_1)	-3.9370E-07	1	0.8464	4.095	0.060	NO
Moisture x Moisture (x_2x_2)	9.9659E-03	1	0.2310	1.118	0.306	NO
Binder x Binder (x_3x_3)	-1.4700E-04	1	0.0008	0.004	0.951	NO
Cure x Cure (x_4x_4)	1.8877E-05	1	0.0639	0.309	0.586	NO

Intercept

Source	Estimate	t Ratio	Intercept Test	
			Prob> t	Significance
Intercept (β)	7.61728	3.36	0.004	YES

Residuals for pellet ash full model**Residuals for pellet ash reduced model**

Pellet ash reduced model**Summary of Fit**

Rsquare	0.598
RSquare Adj	0.451
Root Mean Square Error	0.403
Mean of Response	6.654

Analysis of Variance

Source	DF	Sum of Squares	Mean Square	F Ratio	Model Test	
					Prob > F	Significance
Model	8	5.3113	0.6639	4.083	0.0041	YES
Error	22	3.5772	0.1626			
C. Total	30	8.8885				

Lack Of Fit

Source	DF	Sum of Squares	Mean Square	F Ratio	Lack of Fit Test	
					Prob > F	Significance
Lack Of Fit	16	2.2020	0.1376	0.601	0.8063	NO
Pure Error	6	1.3752	0.2292			
Total Error	22	3.5772		Max RSq	0.8453	

Terms

Source	Estimate	DF	Sum of Squares	F Ratio	Term Test	
					Prob > F	Significance
Particle (x_1)	1.0368E-03	1	0.8729	5.3685	0.030	YES
Moisture (x_2)	-2.6214E-01	1	0.5947	3.6574	0.069	NO
Binder (x_3)	-3.8333E-02	1	1.2696	7.8081	0.011	YES
Cure (x_4)	-6.1670E-03	1	0.3260	2.0046	0.171	NO
Particle x Moisture (x_1x_2)	-7.0870E-05	1	0.5533	3.4031	0.079	NO
Moisture x Cure (x_2x_4)	1.2667E-03	1	0.5776	3.5523	0.073	NO
Particle x Particle (x_1x_1)	-3.8630E-07	1	0.8257	5.0782	0.035	YES
Moisture x Moisture (x_2x_2)	9.5318E-03	1	0.2154	1.3247	0.262	NO

Intercept

Source	Estimate	t Ratio	Intercept Test	
			Prob> t	Significance
Intercept (β)	8.5364	11.48	<.0001	YES

Reduced Model F-Test

Model	SSE	MSE	DF	F_{calc}	$H_0: F_{calc} > F_{0.05, df1, df2}$	
					$F_{0.05, df1, df2}$	Reject H_0 ?
Full	3.3066	0.2067	14	0.2182	2.8477	NO
Reduced	3.5772		8			

Pellet elemental carbon full model**Summary of Fit**

Rsquare	0.721
RSquare Adj	0.478
Root Mean Square Error	0.963
Mean of Response	68.603

Analysis of Variance

Source	DF	Sum of Squares	Mean Square	F Ratio	Model Test	
					Prob > F	Significance
Model	14	38.4221	2.7444	2.960	0.0202	YES
Error	16	14.8354	0.9272			
C. Total	30	53.2574				

Lack Of Fit

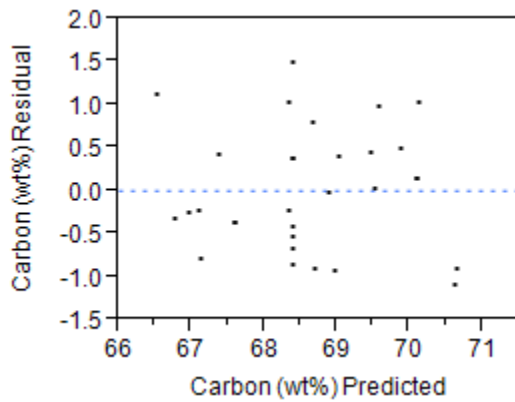
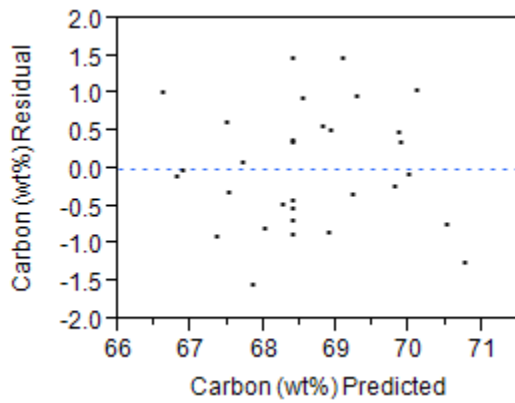
Source	DF	Sum of Squares	Mean Square	F Ratio	Lack of Fit Test	
					Prob > F	Significance
Lack Of Fit	10	10.6880	1.0688	1.546	0.3071	NO
Pure Error	6	4.1473	0.6912			
Total Error	16	14.8354		Max RSq	0.9221	

Terms

Source	Estimate	DF	Sum of Squares	F Ratio	Term Test	
					Prob > F	Significance
Particle (x_1)	2.6740E-04	1	0.0237	0.026	0.875	NO
Moisture (x_2)	-3.1141E-01	1	0.4256	0.459	0.508	NO
Binder (x_3)	-0.6772	1	5.5533	5.989	0.026	YES
Cure (x_4)	-2.4613E-02	1	0.6929	0.747	0.400	NO
Particle x Moisture (x_1x_2)	-1.5400E-04	1	2.6237	2.830	0.112	NO
Particle x Binder (x_1x_3)	7.9044E-05	1	2.7535	2.970	0.104	NO
Moisture x Binder (x_2x_3)	2.3264E-03	1	0.0281	0.030	0.864	NO
Particle x Cure (x_1x_4)	-4.9490E-06	1	0.7497	0.809	0.382	NO
Moisture x Cure (x_2x_4)	8.6250E-04	1	0.2678	0.289	0.598	NO
Binder x Cure (x_3x_4)	5.6460E-04	1	0.4590	0.495	0.492	NO
Particle x Particle (x_1x_1)	-4.9920E-07	1	1.3611	1.468	0.243	NO
Moisture x Moisture (x_2x_2)	5.8908E-03	1	0.0807	0.087	0.772	NO
Binder x Binder (x_3x_3)	8.9033E-03	1	2.9492	3.181	0.094	NO
Cure x Cure (x_4x_4)	8.3700E-05	1	1.2572	1.356	0.261	NO

Intercept

Source	Estimate	t Ratio	Intercept Test	
			Prob> t	Significance
Intercept (β)	80.2172	16.70	<.0001	YES

Residuals for pellet elemental carbon full model**Residuals for pellet elemental carbon reduced model**

Pellet elemental carbon reduced model**Summary of Fit**

Rsquare	0.648
RSquare Adj	0.540
Root Mean Square Error	0.903
Mean of Response	68.603

Analysis of Variance

Source	DF	Sum of Squares	Mean Square	F Ratio	Model Test	
					Prob > F	Significance
Model	7	34.4952	4.9279	6.041	0.0004	YES
Error	23	18.7622	0.8158			
C. Total	30	53.2574				

Lack Of Fit

Source	DF	Sum of Squares	Mean Square	F Ratio	Lack of Fit Test	
					Prob > F	Significance
Lack Of Fit	17	14.6149	0.8597	1.244	0.4196	NO
Pure Error	6	4.1473	0.6912			
Total Error	23	18.7622		Max RSq	0.9221	

Terms

Source	Estimate	DF	Sum of Squares	F Ratio	Term Test	
					Prob > F	Significance
Particle (x_1)	-1.4070E-03	1	1.1624	1.425	0.245	NO
Moisture (x_2)	-8.1388E-02	1	0.4471	0.548	0.467	NO
Binder (x_3)	-5.4450E-01	1	4.6220	5.666	0.026	YES
Cure (x_4)	8.9583E-03	1	4.8151	5.903	0.023	YES
Particle x Moisture (x_1x_2)	-1.5400E-04	1	2.6237	3.216	0.086	NO
Particle x Binder (x_1x_3)	7.9044E-05	1	2.7535	3.375	0.079	NO
Binder x Binder (x_3x_3)	7.8415E-03	1	2.3439	2.873	0.104	NO

Intercept

Source	Estimate	t Ratio	Intercept Test	
			Prob> t	Significance
Intercept (β)	76.8159	25.79	<.0001	YES

Reduced Model F-Test

Model	SSE	MSE	DF	F_{calc}	$H_0: F_{calc} > F_{0.05, df1, df2}$	
					$F_{0.05, df1, df2}$	Reject H_0 ?
Full	14.8354	0.9272	14	0.6050	2.7642	NO
Reduced	18.7622		7			

Pellet elemental hydrogen full model**Summary of Fit**

Rsquare	0.573
RSquare Adj	0.199
Root Mean Square Error	0.140
Mean of Response	5.547

Analysis of Variance

Source	DF	Sum of Squares	Mean Square	F Ratio	Model Test	
					Prob > F	Significance
Model	14	4.2089E-01	3.0063E-02	1.531	0.2056	NO
Error	16	3.1419E-01	1.9637E-02			
C. Total	30	7.3508E-01				

Lack Of Fit

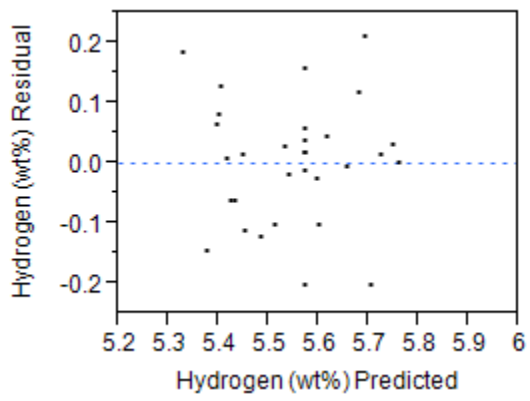
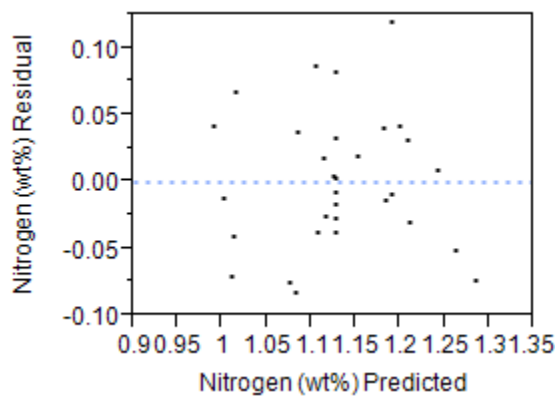
Source	DF	Sum of Squares	Mean Square	F Ratio	Lack of Fit Test	
					Prob > F	Significance
Lack Of Fit	10	2.4365E-01	2.4365E-02	2.072	0.1927	NO
Pure Error	6	7.0543E-02	1.1757E-02			
Total Error	16	3.1419E-01		Max RSq	0.9040	

Terms

Source	Estimate	DF	Sum of Squares	F Ratio	Term Test	
					Prob > F	Significance
Particle (x_1)	-2.9100E-04	1	2.8116E-02	1.432	0.249	NO
Moisture (x_2)	9.8041E-03	1	4.2185E-04	0.022	0.885	NO
Binder (x_3)	0.0289	1	1.0092E-02	0.514	0.484	NO
Cure (x_4)	1.7545E-03	1	3.5206E-03	0.179	0.678	NO
Particle x Moisture (x_1x_2)	-2.1540E-06	1	5.1098E-04	0.026	0.874	NO
Particle x Binder (x_1x_3)	5.7314E-06	1	1.4476E-02	0.737	0.403	NO
Moisture x Binder (x_2x_3)	1.7014E-03	1	1.5006E-02	0.764	0.395	NO
Particle x Cure (x_1x_4)	4.4662E-07	1	6.1047E-03	0.311	0.585	NO
Moisture x Cure (x_2x_4)	8.7500E-05	1	2.7563E-03	0.140	0.713	NO
Binder x Cure (x_3x_4)	-8.5420E-05	1	1.0506E-02	0.535	0.475	NO
Particle x Particle (x_1x_1)	7.0357E-08	1	2.7034E-02	1.377	0.258	NO
Moisture x Moisture (x_2x_2)	-5.0780E-03	1	5.9967E-02	3.054	0.100	NO
Binder x Binder (x_3x_3)	-4.0200E-04	1	5.9980E-03	0.305	0.588	NO
Cure x Cure (x_4x_4)	-6.7820E-06	1	8.2522E-03	0.420	0.526	NO

Intercept

Source	Estimate	t Ratio	Intercept Test	
			Prob> t	Significance
Intercept (β)	5.1013	7.30	<.0001	YES

Residuals for pellet elemental hydrogen full model**Residuals for pellet elemental nitrogen full model**

Pellet elemental nitrogen full model**Summary of Fit**

Rsquare	0.694
RSquare Adj	0.426
Root Mean Square Error	0.0687
Mean of Response	1.130

Analysis of Variance

Source	DF	Sum of Squares	Mean Square	F Ratio	Model Test	
					Prob > F	Significance
Model	14	1.7137E-01	1.2241E-02	2.593	0.0353	YES
Error	16	7.5529E-02	4.7210E-03			
C. Total	30	2.4690E-01				

Lack Of Fit

Source	DF	Sum of Squares	Mean Square	F Ratio	Lack of Fit Test	
					Prob > F	Significance
Lack Of Fit	10	6.5243E-02	6.5240E-03	3.806	0.0578	NO
Pure Error	6	1.0286E-02	1.7140E-03			
Total Error	16	7.5529E-02		Max RSq	0.9583	

Terms

Source	Estimate	DF	Sum of Squares	F Ratio	Term Test	
					Prob > F	Significance
Particle (x_1)	4.2074E-05	1	5.8591E-04	0.124	0.729	NO
Moisture (x_2)	-1.4742E-02	1	9.5381E-04	0.202	0.659	NO
Binder (x_3)	-0.0083	1	8.4373E-04	0.179	0.678	NO
Cure (x_4)	8.9940E-04	1	9.2506E-04	0.196	0.664	NO
Particle x Moisture (x_1x_2)	2.2699E-06	1	5.6769E-04	0.120	0.733	NO
Particle x Binder (x_1x_3)	-1.7290E-08	1	1.3000E-07	0.000	0.996	NO
Moisture x Binder (x_2x_3)	-8.6800E-04	1	3.9063E-03	0.828	0.377	NO
Particle x Cure (x_1x_4)	-6.7010E-08	1	1.3743E-04	0.029	0.867	NO
Moisture x Cure (x_2x_4)	-2.0830E-05	1	1.5625E-04	0.033	0.858	NO
Binder x Cure (x_3x_4)	-1.4580E-05	1	3.0625E-04	0.065	0.802	NO
Particle x Particle (x_1x_1)	-2.6600E-08	1	3.8650E-03	0.819	0.379	NO
Moisture x Moisture (x_2x_2)	2.1971E-03	1	1.1225E-02	2.378	0.143	NO
Binder x Binder (x_3x_3)	6.3165E-05	1	1.4844E-04	0.031	0.862	NO
Cure x Cure (x_4x_4)	-1.0900E-06	1	2.1334E-04	0.045	0.834	NO

Intercept

Source	Estimate	t Ratio	Intercept Test	
			Prob> t	Significance
Intercept (β)	1.3710	4.00	0.001	YES

Pellet elemental sulfur full model**Summary of Fit**

Rsquare	0.694
RSquare Adj	0.426
Root Mean Square Error	0.167
Mean of Response	1.740

Analysis of Variance

Source	DF	Sum of Squares	Mean Square	F Ratio	Model Test	
					Prob > F	Significance
Model	14	1.0096	0.0721	2.593	0.0353	YES
Error	16	0.4450	0.0278			
C. Total	30	1.4546				

Lack Of Fit

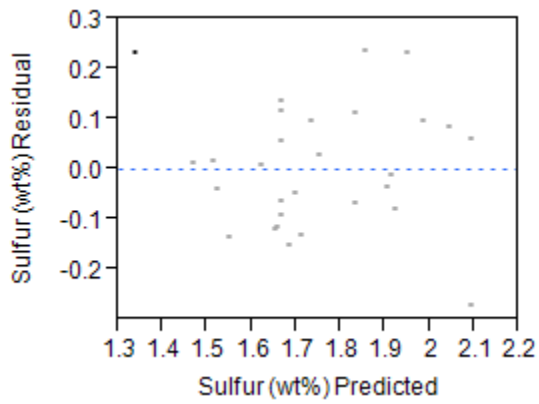
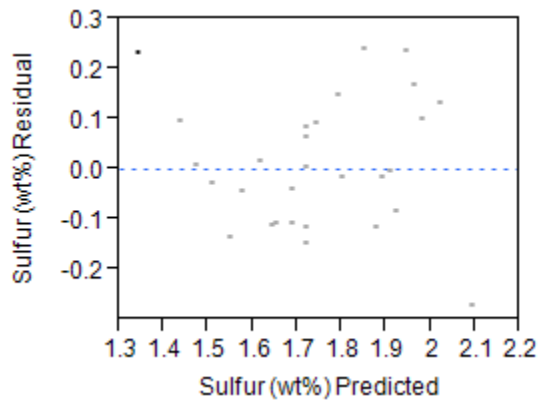
Source	DF	Sum of Squares	Mean Square	F Ratio	Lack of Fit Test	
					Prob > F	Significance
Lack Of Fit	10	0.3841	0.0384	3.781	0.0586	NO
Pure Error	6	0.0609	0.0102			
Total Error	16	0.4450		Max RSq	0.9581	

Terms

Source	Estimate	DF	Sum of Squares	F Ratio	Term Test	
					Prob > F	Significance
Particle (x_1)	8.3231E-05	1	2.2929E-03	0.082	0.778	NO
Moisture (x_2)	-6.3078E-02	1	1.7462E-02	0.628	0.440	NO
Binder (x_3)	-0.0389	1	1.8334E-02	0.659	0.429	YES
Cure (x_4)	5.1080E-04	1	2.9842E-04	0.011	0.919	NO
Particle x Moisture (x_1x_2)	1.3647E-06	1	2.0518E-04	0.007	0.933	NO
Particle x Binder (x_1x_3)	-9.4410E-06	1	3.9281E-02	1.412	0.252	NO
Moisture x Binder (x_2x_3)	1.1458E-03	1	6.8063E-03	0.245	0.628	NO
Particle x Cure (x_1x_4)	1.3500E-08	1	5.5800E-06	0.000	0.989	NO
Moisture x Cure (x_2x_4)	-1.2100E-04	1	5.2563E-03	0.189	0.670	NO
Binder x Cure (x_3x_4)	-5.2000E-05	1	3.9063E-03	0.140	0.713	NO
Particle x Particle (x_1x_1)	5.1218E-08	1	1.4326E-02	0.515	0.483	NO
Moisture x Moisture (x_2x_2)	3.5087E-03	1	2.8627E-02	1.029	0.325	NO
Binder x Binder (x_3x_3)	3.5640E-04	1	4.7245E-03	0.170	0.686	NO
Cure x Cure (x_4x_4)	9.1315E-06	1	1.4961E-02	0.538	0.474	NO

Intercept

Source	Estimate	t Ratio	Intercept Test	
			Prob> t	Significance
Intercept (β)	2.6080	3.13	0.0064	YES

Residuals for pellet elemental sulfur full model**Residuals for pellet elemental sulfur reduced model**

Pellet elemental sulfur reduced model**Summary of Fit**

Rsquare	0.658
RSquare Adj	0.572
Root Mean Square Error	0.144
Mean of Response	1.740

Analysis of Variance

Source	DF	Sum of Squares	Mean Square	F Ratio	Model Test	
					Prob > F	Significance
Model	6	0.9570	0.1595	7.693	0.0001	YES
Error	24	0.4976	0.0207			
C. Total	30	1.4546				

Lack Of Fit

Source	DF	Sum of Squares	Mean Square	F Ratio	Lack of Fit Test	
					Prob > F	Significance
Lack Of Fit	18	0.4367	0.0243	2.388	0.143	NO
Pure Error	6	0.0609	0.0102			
Total Error	24	0.4976		Max RSq	0.9581	

Terms

Source	Estimate	DF	Sum of Squares	F Ratio	Term Test	
					Prob > F	Significance
Particle (x_1)	2.0240E-04	1	2.9788E-02	1.437	0.242	NO
Moisture (x_2)	-4.6523E-02	1	3.3262E-02	1.604	0.218	NO
Binder (x_3)	-2.1179E-02	1	1.2111E-01	5.841	0.024	YES
Cure (x_4)	7.4170E-04	1	3.3004E-02	1.592	0.219	NO
Particle x Binder (x_1x_3)	-9.4410E-06	1	3.9281E-02	1.895	0.181	NO
Moisture x Moisture (x_2x_2)	3.3329E-03	1	2.6465E-02	1.277	0.270	NO

Intercept

Source	Estimate	t Ratio	Intercept Test	
			Prob> t	Significance
Intercept (β)	2.3212	9.31	<.0001	YES

Reduced Model F-Test

Model	SSE	MSE	DF	F_{calc}	$H_0: F_{calc} > F_{0.05, df1, df2}$	
					$F_{0.05, df1, df2}$	Reject H_0 ?
Full	0.4450	0.0278	14	0.2364	2.6987	NO
Reduced	0.4976		6			

Pellet elemental oxygen full model**Summary of Fit**

Rsquare	0.758
RSquare Adj	0.547
Root Mean Square Error	1.232
Mean of Response	16.309

Analysis of Variance

Source	DF	Sum of Squares	Mean Square	F Ratio	Model Test	
					Prob > F	Significance
Model	14	76.1833	5.4417	3.585	0.0083	YES
Error	16	24.2883	1.5180			
C. Total	30	100.4716				

Lack Of Fit

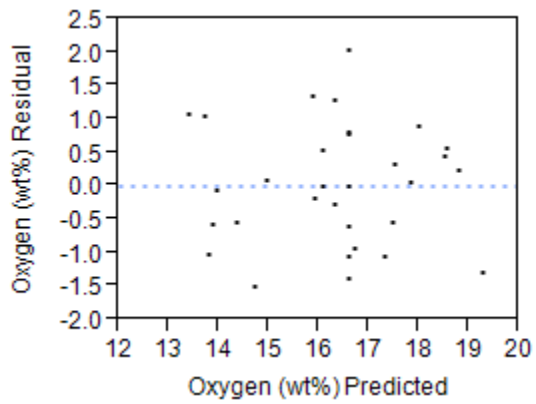
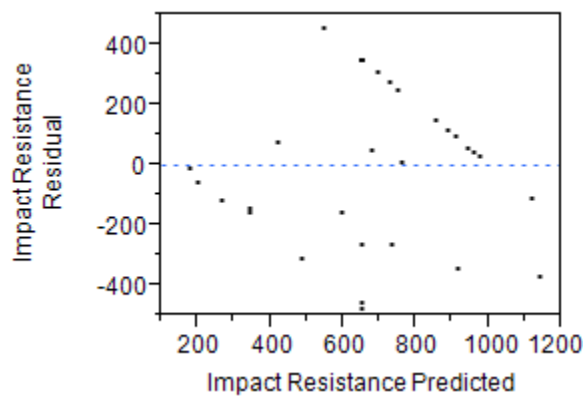
Source	DF	Sum of Squares	Mean Square	F Ratio	Lack of Fit Test	
					Prob > F	Significance
Lack Of Fit	10	15.5393	1.5539	1.066	0.4911	NO
Pure Error	6	8.7490	1.4582			
Total Error	16	24.2883		Max RSq	0.9129	

Terms

Source	Estimate	DF	Sum of Squares	F Ratio	Term Test	
					Prob > F	Significance
Particle (x_1)	-8.5100E-04	1	0.2394	0.158	0.697	NO
Moisture (x_2)	7.4363E-01	1	2.4270	1.599	0.224	NO
Binder (x_3)	0.6657	1	5.3670	3.536	0.078	NO
Cure (x_4)	3.6676E-02	1	1.5384	1.013	0.329	NO
Particle x Moisture (x_1x_2)	2.0170E-04	1	4.4824	2.953	0.105	NO
Particle x Binder (x_1x_3)	-9.4000E-05	1	3.8986	2.568	0.129	NO
Moisture x Binder (x_2x_3)	-6.0420E-03	1	0.1892	0.125	0.729	NO
Particle x Cure (x_1x_4)	7.0290E-06	1	1.5120	0.996	0.333	NO
Moisture x Cure (x_2x_4)	-2.1830E-03	1	1.7161	1.131	0.304	NO
Binder x Cure (x_3x_4)	-1.5000E-04	1	0.0324	0.021	0.886	NO
Particle x Particle (x_1x_1)	7.8041E-07	1	3.3261	2.191	0.158	NO
Moisture x Moisture (x_2x_2)	-1.9285E-02	1	0.8648	0.570	0.461	NO
Binder x Binder (x_3x_3)	-7.4950E-03	1	2.0899	1.377	0.258	NO
Cure x Cure (x_4x_4)	-1.6100E-04	1	4.6465	3.061	0.099	NO

Intercept

Source	Estimate	t Ratio	Intercept Test	
			Prob> t	Significance
Intercept (β)	2.1897	0.36	0.7263	NO

Residuals for pellet elemental oxygen full model**Residuals for pellet impact resistance full model**

Pellet impact resistance full model**Summary of Fit**

Rsquare	0.478
RSquare Adj	0.021
Root Mean Square Error	355.70
Mean of Response	676.06

Analysis of Variance

Source	DF	Sum of Squares	Mean Square	F Ratio	Model Test	
					Prob > F	Significance
Model	14	1853208	132372	1.046	0.4612	NO
Error	16	2024408	126525			
C. Total	30	3877616				

Lack Of Fit

Source	DF	Sum of Squares	Mean Square	F Ratio	Lack of Fit Test	
					Prob > F	Significance
Lack Of Fit	10	1025464	102546	0.616	0.7626	NO
Pure Error	6	998944	166491			
Total Error	16	2024408		Max RSq	0.7424	

Terms

Source	Estimate	DF	Sum of Squares	F Ratio	Term Test	
					Prob > F	Significance
Particle (x_1)	1.9062E-01	1	12026	0.095	0.762	NO
Moisture (x_2)	71.8249	1	22641	0.179	0.678	NO
Binder (x_3)	-233.8454	1	662227	5.234	0.036	YES
Cure (x_4)	-8.1201	1	75411	0.596	0.451	NO
Particle x Moisture (x_1x_2)	-3.6040E-02	1	143102	1.131	0.303	NO
Particle x Binder (x_1x_3)	-9.2110E-03	1	37393	0.296	0.594	NO
Moisture x Binder (x_2x_3)	4.6076	1	110058	0.870	0.365	NO
Particle x Cure (x_1x_4)	5.6750E-04	1	9856	0.078	0.784	NO
Moisture x Cure (x_2x_4)	-3.8625E-01	1	53708	0.425	0.524	NO
Binder x Cure (x_3x_4)	6.7521E-01	1	656505	5.189	0.037	YES
Particle x Particle (x_1x_1)	8.0000E-05	1	34953	0.276	0.606	NO
Moisture x Moisture (x_2x_2)	-7.5351	1	132028	1.044	0.322	NO
Binder x Binder (x_3x_3)	2.6787	1	266965	2.110	0.166	NO
Cure x Cure (x_4x_4)	-1.7977E-02	1	57981	0.458	0.508	NO

Intercept

Source	Estimate	t Ratio	Intercept Test	
			Prob> t	Significance
Intercept (β)	3563.3131	2.01	0.0618	NO

Pellet indirect tensile strength full model**Summary of Fit**

Rsquare	0.504
RSquare Adj	0.070
Root Mean Square Error	211.97
Mean of Response	353.03

Analysis of Variance

Source	DF	Sum of Squares	Mean Square	F Ratio	Model Test	
					Prob > F	Significance
Model	14	730522	52180	1.161	0.3836	NO
Error	16	718903	44931			
C. Total	30	1449425				

Lack Of Fit

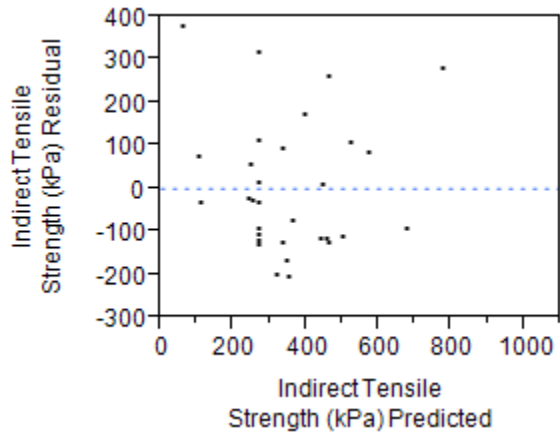
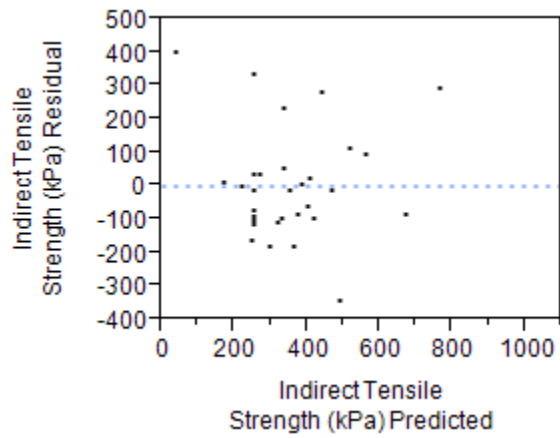
Source	DF	Sum of Squares	Mean Square	F Ratio	Lack of Fit Test	
					Prob > F	Significance
Lack Of Fit	10	568891	56889	2.275	0.1633	NO
Pure Error	6	150012	25002			
Total Error	16	718903		Max RSq	0.8965	

Terms

Source	Estimate	DF	Sum of Squares	F Ratio	Term Test	
					Prob > F	Significance
Particle (x_1)	7.4813E-02	1	1853	0.041	0.842	NO
Moisture (x_2)	-163.4858	1	117302	2.611	0.126	NO
Binder (x_3)	24.4787	1	7257	0.162	0.693	NO
Cure (x_4)	-4.9443	1	27959	0.622	0.442	NO
Particle x Moisture (x_1x_2)	9.6624E-03	1	10286	0.229	0.639	NO
Particle x Binder (x_1x_3)	12.6801	1	10053	0.224	0.643	NO
Moisture x Binder (x_2x_3)	1.3542	1	9506	0.212	0.652	NO
Particle x Cure (x_1x_4)	1.0410E-03	1	33162	0.738	0.403	NO
Moisture x Cure (x_2x_4)	-1.9417E-01	1	13572	0.302	0.590	NO
Binder x Cure (x_3x_4)	-5.9583E-02	1	5112	0.114	0.740	NO
Particle x Particle (x_1x_1)	-9.3330E-05	1	47565	1.059	0.319	NO
Moisture x Moisture (x_2x_2)	-4.7760E-03	1	373876	8.321	0.011	YES
Binder x Binder (x_3x_3)	-5.6608E-01	1	11922	0.265	0.614	NO
Cure x Cure (x_4x_4)	2.7798E-02	1	138649	3.086	0.098	NO

Intercept

Source	Estimate	t Ratio	Intercept Test	
			Prob> t	Significance
Intercept (β)	797.1258	0.75	0.4619	NO

Residuals for pellet indirect tensile strength full model**Residuals for pellet indirect tensile strength reduced model**

Pellet indirect tensile strength reduced model**Summary of Fit**

Rsquare	0.439
RSquare Adj	0.269
Root Mean Square Error	187.95
Mean of Response	353.03

Analysis of Variance

Source	DF	Sum of Squares	Mean Square	F Ratio	Model Test	
					Prob > F	Significance
Model	7	636908	90987	2.576	0.0408	YES
Error	23	812517	35327			
C. Total	30	1449425				

Lack Of Fit

Source	DF	Sum of Squares	Mean Square	F Ratio	Lack of Fit Test	
					Prob > F	Significance
Lack Of Fit	17	662505	38971	1.559	0.3039	NO
Pure Error	6	150012	25002			
Total Error	23	812517		Max RSq	0.8965	

Terms

Source	Estimate	DF	Sum of Squares	F Ratio	Term Test	
					Prob > F	Significance
Particle (x_1)	1.5208E-01	1	25412	0.7193	0.405	NO
Moisture (x_2)	-146.8459	1	327213	9.2624	0.006	YES
Binder (x_3)	-6.7778	1	39691	1.1235	0.300	NO
Cure (x_4)	-6.6379	1	131804	3.7310	0.066	NO
Particle x Particle (x_1x_1)	-9.7270E-05	1	52043	1.4732	0.237	NO
Moisture x Moisture (x_2x_2)	12.9131	1	391889	11.0932	0.003	YES
Cure x Cure (x_4x_4)	2.8637E-02	1	148716	4.2097	0.052	NO

Intercept

Source	Estimate	t Ratio	Intercept Test	
			Prob> t	Significance
Intercept (β)	1165.4642	3.92	0.0007	YES

Reduced Model F-Test

Model	SSE	MSE	DF	F_{calc}	$H_0: F_{calc} > F_{0.05, df1, df2}$	
					$F_{0.05, df1, df2}$	Reject H_0 ?
Full	718903	44931	14	0.2976	2.8477	NO
Reduced	812517		7			

Pellet abrasion resistance full model**Summary of Fit**

Rsquare	0.361
RSquare Adj	-0.198
Root Mean Square Error	16.20
Mean of Response	89.87

Analysis of Variance

Source	DF	Sum of Squares	Mean Square	F Ratio	Model Test	
					Prob > F	Significance
Model	14	2375.87	169.71	0.647	0.791	NO
Error	16	4199.61	262.48			
C. Total	30	6575.48				

Lack Of Fit

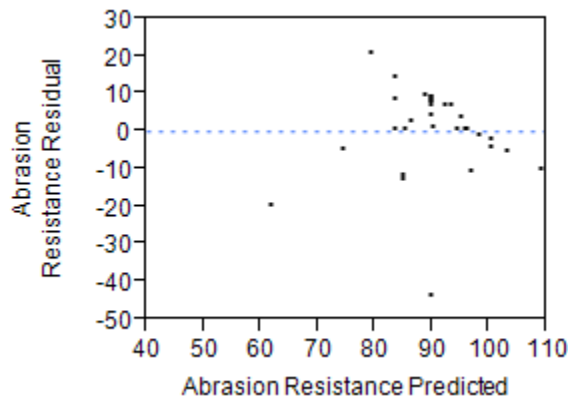
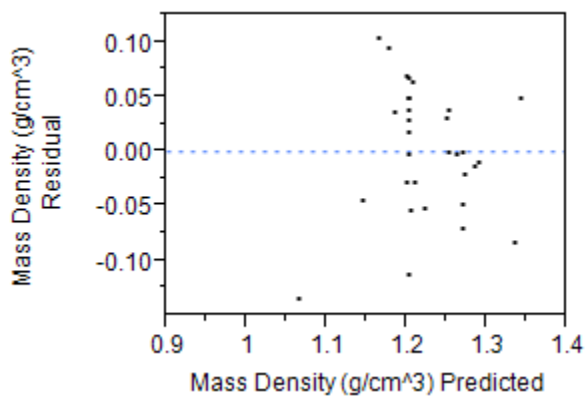
Source	DF	Sum of Squares	Mean Square	F Ratio	Lack of Fit Test	
					Prob > F	Significance
Lack Of Fit	10	1908.76	190.88	0.500	0.8411	NO
Pure Error	6	2290.86	381.81			
Total Error	16	4199.61		Max RSq	0.6516	

Terms

Source	Estimate	DF	Sum of Squares	F Ratio	Term Test	
					Prob > F	Significance
Particle (x_1)	3.9750E-03	1	5.230	0.020	0.890	NO
Moisture (x_2)	0.1970	1	0.170	0.001	0.980	NO
Binder (x_3)	-1.2366	1	18.518	0.071	0.794	NO
Cure (x_4)	-0.5672	1	367.921	1.402	0.254	NO
Particle x Moisture (x_1x_2)	-3.8000E-04	1	15.943	0.061	0.809	NO
Particle x Binder (x_1x_3)	-8.8100E-04	1	342.029	1.303	0.270	NO
Moisture x Binder (x_2x_3)	0.1667	1	144.000	0.549	0.470	NO
Particle x Cure (x_1x_4)	7.3900E-05	1	167.156	0.637	0.437	NO
Moisture x Cure (x_2x_4)	-1.8333E-02	1	121.000	0.461	0.507	NO
Binder x Cure (x_3x_4)	2.5000E-02	1	900.000	3.429	0.083	NO
Particle x Particle (x_1x_1)	2.8399E-06	1	44.044	0.168	0.688	NO
Moisture x Moisture (x_2x_2)	-0.0865	1	17.416	0.066	0.800	NO
Binder x Binder (x_3x_3)	-0.0390	1	56.580	0.216	0.649	NO
Cure x Cure (x_4x_4)	2.3840E-04	1	10.201	0.039	0.846	NO

Intercept

Source	Estimate	t Ratio	Intercept Test	
			Prob> t	Significance
Intercept (β)	133.7392	1.65	0.1175	NO

Residuals for pellet abrasion resistance full model**Residuals for pellet mass density full model**

Pellet mass density full model**Summary of Fit**

Rsquare	0.473
RSquare Adj	0.011
Root Mean Square Error	0.080
Mean of Response	1.225

Analysis of Variance

Source	DF	Sum of Squares	Mean Square	F Ratio	Model Test	
					Prob > F	Significance
Model	14	9.0854E-02	6.4900E-03	1.025	0.4768	NO
Error	16	1.0131E-01	6.3320E-03			
C. Total	30	1.9217E-01				

Lack Of Fit

Source	DF	Sum of Squares	Mean Square	F Ratio	Lack of Fit Test	
					Prob > F	Significance
Lack Of Fit	10	8.2228E-02	8.2230E-03	2.585	0.1286	NO
Pure Error	6	1.9086E-02	3.1810E-03			
Total Error	16	1.0131E-01		Max RSq	0.9007	

Terms

Source	Estimate	DF	Sum of Squares	F Ratio	Term Test	
					Prob > F	Significance
Particle (x_1)	-1.7400E-04	1	9.9874E-03	1.577	0.227	NO
Moisture (x_2)	-2.7401E-02	1	3.2952E-03	0.520	0.481	NO
Binder (x_3)	1.8565E-02	1	4.1740E-03	0.659	0.429	NO
Cure (x_4)	-3.5750E-03	1	1.4621E-02	2.309	0.148	NO
Particle x Moisture (x_1x_2)	2.1932E-06	1	5.2998E-04	0.084	0.776	NO
Particle x Binder (x_1x_3)	-1.8130E-06	1	1.4488E-03	0.229	0.639	NO
Moisture x Binder (x_2x_3)	7.9860E-04	1	3.3063E-03	0.522	0.480	NO
Particle x Cure (x_1x_4)	5.3164E-07	1	8.6500E-03	1.366	0.260	NO
Moisture x Cure (x_2x_4)	2.0833E-05	1	1.5625E-04	0.025	0.877	NO
Binder x Cure (x_3x_4)	9.7917E-05	1	1.3806E-02	2.180	0.159	NO
Particle x Particle (x_1x_1)	5.8453E-08	1	1.8659E-02	2.947	0.105	NO
Moisture x Moisture (x_2x_2)	6.4300E-04	1	9.6154E-04	0.152	0.702	NO
Binder x Binder (x_3x_3)	-6.0300E-04	1	1.3534E-02	2.137	0.163	NO
Cure x Cure (x_4x_4)	3.3150E-06	1	1.9717E-03	0.311	0.585	NO

Intercept

Source	Estimate	t Ratio	Intercept Test	
			Prob> t	Significance
Intercept (β)	1.2984	3.3	0.0048	YES

Pellet particle density full model**Summary of Fit**

Rsquare	0.848
RSquare Adj	0.715
Root Mean Square Error	0.022
Mean of Response	1.367

Analysis of Variance

Source	DF	Sum of Squares	Mean Square	F Ratio	Model Test	
					Prob > F	Significance
Model	14	4.4080E-02	3.1490E-03	6.382	0.0004	YES
Error	16	7.8940E-03	4.9300E-04			
C. Total	30	5.1974E-02				

Lack Of Fit

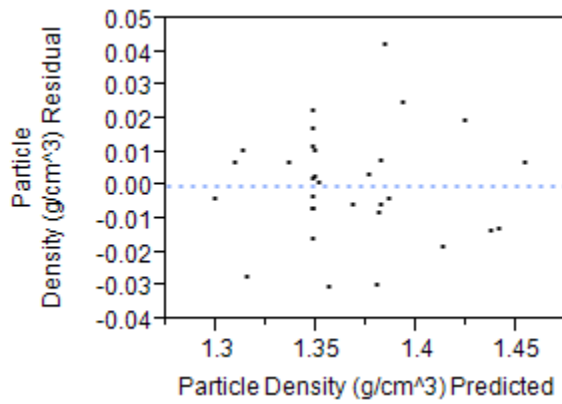
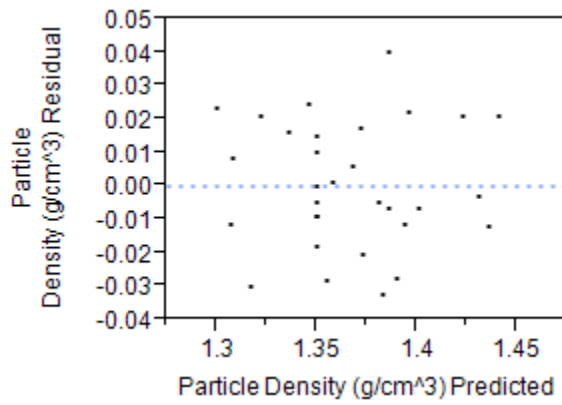
Source	DF	Sum of Squares	Mean Square	F Ratio	Lack of Fit Test	
					Prob > F	Significance
Lack Of Fit	10	7.0946E-03	7.0900E-04	5.325	0.0266	YES
Pure Error	6	7.9943E-04	1.3300E-04			
Total Error	16	7.8940E-03		Max RSq	0.9846	

Terms

Source	Estimate	DF	Sum of Squares	F Ratio	Term Test	
					Prob > F	Significance
Particle (x_1)	-1.0100E-04	1	3.3775E-03	6.846	0.019	YES
Moisture (x_2)	2.5511E-02	1	2.8563E-03	5.789	0.029	YES
Binder (x_3)	-1.1194E-02	1	1.5175E-03	3.076	0.099	NO
Cure (x_4)	3.0420E-04	1	1.0583E-04	0.215	0.650	NO
Particle x Moisture (x_1x_2)	1.8579E-06	1	3.8032E-04	0.771	0.393	NO
Particle x Binder (x_1x_3)	1.2883E-06	1	7.3143E-04	1.483	0.241	NO
Moisture x Binder (x_2x_3)	-2.7100E-04	1	3.8025E-04	0.771	0.393	NO
Particle x Cure (x_1x_4)	-2.3140E-07	1	1.6393E-03	3.323	0.087	NO
Moisture x Cure (x_2x_4)	-9.9170E-05	1	3.5403E-03	7.176	0.017	YES
Binder x Cure (x_3x_4)	2.0417E-05	1	6.0025E-04	1.217	0.286	NO
Particle x Particle (x_1x_1)	3.3326E-08	1	6.0654E-03	12.294	0.003	YES
Moisture x Moisture (x_2x_2)	-1.5500E-04	1	5.5680E-05	0.113	0.741	NO
Binder x Binder (x_3x_3)	1.0020E-04	1	3.7357E-04	0.757	0.397	NO
Cure x Cure (x_4x_4)	3.9293E-07	1	2.7700E-05	0.056	0.816	NO

Intercept

Source	Estimate	t Ratio	Intercept Test	
			Prob> t	Significance
Intercept (β)	1.4758	13.3	<.0001	YES

Residuals for pellet particle density full model**Residuals for pellet particle density reduced model**

Pellet particle density reduced model**Summary of Fit**

Rsquare	0.799
RSquare Adj	0.737
Root Mean Square Error	0.0213
Mean of Response	1.367

Analysis of Variance

Source	DF	Sum of Squares	Mean Square	F Ratio	Model Test	
					Prob > F	Significance
Model	7	4.1506E-02	5.9290E-03	13.028	<.0001	YES
Error	23	1.0468E-02	4.5500E-04			
C. Total	30	5.1974E-02				

Lack Of Fit

Source	DF	Sum of Squares	Mean Square	F Ratio	Lack of Fit Test	
					Prob > F	Significance
Lack Of Fit	17	9.6683E-03	5.6900E-04	4.269	0.0407	YES
Pure Error	6	7.9943E-04	1.3300E-04			
Total Error	23	1.0468E-02		Max RSq	0.9846	

Terms

Source	Estimate	DF	Sum of Squares	F Ratio	Term Test	
					Prob > F	Significance
Particle (x_1)	-6.0120E-05	1	2.6372E-03	5.795	0.0245	YES
Moisture (x_2)	1.9122E-02	1	8.1932E-03	18.002	0.0003	YES
Binder (x_3)	-4.1940E-03	1	1.5201E-02	33.399	<.0001	YES
Cure (x_4)	8.8850E-04	1	5.1485E-03	11.312	0.0027	YES
Particle x Cure (x_1x_4)	-2.3140E-07	1	1.6393E-03	3.602	0.0703	NO
Moisture x Cure (x_2x_4)	-9.9170E-05	1	3.5403E-03	7.779	0.0104	YES
Particle x Particle (x_1x_1)	3.3840E-08	1	6.3666E-03	13.989	0.0011	YES

Intercept

Source	Estimate	t Ratio	Intercept Test	
			Prob> t	Significance
Intercept (β)	1.3566	35.35	<.0001	YES

Reduced Model F-Test

Model	SSE	MSE	DF	F_{calc}	$H_0: F_{calc} > F_{0.05, df1, df2}$	
					$F_{0.05, df1, df2}$	Reject H_0 ?
Full	7.8940E-03	4.9300E-04	14	0.7458	2.7642	NO
Reduced	1.0468E-02		7			